



Study of the role of the deglutamyating enzyme CCP5 in microtubules function regulation during mouse spermatogenesis

Tiziana Giordano

► To cite this version:

Tiziana Giordano. Study of the role of the deglutamyating enzyme CCP5 in microtubules function regulation during mouse spermatogenesis. Cellular Biology. Université Paris Saclay (COMUE), 2016. English. NNT : 2016SACLS574 . tel-01796055

HAL Id: tel-01796055

<https://theses.hal.science/tel-01796055>

Submitted on 19 May 2018

HAL is a multi-disciplinary open access archive for the deposit and dissemination of scientific research documents, whether they are published or not. The documents may come from teaching and research institutions in France or abroad, or from public or private research centers.

L'archive ouverte pluridisciplinaire **HAL**, est destinée au dépôt et à la diffusion de documents scientifiques de niveau recherche, publiés ou non, émanant des établissements d'enseignement et de recherche français ou étrangers, des laboratoires publics ou privés.

THESE DE DOCTORAT
DE
L' UNIVERSITE PARIS-SACLAY
PREPAREE A
UNIVERSITE PARIS SUD-XI

ECOLE DOCTORALE N° 577
Structure et Dynamique des Systèmes Vivants
Discipline: Sciences de la Vie et de la Santé

Par

Tiziana GIORDANO

**ETUDE DU RÔLE DE L'ENZYME DEGLUTAMYLASE CCP5
DANS LA RÉGULATION DE LA FONCTION DES
MICROTUBULES AU COURS DE LA SPERMIOGENÈSE CHEZ
LA SOURIS**

Thèse présentée et soutenue à Orsay, le 13 Décembre 2016

Composition du Jury:

Dr.: Christian Pous, Professeur, Université Paris-Saclay, Président du jury
Dr. : Francois Lanza, Directeur de recherche, Université de Strasbourg, Rapporteur
Dr. : Aminata Toure, Directrice de recherche, Université Paris Descartes, Rapporteur
Dr. : Christophe Arnoult, Directeur de recherche, Université de Grenoble, Examineur
Dr. : Filippo Del Bene, Directeur de recherche, Institut Curie, Examineur
Dr. : Stefan Geimer, Professeur, Université de Bayreuth, Examineur
Dr. : Carsten Janke, Directeur de recherche, Université Paris-Saclay, Directeur de thèse
Dr. : Véronique Marthiens, Post-doctorante, Institut Curie, Examineur

ACKNOWLEDGEMENTS

I would like first to thank my thesis supervisor Dr. Carsten Janke who allowed me to work in this interesting and challenging project. Beside my supervisor, I would like to thank all the members of the laboratory. Among them, I am really grateful to Sudarshan who helped me out with several experiments during the last months on my thesis. Many thanks for the time you spent with me in the cold room even if you were about to lose your fingers for the low temperature! ! I thank Satish for all stimulating discussions we had and, of course, for your help and complete availability during the writing of my thesis manuscript. Thanks to Kathiresan and Puja for all the good moments we had spent together.

I would like to express my sincere gratitude to my collaborator Christophe Arnoult. When we decided to work on spermatogenesis I was a bit afraid because of the novelty of this scientific field for our lab. Thanks to your scientific and technical advice I have been able to perform a great research and I have learned really a lot of new things. Many thanks also to all your lab members that have been really welcoming when I came to Grenoble.

Thanks also to Dr Stefan Geimer and his student Sebastian that have performed all the electron microscopy studies. I really appreciate to collaborate with both of you and I would like to thank you for helping me to proceed with my research.

During my thesis I was fortunate enough to meet wonderful colleagues that now have become truly friends: thanks to Cecilia, Patricia, Montsè, Julie, Olivia, Judith, Annemarie, Lulu and Lolo. I miss all our coffee breaks but fortunately we still have our dinner sections! Special thanks to Lolo, for have been on my side during a very difficult moment. Thanks to Vincent, Alexi, Sandrine, Sylvain et all my meal-friends!

Il più grande dei ringraziamenti va alla mia famiglia, in particolare alla mia mamma, a mia sorella e alla nonna. Il ringraziamento più sentito va al mio compagno di viaggio... grazie per la tua tenacia. Tutto ciò non avrebbe avuto senso senza di te.

È stato un cammino lungo e difficile, vi ringrazio per la forza che mi avete trasmesso permettendomi di arrivare a questo traguardo.

INDEX

MAIN ABBREVIATION LIST	6
1. INTRODUCTION	8
MICROTUBULES	8
1.1.1 <i>Microtubule structure</i>	9
1.1.2 <i>Functions of Microtubules</i>	12
1.1.3 <i>The Tubulins: the different tubulin genes and their expression profile</i>	13
1.1.4 <i>Tubulin post-translational modifications</i>	15
1.1.4.1 Detyrosination and tyrosination	17
1.1.4.2 $\Delta 2$ - and $\Delta 3$ -tubulin	17
1.1.4.3 Acetylation	18
1.1.4.4 Glutamylation	19
1.1.4.5 Glycylation	27
1.2 SPERMATOGENESIS	29
1.2.1 <i>General aspects of spermatogenesis</i>	30
1.2.2 <i>The mitotic phase: spermatogonial proliferation</i>	35
1.2.3 <i>The meiotic phase: production of haploid germ cells</i>	36
1.2.4 <i>Spermiogenesis: cytodifferentiation of round spermatids into spermatozoa</i>	38
1.2.4.1 Acrosome, perinuclear theca and acroplaxome	40
1.2.4.2 The microtubule-based manchette	45
1.2.4.3 Spermatid nuclear condensation	51
1.2.4.4 Sperm tail formation, structure and functions	53
1.2.4.4.1 Axoneme structure and development	53
1.2.4.4.2 The connecting piece	56
1.2.4.4.3 The midpiece	58
1.2.4.4.4 The principal and distal piece	62
1.2.4.5 Importance of intraflagellar and intramanchette based transport in spermatid development	63
1.2.4.6 Microtubule polyglutamylation in flagella	68
2. AIM OF THE STUDY	75
3. MATERIAL AND METHODS	77
ANIMAL EXPERIMENTATION	77
TESTICULAR GERM CELL DISSOCIATION.	78
BSA DENSITY GRADIENT-BASED TESTICULAR GERM CELL FRACTIONATION	79
COMPUTER-ASSISTED MOTILITY ANALYSIS	80
SPERM COUNTING	80
SAMPLE PREPARATION FOR ELECTRON MICROSCOPY ANALYSIS	81
GERM CELLS DEPLETION FROM MOUSE TESTIS SEMINIFEROUS TUBULES	82
HISTOLOGY AND IMMUNOFLUORESCENCE	82
MICROSCOPY AND IMAGING	83
QUANTIFICATION OF CCP5 KO-RELATED PHENOTYPES	83
WESTERN BLOT	85
RNA EXTRACTION	85
REAL-TIME QUANTITATIVE REVERSE TRANSCRIPTION PCR	86
STATISTICAL ANALYSIS	86
4. RESULTS	88
4.1 INFERTILITY PHENOTYPE IN CCP5 ^{-/-} MICE IS MAINLY DUE TO DEFECTS IN HAPLOID POST MEIOTIC GERM CELLS.	88
4.2 HIGH CCP5 EXPRESSION LEVELS IN WILD TYPE TESTICULAR TISSUE	99

4.5 CCP5 ^{-/-} ELONGATING SPERMATIDS ARE CHARACTERIZED BY SUPERNUMERARY BASAL BODIES..	102
4.3 CCP5 ^{-/-} TESTICULAR GERM CELLS PRESENT INCREASED TUBULIN PTMS LEVELS.	105
4.4 CCP5 ^{-/-} SPERMATIDS ARE CHARACTERIZED BY SEVERAL MORPHOLOGICAL DEFECTS AND OVERALL INCREASED LEVEL OF TUBULIN PTMS	108
4.5 CCP5 ^{-/-} ELONGATING SPERMATIDS ARE CHARACTERIZED BY SUPERNUMERARY BASAL BODIES..	120
4.6 CCP5 ^{-/-} SPERMATIDS ARE CHARACTERIZED BY ULTRASTRUCTURAL DEFECTS ON ACROSOMES, MANCHETTES AND FLAGELLA.....	122
4.7 GENERATION OF A GERM-CELL-SPECIFIC CCP5 CONDITIONAL KNOCKOUT MOUSE: THE CCP5 ^{F/F} STRA8-CRE ^{+/+} MOUSE MODEL	128
4.8 INCREASED SPERM PRODUCTION IN CONDITIONAL CCP5 ^{-/-} MICE.	129
4.9 NO CHANGES IN PTMS BETWEEN TOTAL CCP5 ^{-/-} AND CONDITIONAL CCP5 ^{-/-} TESTICULAR GERM CELLS, BUT LOWER PENETRANCE OF CCP5 ^{-/-} -LIKE PHENOTYPES	133
4.10 PRESENCE OF MULTIPLE BASAL BODIES IN CONDITIONAL CCP5 ^{-/-} SPERMATIDS.	137
4.11 COMMON ULTRASTRUCTURAL DEFECTS IN CONDITIONAL CCP5 ^{-/-} AND TOTAL CCP5 ^{-/-} ELONGATING SPERMATIDS.	139
4.12 INCOMPLETE CRE-MEDIATED DEFLOXING IN CONDITIONAL CCP5 ^{-/-} TESTICULAR GERM CELLS ..	143
5. DISCUSSION	148
5.1 REDUCED SPERM OUTPUT IN CCP5 ^{-/-} IS DUE DO DEFECTIVE IN THE POST-MEIOTIC PHASE OF SPERMATOGENESIS.....	150
5.2 THE ENTIRE PROCESS OF SPERMIOGENESIS IS DEFECTIVE IN THE CCP5 ^{-/-} MOUSE	151
5.2.1 <i>CCP5 is important for acrosome elongation as well as for nucleus-acrosome anchoring.</i>	152
5.2.2 <i>CCP5^{-/-} elongating spermatids are characterized by a hypermodified and ultrastructural defective manchettes</i>	154
5.2.3 <i>Formation of multiple defective flagella in CCP5^{-/-} elongating spermatids</i>	156
5.2.4 <i>CCP5-mediated glutamylation participates in the regulation of the acrosome-acroplaxome-manchette-tail system.</i>	158
5.3 IMPLICATION OF SERTOLI CELLS IN THE CCP5 ^{-/-} INFERTILITY PHENOTYPE	159
6. CONCLUSION.....	162
BIBLIOGRAPHY	164

INDEX OF FIGURES

Introduction

Figure 1. Structure and dynamic instability of microtubules	11
Figure 2. Heterogeneity in the C-terminal tails of tubulin isotypes and their associated PTMs	14
Figure 3. Differential tubulin subpopulation generated by PTMs	16
Figure 4: Enzymes involved in the generation of PTMs in the C-terminal tail of tubulin	21
Figure 5: Reaction and substrate preference for TTLLs and CCPs	22
Figure 6: Schematic representation of mouse spermatogenesis	33
Figure 7: Schematic representation of spermiogenesis	39
Figure 8: Schematic representation of the structural components of the mammalian sperm head	44
Figure 9: Ultrastructure of mammalian spermatid manchette	49
Figure 10. Subcellular structures involved in the shaping of the spermatid head	50
Figure 11: Cross section representation of the sperm central axoneme	55
Figure 12: Electron micrograph of sperm connecting piece	57
Figure 13: Architecture of mammalian sperm flagellum	60
Figure 14: Role of microtubule-based transport in spermatid development	67

Results

Figure 4.1: Poor sperm production in CCP5 ^{-/-} mice	92
Figure 4.2: Infertility in CCP5 ^{-/-} mice	93
Figure 4.3: Disorganized testis cytoarchitecture in 4-months-old CCP5 ^{-/-} mice	95
Figure 4.4: Histological examination of 1-year-old CCP5 ^{-/-} testis: Absence of age-related pejorative phenotype	96
Figure 4.5 Motility analysis of CCP5 ^{+/-} spermatozoa	98
Figure 4.6: Relative expression levels of CCP5 in wild type adult murine tissues	100
Figure 4.7: Expression levels of selected CCPs and TTLLs in wild type mouse testis	101
Figure 4.8 Absence of up- or down-regulation of expression levels TTLLs and CCPs in CCP5 ^{-/-} testicular germ cells	103
FIG 4.9: Analyses of tubulin PTMs in testicular fractionated cells	107
FIG 4.9: Localisation of glutamylated tubulin in CCP5 ^{+/+} and CCP5 ^{-/-} testicular dissociated cells	110
Figure 4.10: Tubulin and polyglutamylation signals in round and elongating spermatids in CCP5 ^{+/+} and CCP5 ^{-/-} mice	113
Figure 4.12: Augmented frequency of defective germ cells in CCP5 ^{-/-} mice	116
Figure 4.13 Immunodetection of a range of tubulin posttranslational modifications in round and elongating spermatids	119
Figure 4.14: Presence of supernumerary centrioles/basal bodies in CCP5 ^{-/-} elongating spermatids	121
Figure 4.15: Ultrastructural defects in CCP5 ^{-/-} elongating spermatids	124
Figure 4.16: The acrosome is detached from the nuclear membrane in degenerating elongated spermatids of CCP5 ^{-/-}	125
Figure 4.17: Electron microscopy serial sections of a CCP5 ^{-/-} condensed spermatid showing axonemal integrity defects	126
Figure 4.18: Presence of spermatozoa in conditional CCP5 ^{-/-} semen	130
Figure 4.19: Disorganized testis cytoarchitecture in 2-months-old conditional CCP5 ^{-/-} mice	132
Figure 4.20: Posttranslational modifications in conditional CCP5 ^{-/-} testicular germ cells	135
Figure 4.21: Percentage of defective germ cells in conditional CCP5 ^{-/-} spermatids	136
Figure 4.22: Presence of supernumerary basal bodies in conditional CCP5 ^{-/-} elongating spermatids	138
Figure 4.23: Characterization of ultrastructural defects of conditional CCP5 ^{-/-} spermatids by electron microscopy	141
Figure 4.24: Incomplete Cre-mediated defloxing in conditional CCP5 ^{-/-} testicular germ cells	146
Figure 4.25: Glutamylation levels in wild type and CCP5-mutant Sertoli cells	147

MAIN ABBREVIATION LIST

ATP: Adenosine triphosphate

Azh: Abnormal Spermatozoon Head Shape

CCPs: Cytosolic carboxypeptidases

CTT: C-terminal tail of the tubulin

ES: Ectoplasmic specialization

Fleer/lft70: Tetratricopeptide (TRP) repeat protein

FS: Fibrous sheath

GDP: Guanosine diphosphate

GTP: Guanosine triphosphate

HDAC6: Histone deacetylase family member 6

IFT: Intraflagellar-transport

IMT: Intramanchette transport

K40: Lysine 40

KLC3: Kinesin light chain 3

MAPs: Microtubule associates proteins

MTOCs: MT-organizing centers

MTs: Microtubules

NAPs: Nucleosome assembly proteins

ODF: Outer dense fibers

PAS: Post-acrosomal sheath

PCD: Purkinje Cell Degeneration

PCM: Pericentriolar material

PRM: Protamines

PT: Perinuclear theca

PTMs: Post-translational modification

RT PCR: Reverse transcriptase polymerase chain reaction

SAL: Subacrosomal layer of PT

Sirt2: Sirtuin type 2

SSC: Spermatogonial stem cells

TNP: Transition proteins

TTL: Tubulin Tyrosine Ligase

TTLLs: Tyrosine Ligase Like

α -TAT1: α -tubulin N-acetyl transferase 1

1. INTRODUCTION

MICROTUBULES

The cell is a basic structural and functional unit for all the life forms. It facilitates the stringent control of various biochemical processes by maintaining distinct compartments and by coordinating chemical fluxes across them. Also, it has a well-defined structure and is capable of exerting forces. In case of complex organisms such as animals and plants, every cell provides some mechanical force to the tissue it builds. Further, processes such as cellular motility, division and adhesion are linked to the exertion of mechanical forces. These processes are coordinated by dynamic changes in the cellular architecture that is ensured by cytoskeleton.

Three main types of cytoskeletal protein structures exist in almost all eukaryotic cells i) the microtubules (MTs), ii) the actin filaments and iii) the intermediate filaments. Actin filaments and MTs are active filaments whose functions depend respectively on ATP and GTP hydrolysis, while intermediate filaments are structural elements. These filaments serve diverse roles in the cell: providing and maintaining structural stability; facilitating directional intracellular trafficking (actin filaments and MTs act as tracks for motor proteins); and ensuring the equal distribution of chromosomes during cell division.

In the context of my PhD project this first part of the introduction will focus on the description of MT and will present an up-to-date description of the post-translational modification MT proteins and their functions.

1.1.1 Microtubule structure

Structurally, a MT is built as a polymer from globular tubulin subunits, which are arranged in the form of a hollow cylindrical tube. The cylinder is 25 nm in outer diameter with a 17 nm interior space diameter. However, the tube length can vary from a fraction of a micrometer to hundreds of micrometers. The building block of a MT consist of a dimer of the α - and β -tubulin, monomers of each of these two proteins have a molecular weight of 55 kDa. Interactions between the ends of adjoining tubulin dimers connect the subunits head to tail to form a linear protofilament. In each protofilament, the dimeric subunit repeats itself every 8 nm (Fig. 1A). Protofilaments associate through lateral interactions into a cylinder, which is the MT (Fig. 1B). The heterodimer assembly is dependent on the presence of Guanosine triphosphate (GTP). GTP binding and hydrolysis on β -tubulin control the stability of MTs at the more dynamic MT-plus end (Akhmanova & Steinmetz 2008). There are two GTP-binding sites on tubulin, a hydrolysable site at the β -tubulin and a non-hydrolysable site at the α -subunit. The GTP at the β -tubulin is shortly retained after assembly, because its hydrolyzation to Guanosine diphosphate (GDP). (Akhmanova & Steinmetz 2008). Thus, the majority of β -tubulin in the MT polymer is in the GDP-bound form, whereas at the plus end, the MTs are “capped” with GTP-bound β -tubulin (Fig. 1C). In most cases, every MT is built as a single tube of 13 protofilaments, but in functionally specialized structures such as cilia and flagella, MT are organized in doublets (Ishikawa & Marshall 2011).

A MT is a polar structure. The polarity of the MT emerges from the arrangement of the tubulin heterodimers in the head to tail orientation within the protofilament. Due to the same orientation of all protofilaments in the cylinder, one end of the MT, called the minus-end, is exposes a ring of α -tubulins, while the other end of the MT, which is called plus-end, exposes β -tubulins, which in growing MTs carry GTP molecules.

MTs are highly dynamic as they can polymerize (growth) and depolymerize (shrink or catastrophe) at their free ends (Fig. 1C). The plus end of the MTs is more dynamic, whereas the minus-end is less dynamic. MTs can alternate between a period of polymerization and depolymerization, a phenomenon known as dynamic instability (Hawkins et al 2010).

MT nucleation takes place at MT-organizing centers (MTOCs), which in most cells is associated with the centrosomes. The direct templating mechanism is carried out by another type of tubulin, the γ -tubulin. γ -tubulin along with its interacting proteins forms the γ -tubulin complex, which is found at the MTOCs and plays an important role in the nucleation of MTs (Kollman et al 2011).

Centrosomes are composed of a pair of centrioles, a mature (mother) centriole and a daughter centriole. Each centriole consists of nine triplet MTs that form a conserved, barrel-like structure. The centrioles are embedded in a cloud of yet not fully analyzed pericentriolar material (PCM). In resting cells, the mature centriole docks to the plasma membrane and templates the outgrowth of a cilium or flagellum axoneme. This centriole is then referred to as basal body. In dividing cells centrosomes replicate during cell division and migrate to opposite poles of the nucleus to focus the two poles of the bipolar spindle, which will segregate the replicated chromosome into the daughter cells (Bettencourt-Dias & Glover 2007). Abnormal centrosome behavior can impair proper spindle formation during mitosis and meiosis thus contributing to chromosome segregation errors that cause aneuploidy

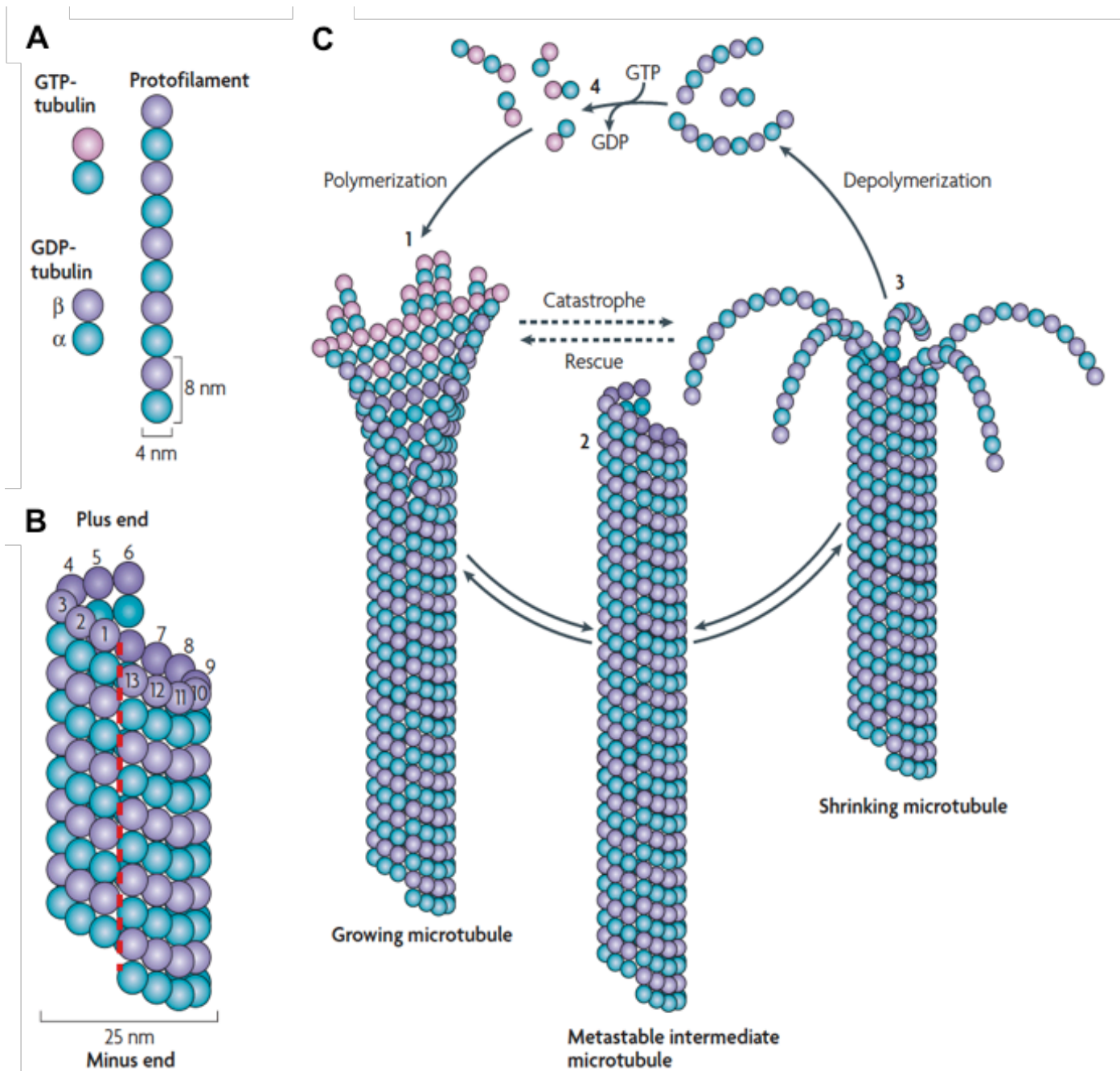


Figure 1. Structure and dynamic instability of microtubules (A) MTs are formed from α -tubulin and β -tubulin heterodimers that are arranged in a polar head-to-tail orientation to form linear protofilaments. (B) Lateral association between the protofilaments forms a cylindrical and helical MT wall, which typically comprises of 13 parallel protofilaments. (C) Assembly–polymerization and disassembly–depolymerization of MTs is carried out by the binding and hydrolysis of GTP on the β -tubulin monomer. The delay in hydrolysis of GTP allows to form a GTP-cap that promotes the growth of MTs. The polymerization–depolymerization cycle is accomplished by interchanging GDP of the disassembled subunits with GTP. (Akhmanova & Steinmetz 2008).

1.1.2 Functions of Microtubules

The internal organization of a cell, its shape and motility are controlled by the cytoskeleton. Considering that MTs are the main component of the cytoskeleton, they might have important roles on all these processes, as well as on the eukaryotic cell cycle control. Thus, MTs have highly divergence functions. In neurons, MTs are involved in the initial steps of establishing neuronal polarity. They are also important for maintaining neuronal morphology. MTs are locally challenged by MT-severing enzymes such as spastin and katanin (Lacroix et al 2010, Valenstein & Roll-Mecak 2016).

In dividing cells MTs form a dynamic structure, the bipolar spindle, responsible for the accurate segregation of the chromosomes into daughter cells. MTs are also the prominent components of the midbody, another transitory structure formed during cell division that connects the two daughter cells prior to the cytokinetic abscission. MTs are also the structural component of cilia and flagella, where they assemble into an axoneme. As there is no protein synthesis in these structures, MTs play a crucial role in facilitating the transport of protein complexes and organelles, a process known as Intraflagellar-transport (IFT).

Although MTs are structurally highly conserved, they participate in diverse functions within a cell. Such diverse functions are facilitated by the cooperation of a number of accessory proteins that mediate the interaction of MTs to other cellular components. Microtubule-associated proteins (MAPs) form a heterogeneous family of proteins, including molecular motors that convert the chemical energy of ATP hydrolysis into mechanical force, which for instance is used for the transportation of particles along axonemes in IFT.

Different functions of the MTs may require a specific set of MAPs and motors. Therefore, a cell needs to generate a large range of distinct MT population. One of the factors that can facilitate the formation of such heterogeneous MT population is post-translational modification of tubulin (PTMs) (Janke & Bulinski 2011). Most known PTMs occur on the C-

terminal tail (CTT) of the tubulin. As CTTs of the tubulin vary in terms of amino acid sequence within isotypes (Fig. 2), the presence of multiple tubulin isotypes together with the PTMs creates a very complex tubulin code that is able to specify different MT functions (Fig. 2). In the spermatogenesis chapter I will discuss the different roles of MTs in the spermatogenesis process in more detail.

1.1.3 The Tubulins: the different tubulin genes and their expression profile

The α - and β -tubulin amino acid sequences are highly conserved across all the eukaryotes. It has been demonstrated that in many species, multiple closely related genes encode α - and β -tubulins (Ludueña & Banerjee 2008). In mammals there are several tubulin isotypes, with a specific tissue expression profile (Fukushima et al 2009). The differences between the amino acid sequences of different α - and β -tubulin isotypes are subtle differences,, and most divergence is found in their CTTs (Fig. 2).

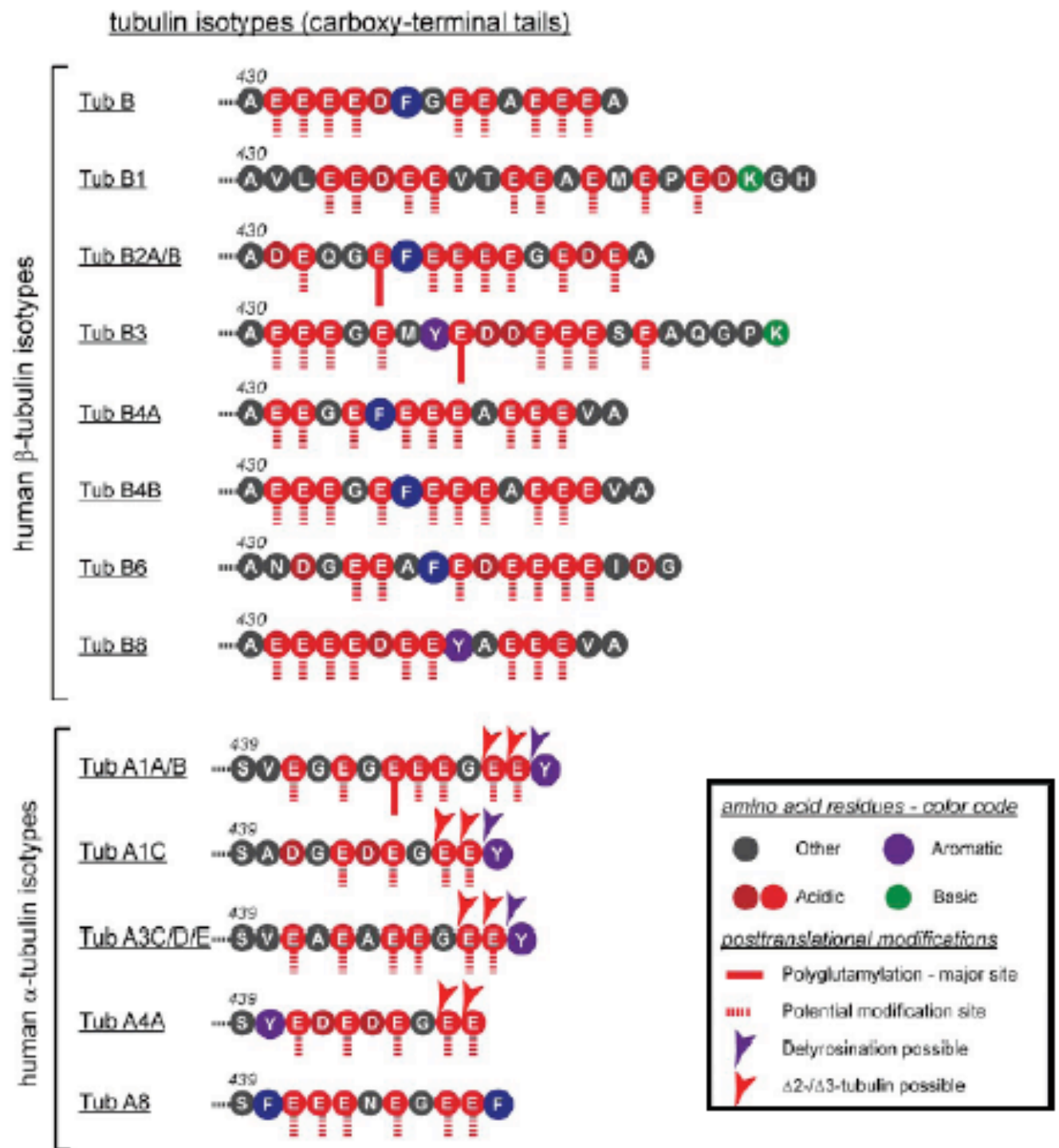


Figure 2. Heterogeneity in the C-terminal tails of tubulin isotypes and their associated PTMs.

Schematic representation of the C-terminal amino acid sequence of human alpha- and beta-tubulin isotypes. The different sites for glutamylation, detyrosination and $\Delta 2/\Delta 3$ modification are indicated. The presence of tubulin isotypes together with post-translational modification contributes to create a complex and unique identity code on MTs (from (Janke 2014))

1.1.4 Tubulin post-translational modifications

Tubulin is modified by a range of post-translational modification (PTMs) (Janke & Bulinski 2011) (Fig. 3). The first PTMs that have been discovered are the mono-modifications, such as detyrosination/tyrosination, and acetylation, $\Delta 2$ - and $\Delta 3$ -tubulin generation. In addition to the mono-modifications, another group of MT-modification, called poly-modification, have been recently discovered: polyglutamylation and polyglycylation. Mono-modifications are capable of generating a binary signal, an “on/off” mode. Poly-modifications can generate a variety of signals by regulating the length of the added side chains, thereby fine-tuning the signal (Janke & Kneussel 2010, van Dijk et al 2008b). Therefore, diversity of MT population within a cell might be a result of the differential pattern of expression of the modifying and de-modifying enzymes.

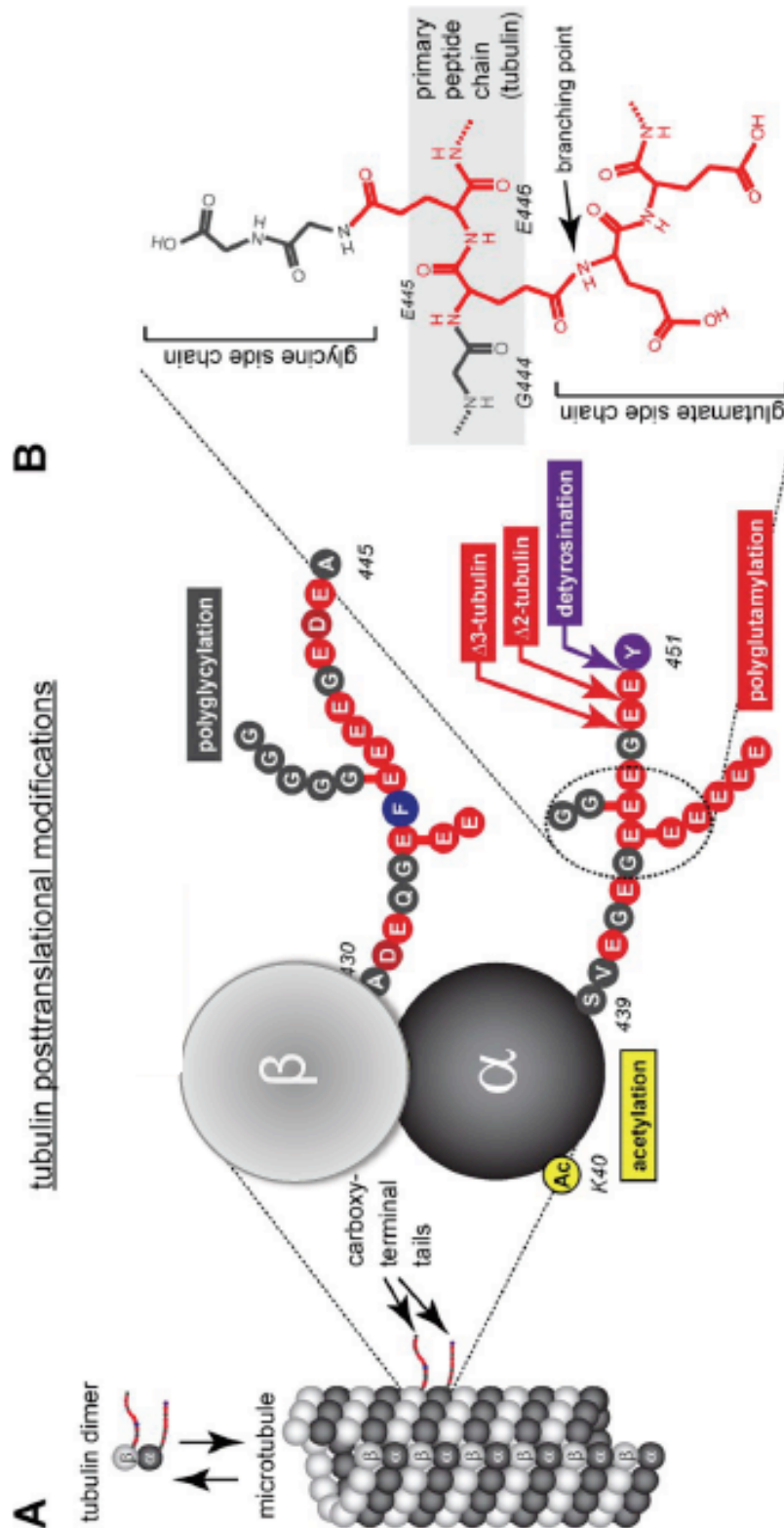


Figure 3. Differential tubulin subpopulation generated by PTMs.

(A) Schematic representation of the differential distribution of various PTMs on the α -tubulin and β -tubulin heterodimers with regards to their location in the microtubule lattice. Acetylation (Ac) is found within the tubulin, whereas other modifications such as polyglutamylation, polyglycylation, detyrosination, and C-terminal $\Delta 2$ tubulin occur on the CTT of the tubulin that are looped out from the lattice surface. (B) Chemical structure of the side chain peptide formed by either polyglutamylation or polyglycylation, using the γ -carboxyl groups of the acceptor glutamate residue has been shown. (from (Janke 2014))

1.1.4.1 Detyrosination and tyrosination

Almost all the α -tubulin genes across various species encode a C-terminal tyrosine residue (Fig. 3) that can be removed by a yet unidentified enzyme. The C-terminal tyrosine residue of α -tubulin thus undergoes cycles of detyrosination and retyrosination.

Detyrosination is a reversible reaction; the Tubulin Tyrosine Ligase enzyme (TTL) is able to catalyze tubulin tyrosination (Fig.4). The TTL enzyme is the first tubulin-modifying enzyme that has been identified and purified from porcine brain (Raybin & Flavin 1995, Schroder et al 1985). TTL modifies non-polymerized tubulin dimers exclusively, whereas the unidentified detyrosinase enzyme acts mostly on polymerized MTs, thus regulating a particular population of MTs inside the cell (Gundersen et al 1987).

Both tyrosinated and detyrosinated α -tubulin are present in most cell types. However, detyrosination was mostly found on stable and long-lived MTs in the cells such as neurons. Recently it has been shown that detyrosination protects MTs from the depolymerizing activity of Kinesin-13-type motor proteins, thus increasing MTs longevity (Peris et al 2009). From these observations, it was believed that detyrosination promotes MTs stability.

1.1.4.2 $\Delta 2$ - and $\Delta 3$ -tubulin

Once the tubulin C-terminal tyrosine residue is detyrosinated, then the penultimate C-terminal glutamate residue of the primary protein sequence can be removed to generate the so-called $\Delta 2$ -tubulin (Fig. 3, Fig. 4). $\Delta 2$ -tubulin is an irreversible modification as only presence of α -tubulin tails with two consecutive glutamate amino acids on their C termini can be retyrosinated (Prota et al 2013). The escape of $\Delta 2$ -tubulin from the tyrosination cycle is one of the reasons for the stabilization and functional specialization of MTs in the neurons, axonemes, and centrioles (Konno et al 2012). The enzymes responsible for

the generation of $\Delta 2$ -tubulin belong to the family of cytosolic carboxypeptidases (CCPs) (Fig. 4). These enzymes are also capable of generating $\Delta 3$ -tubulin (Fig. 3) (Aillaud et al 2016). So far, there have been no reports about the specific biochemical role of $\Delta 2$ -tubulin or $\Delta 3$ -tubulin in a cell. One possibility is that these modifications ensure that the tubulin is always in the detyrosinated state, however the functional importance of this process is yet unknown.

1.1.4.3 Acetylation

Tubulin acetylation was discovered in the flagellar α -tubulin of *Chlamydomonas reinhardtii* (L'Hernault & Rosenbaum 1985). This acetylation was found in the inner surface of polymerized MTs at the Lysine 40 (K40) residue (Fig. 3) of α -tubulin. This PTM is particularly enriched in sperm and cilia axonemes, as well as in neurons. Acetylation can also be found in other MT-based structures such as centrioles, mitotic spindle and midbodies. It has been shown that acetylation levels increase in several cultured cells treated with the MT-stabilizing agent Taxol, (Schulze et al 1987). As tubulin K40 acetylation appears after MT assembly and is shown to be enhanced in stable MTs, this modification is used as a marker for MT age and stability (Piperno et al 1987). However, direct interplay between tubulin K40 acetylation and MT stabilization has not yet been understood.

There are three enzymes that are capable of catalyzing tubulin K40 acetylation, the histone deacetylase family member 6 (HDAC6), the sirtuin type 2 (Sirt2) and the α -tubulin N-acetyl transferase 1 (α -TAT1). HDAC6 and Sirt2 are two enzymes that can also deacetylate substrates other than tubulin. In addition α -TAT1 acts selectively of α -tubulin K40. A recent study in the α -TAT1 knock out mouse analyzed the specific functions of α -tubulin acetylation in mammals (Kalebic et al 2013). Interestingly, the α -TAT1 knock out

mouse is viable with no major developmental defects. No phenotypes were detected in ciliated organs, although acetylation was completely abolished in these organs. However, a reduced male fertility was reported for this knock out model. No defects were found in the development of germinal stem cells into spermatozoa, suggesting that tubulin acetylation does not play an essential role in the early stages of spermatogenesis (Kalebic et al 2013) . On the other hand, slight phenotypes were detected in mature sperm, such as shortened flagellum and lower sperm motility, indicating that the α -tubulin K40 acetylation by α -TAT1 could play a role in full function of MTs in flagella.

Defects in early steps of sperm axoneme assembly are often associated with a disorganization of the 9+2 MT organization typical for motile cilia (O'Donnell 2014). However no defects in the normal axoneme organization were detected in the flagellum of the α -TAT1 knock out mouse, indicating that acetylation is not fundamental for early stages of flagellum formation (Kalebic et al 2013).

1.1.4.4 Glutamylation

Glutamylation is classified as poly-modifications. It consists in the addition, through covalent bond, of a polypeptide chain of a variable number of glutamate residues onto the γ -carboxyl group of a glutamate acceptor residue in the tubulin CTT (Fig. 3). Glutamylation was first discovered in 1990 on α -tubulin from brain tissue (Edde et al 1990), and later also detected on β -tubulin (Rüdiger et al 1992) (Alexander et al 1991) It is abundant in MTs forming axons, dendrites, mitotic spindles, midbodies, cilia and flagella axonemes, as well as basal bodies and centrosomes. After the discovery of glutamylation on tubulin, studies have shown that this modification can also occur on other proteins (van Dijk et al 2008b)

The enzymes that catalyze glutamylation are called glutamylases and belong to the Tubulin Tyrosine Ligase Like (TTLL) family (Janke et al 2005, van Dijk et al 2008b) and

have homology with the TTL enzyme that catalyzes tubulin tyrosination (Ersfeld et al 1993). In mammals, there are seven well characterized glutamylases: TTLL1, TTLL4, TTLL5, TTLL6, TTLL7, TTLL11 and TTLL13). The TTLL1, TTLL5, TTLL6, TTLL11, TTLL13 enzymes modify the α -tubulin, whereas the TTLL4, TTLL7 are specific for β -tubulin (van Dijk et al 2008b). The TTLL4, TTLL5 and TTLL7 catalyze preferentially the initiation reaction by adding the first glutamate residues of the side chain, while the others (TTLL1, TTLL6, TTLL11 and TTLL13) promote the elongation of the added side chain (van Dijk et al 2008b). TTLL9 and TTLL2 are glutamylases as well, but little is known about their substrate and reaction preferences (Fig. 5).

Several studies have described the importance of glutamylation in the regulation of cilia and flagella structure and functions (Bosch Grau et al 2013, Campbell et al 2002, Kim et al 2011, Konno et al 2016, Lee et al 2013). The role of glutamylation in sperm flagellum formation and maintenance will be discussed later in the section 1.2.4.6.

Posttranslational modifications of carboxy terminal tails

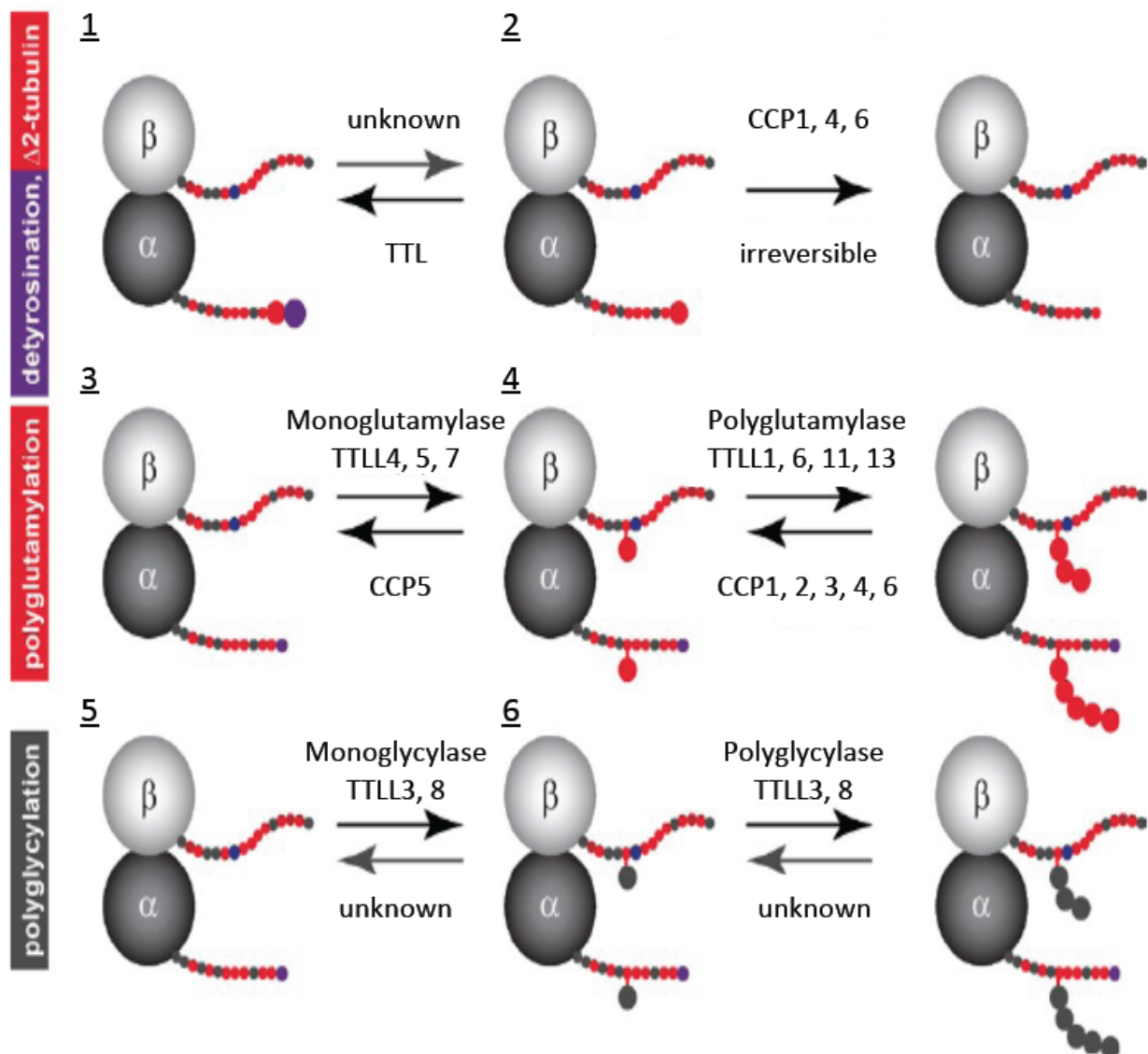


Figure 4: Enzymes involved in the generation of PTMs in the C-terminal tail of tubulin.

1) α -tubulin detyrosination is catalyzed by an unknown enzyme, whereas the Tubulin Tyrosine Ligase enzyme (TTL) catalyzes tyrosination. 2) Cytosolic carboxypeptidases-1, -4, and -6 are able to remove the penultimate C-terminal glutamate residue of the detyrosinated α -tubulin primary chain generating $\Delta 2$ tubulin. 3) The glutamylation initiation reaction is catalyzed by the Tubulin Tyrosine Ligase Like enzyme TTLL4, TTLL5 and TTLL7. The added glutamate branching point can be removed by the Cytosolic carboxypeptidase CCP5. 4) TTLL1, TTLL6, TTLL11 and TTLL13 elongate the glutamate side chain, whereas CCP1, CCP2, CCP3, CCP4 and CCP6 shorten the added glutamate side chain. 5) Monoglycylase is mediated by TTLL3 and TTLL8 whereas the elongating of the glycine side chain is catalyzed by TTLL10. (modified from (Janke 2014))

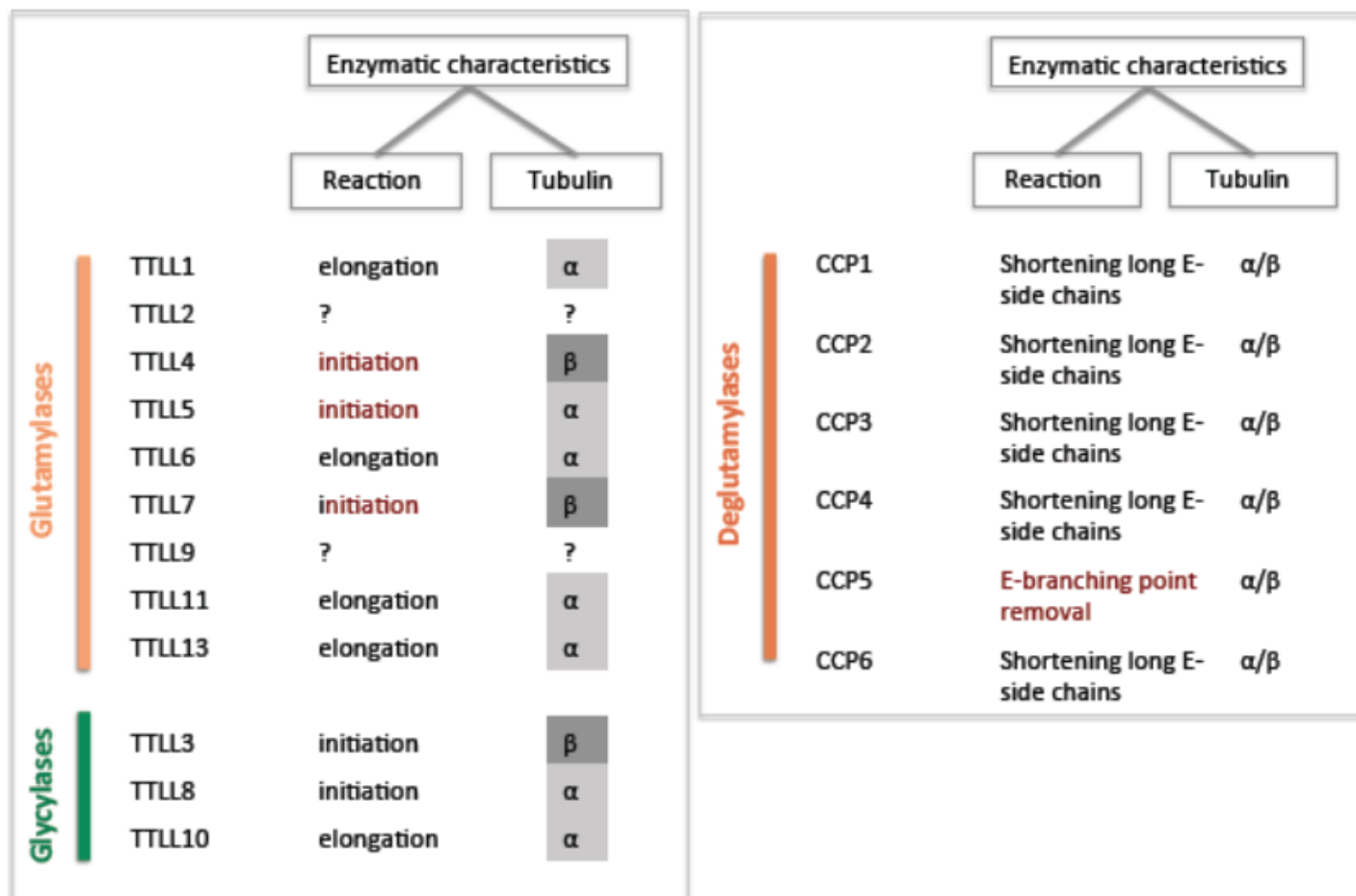


Figure 5: Reaction and substrate preference for TLLs and CCPs.

The Tubulin Tyrosine Ligase Like enzymes are divided into two groups: glutamylases and glycylases. The enzymes have their own predefined reaction preferences; they can catalyze the initiation or the elongation reaction on α - or β -tubulin. Among the CCPs, CCP5 is the only enzyme able to remove the glutamate branching point. No substrate preference has been reported for CCP enzymes.

Despite the presence of several glutamylases in certain ciliated cells and tissue, the lack of expression of a single enzyme can be sufficient to provoke a ciliary-related phenotype. For example, it has been shown that the silencing of TTLL6 on ependymal multi-ciliated cells leads to a reduced ciliary beating frequency (Bosch Grau et al 2013). Moreover, knock-out mice for certain TTLL enzymes show defective sperm flagella and male infertility (Campbell et al 2002, Handel & Dawson M. 1981, Kim et al 2011, Konno et al 2016, Lee et al 2013, Vogel et al 2010) (See section 1.2.4.6.) Thus, the TTLLs are not always redundant suggesting that they have very specific roles in a given cellular context. Interestingly, the importance of a given TTLL enzyme in a specific biological context does not always correlate with its expression levels.

Unlike detyrosination, glutamylation is a reversible reaction. The deglutamylases are members of the cytosolic carboxypeptidase (CCP) family (Kimura et al 2010, Rogowski et al 2010, Tort et al 2014) In an elegant phylogenetic work the authors tried to reconstruct the evolutionary history of CCPs. They found out that the CCP genes are conserved in most eukaryotic groups and few bacteria, and that these enzymes are only found in organisms that have cilia (Otazo et al 2013), suggesting that CCPs belong to a set of ancestral proteins with a role in building up cilia and basal bodies and their related functions. Among these enzymes CCP1, CCP2, CCP3, CCP4 and CCP6 shorten the elongated side chain acting on bond between the carboxyl group and the amino group of two consecutive glutamate residues. In contrast, CCP5 is the only deglutamylase that efficiently cleaves the γ -linked glutamate of the glutamate branching point of the side chain (Rogowski et al 2010). It has been shown that CCPs can also hydrolyze gene-encoded glutamate residues at the C-terminal tails of tubulin sequence, thus generating $\Delta 2$ - and $\Delta 3$ -tubulin (Berezniuk et al 2013, Rogowski et al 2010). The expression profile of CCPs has been studied in different murine tissues by RT-PCR. While CCP1 is highly expressed

in all the organs, other CCPs show a tissue-specific expression pattern profile (Kalinina et al 2007). Interestingly, CCP5 is less broadly expressed in the different tissues compared to others CCPs, with particularly high expression level in testis. All CCPs show a cytosolic localization, except for CCP5 that can also be detected in the nucleus (Kalinina et al 2007).

The combination of the expression of specific TTLLs together with CCPs in a given tissue allows the generation of a broad PTM pattern profile that can be tissue-specific. Thus, a fine regulation and coordination of both TTLLs and CCPs within an organ or even at a single cell level is necessary to maintain the correct PTM profile and ensure MTs functions in specific biological context.

The first studied knockout model for CCPs is the Purkinje Cell Degeneration (PCD) mouse model. This mutant is a well-known mouse model characterized by cerebellar ataxia caused by the degeneration of the cerebellar Purkinje cells (Mullen et al 1976). Interestingly, the mutation in the PCD mouse affects the *ccp1* gene (Fernandez-Gonzalez et al 2002), which is the major deglutamylase expressed in the cerebellum (Rogowski et al 2010). In 2010, a direct link between cerebellar tubulin hyperglutamylation and Purkinje-cell loss has been reported. Moreover, the re-equilibration of glutamylation levels by the silencing TTLL1, major glutamylase in the brain, rescued the degenerative phenotype (Rogowski et al 2010). Further, mutations in CCP1 have been linked to defects in the nervous system in *C. elegans*, where a remarkable hyperglutamylation of the sensory cilia is correlated with defective B-tubules of the ciliary axoneme (O'Hagan et al 2011).

Further studies have focused on understanding the function of CCP5. The biological function of this deglutamylase have been analyzed in Zebrafish embryos by RT-PCR and knockout approaches using morpholino antisense oligonucleotides (Lyons et al 2013). Although CCP5 is broadly expressed throughout the whole embryo, it is particularly strongly expressed in the olfactory placode, a part of the peripheral nervous system from

which the olfactory epithelium originates. Silencing of CCP5 causes hydrocephalus and a strong axial body curvature (Lyons et al 2013). Immunolabeling of the olfactory placode using anti-glutamylation antibody, which stains glutamylated multiple cilia, reveals an overall disorganized and atrophic tissue with tightly clustered cilia. Moreover, knocking down CCP5 causes a general hyperglutamylation in the whole embryo. Interestingly, the silencing of CCP1 leads to the same phenotypes as the ones found after morpholino treatment to CCP5, although with lower penetrance (Lyons et al 2013). However, no changes in glutamylation levels were detected in the whole CCP1-deficient embryo. This result supports the hypothesis that CCP1 share its deglutamylating function with other CCPs, whereas CCP5 is the only one able to specifically regulate the equilibrium between unmodified MTs and monoglutamylated ones. Recent studies have highlighted the importance of CCP5 in cilia formation and function in Zebrafish (Pathak et al 2014). A complete expression analysis for CCPs reveals that CCP5 is in general abundant in all ciliated tissues (Pathak et al 2014). Analyses of the beating of multicilia in the pronephron after CCP5 ablation reveals an uncoordinated beating, with single cilia paralyzed or moving independently with reduced amplitude. As it has been previously demonstrated, mutation in the Tetratricopeptide (TRP) repeat protein Fleeer/Ift70 correlates with decreased tubulin glutamylation in primary cilia and to a impaired multiciliogenesis (Pathak et al 2007). CCP5 was knocked down in the Fleeer mutant to check if it is able to rescue the ciliary phenotype by an increase in glutamylation. Cilia of *fleeer/ccp5* deficient Zebrafish larvae showed a rescued glutamylation level and multiciliated double-mutant cells were able to extend short apical multicilia (Pathak et al 2014). Altogether these studies highlight a potential role of CCP5 as a regulator on multiciliogenesis in Zebrafish.

Multiple roles for tubulin polyglutamylation in the regulation of MT functions are well documented. It is known that MAPs bind to MTs, and their interaction is in part regulated

by phosphorylation of MAPs (Drewes et al 1997). However, the binding between MTs and MAPs is highly selective with MAPs binding to a specific subgroup of MTs inside the cells. Thus, MTs may have a kind of “identity code” in order to attract and interact with a specific subset of MAPs and motors proteins. Polyglutamylation may provide this “identity code” by creating different modified MTs by the coordinated action of specific TTLLs and CCPs. Several studies have shown that MT glutamylation regulates MAP binding *in vitro*. For example, TAU, MAP2, MAP1B have a high binding affinity for MTs modified by 1 to 3 glutamate residues, while MAP1A has a preference for MTs with long glutamate side chains (Bonnet et al 2001, Boucher et al 1994). Polyglutamylation was further shown to regulate the binding affinity for several kinesin proteins *in vivo* in the mouse. The ROSA22 mouse model lacks the PGs1, a subunit of TTLL1, leading to a loss of long glutamate side chains in neuronal MTs. In these animals the alteration in MT polyglutamylation correlates with a mislocalization of kinesin motor protein KIF1A and impaired synaptic transmission in hippocampal neurons (Ikegami et al 2007, Janke et al 2005) suggesting that polyglutamylation can regulate kinesin traffic.

Glutamylation can regulate MT functions also by enhancing or inhibiting the activity of MT-severing proteins such as spastin and katanin. MT-severing enzymes sever and disassemble MTs, playing a role in several MT-based processes such as neuronal morphogenesis, cilia biogenesis/disassembly, cell migration and cell cycle regulation (Sharp & Ross 2012). Several studies demonstrate that there is a relationship between polyglutamylation levels and MT-severing activity. In mammalian cells, the presence of long glutamate side chains on MTs activates spastin and induces MTs severing (Lacroix et al 2010) regulating MTs turnover. However it has been demonstrate that although spastin activity for MT severing increases with the number of glutamate residues added to the tubulin tail, its activity decrease over a given threshold (Valenstein & Roll-Mecak 2016).

As mentioned before, glutamylases can modify substrates other than tubulin. The histone

chaperones Nucleosome Assembly Proteins-1 and -2 (NAP1 and NAP2) are two well-known substrates for glutamylation (Regnard et al 2000). However, little is known about the significance of glutamylation on these two proteins. NAP1 and NAP2 are implicated in the deposition of core histones H2A, H2B, H3 and H4 that are assembled into stable octameric units around which DNA is encircled to form a nucleosome. Recent studies on *Xenopus laevis* egg extract have shown that glutamylation of NAP1 is required for mitotic chromosome condensation and that preventing this modification alters the deposition of the linker histone 1 (H1) on mitotic chromosomes (Miller & Heald 2015). In the past decade, novel substrates for glutamylation have been described. Most of them are nucleocytoplasmic shuttling proteins, including several chromatin-binding proteins (van Dijk et al 2008a); however the biological function of glutamylation on these proteins is yet to be identified.

1.1.4.5 Glycylation

Tubulin is subjected to a second type of polymodification called glycylation. This modification was first discovered on *Paramecium* axonemal α - and β -tubulin (Redeker et al 1994). The modification consists in the addition of one or more glycine residues on a glutamate acceptor site in the CTT of tubulin by glycylation enzymes (Fig. 3). The glycylation enzymes, like glutamylases, belong to the TTLL family. In mammals three glycylation enzymes are known: TTLL3, TTLL8 and TTLL10 (Rogowski et al 2009). Deglycylation enzymes have not yet been identified. All glycylation enzymes can modify both α - and β -tubulin, although TTLL8 and TTLL10 show a preference for α -tubulin (Rogowski et al 2009) (Fig.5). The two enzymes, TTLL3 and TTLL8, first catalyze the initial transfer of a glycine onto a glutamate residue in the CTT of tubulin, while TTLL10 elongates the glycine side chains (Fig. 4). A previous

observation in human sperm reveals that the flagellum is not polyglycylated, but just monoglycylated {Marie-Hélène Bré, 1996

#150}. Indeed, TTLL10 is not active in human due to the presence of two mutations in its catalytic domain (Rogowski et al 2009), suggesting that the elongation of glycine side chains is not an essential aspect of this PTM.

Glycylation is less broadly represented PTM as compared to glutamylation and appear to be restricted mostly to cilia and flagella. Several studies carried out in different model systems correlate a malfunctioning glycylation activity with cilia and flagella biogenesis and maintenance defects. A study on mouse ependymal multicilia reveal that monoglycylation appear early during cilia maturation, whereas polyglycylation is detectable only in mature multi-cilia,. Silencing of TTLL8 in the TTLL3-knockout mouse provokes multicilia loss in the brain ependymal cells (Grau et al 2013). The expression of an inactive form of TTLL3A in Tetrahymena leads to ciliary axoneme defects such as shortened axoneme, lack of MT central pairs, and rotated peripheral doublets (Wloga et al 2009). In zebrafish, morpholino-mediated silencing of TTLL3 provokes right-left axis defects in embryos (Wloga et al 2009). Interestingly, the level of tubulin glutamylation in cilia increases upon glycylation suppression in several ciliated tissues, leading to the hypothesis that glutamylation and glycylation levels could be inversely correlated (Wloga et al 2009). Altogether, these findings suggest that glycylation is extremely important to assure a correct axonemal ultrastructure. Moreover, axonemes in mouse and Drosophila depleted of glycylation enzymes disassemble after initial assembly, suggesting that glycylation is more likely to have a role in axoneme maintenance rather than in ciliogenesis (Bosch Grau et al 2013, Rogowski et al 2009).

1.2 SPERMATOGENESIS

On an average, men produce at least 1500 sperm cells every second. Thus, a daily sperm production is about 130 million of sperm cells. However, fertilization is quite inefficient process, with only one or few sperm cells managing to penetrate the ovum and start fertilization. On top of it, the declining birth rate is becoming one of the most serious problems of our society. Indeed, 10-15% of the couples suffer of infertility, with approximately equal contribution from the two partners. Thus, understanding the possible causes of male infertility is becoming a central social issue.

Studies using knockout mouse models have recently linked many genes to spermatogenesis. Abnormal shaped head spermatozoa, which result in partial or total infertility, is one of the common feature of male sterility (Cooke & Saunders 2002) and have been observed in several knockout mice. In turn, infertility is associated with defects in flagellar assembly and/or motility causing sperm inability to pass through the female genital tract.

MTs represent a key-regulatory factor of spermatogenesis. During spermatozoa differentiation MTs participate in mechanisms involved in acrosome development, sperm head shaping and flagellum formation, mostly acting as tracks on which specific molecules move to reach their final destination. Tubulin PTMs are known to participate in the regulation of MT-based transport by influencing motor protein velocity, processivity and MT depolymerization rate (Sirajuddin et al 2014). A deeper understanding of the role of MT PTMs during spermatogenesis is now possible because of the available of novel knockout mouse models.

During my PhD, I have characterized a new mouse model for tubulin glutamylation: the

CCP5-knockout mouse. This mouse model lacks the unique deglutamylating enzyme able to remove the glutamate branching point of the added side chain, causing deregulation of the MT glutamylation level. Interestingly, CCP5-knockout males are infertile due to the abnormalities in most of the processes involved in the cyto-differentiation of spermatids into spermatozoa, a process called spermiogenesis.

Thus, the spermiogenesis phase will be further discussed focusing on the role of MTs and MT-PTM-related functions. Also, the earlier stages of spermatogenesis will be briefly introduced.

1.2.1 General aspects of spermatogenesis

In mammals, spermatogenesis takes place in the testis, the organ that is dedicated to the production of spermatozoa (Fig. 6A). A dense fibrous capsule, the tunica albuginea, surrounds and protects the highly convoluted seminiferous tubules, and covers each testis. The seminiferous tubules end in the rete testis that collects and carries spermatozoa from the testis to the head of the epididymis (Fig. 6A). The epididymal duct is composed of a head, a corpus and a tail called caput, corpus and cauda epididymis, respectively. The major function of epididymis is to accumulate, bring to complete maturation, and to store mature spermatozoa. Immature sperm cells are located in the caput, whereas mature spermatozoa fill the cauda epididymis (Knoblauch D & L. 2012). The sperm production takes place in the seminiferous epithelium (Fig. 6C) within each seminiferous tubule. In the interstitial space between the tubules are Leydig cells and vessels. Leydig cells are somatic cells producing testosterone under the regulation of the pituitary luteinizing hormone, participating in the hormonal regulation of the spermatogenic process (Walker 2011). The seminiferous tubule comprises the germ epithelium and the peritubular tissue, also called lamina propria. The peritubular tissue consists of myofibroblasts and connective tissue. The myofibroblasts generate peristaltic contractions

of the seminiferous tubule that facilitates the migration of the immotile spermatozoa to reach the rete testis.

The germinal epithelium comprises cells at different germ-cell developmental stages, namely spermatogonia, primary and secondary spermatocytes and spermatids (Fig. 6B, 6C). These cells are situated within the invaginations of epithelial cells of the seminiferous epithelium, called Sertoli cells. Tight junctions connect Sertoli cells to each other. This separates the germ epithelium into two compartments: basal and adluminal compartment (Yan et al 2008). The tight junctions between these cells also serve as the blood-testis barrier. During maturation, the germ cells progressively pass this barrier to enter the adluminal compartment where they find protection from diffusion of extraneous substances (Fig. 6C). The Sertoli cell cytoplasm extends all around the germ cells providing them a physical support and providing all required molecules and nutrients to sustain their development (Fig. 6C). At all stages of spermatogenesis, the germ cells are in close contact with the Sertoli cells through anchoring junctions and gap junctions. MTs in Sertoli cells extend along the entire longitudinal axis of the cell, showing a radial spoke like pattern in cross sections. Moreover, Sertoli cell MTs have to be highly dynamic in order to rapidly respond to changes of developing germ cells. The maintenance of the dynamics and organization of MTs seems to have an important role in assuring a physical support to germ cells, as the disruption of MTs in Sertoli cells leads to a premature exfoliation of immature germ cells from the epithelium (Smith et al 2012). Indeed, it has recently been demonstrated that the MT-severing enzyme Katanin-like protein1, which regulates MT dynamics, is important in spermatogenesis. A mutation in KATNAL1 gene causes a disruption of the MT network in Sertoli cells leading to a premature release of round spermatids from the seminiferous epithelium (Smith et al 2012).

Another well-known function of MTs in Sertoli cells is the motor protein dependent movement of spermatids through the seminiferous epithelium (Guttman et al 2000). As spermatids start to elongate, they move to invaginations in the apices of Sertoli cell cytoplasm. During spermatid development, crypts become deeper resulting in the repositioning of spermatids near the base of Sertoli cells. Towards the end of differentiation, the crypts become shallow again, so that the spermatids are moved again to the apex. A structure that plays an important role in this process is the ectoplasmic specialization, which is formed of three elements: the plasma membrane of Sertoli cells which is attached to the spermatid head, and a layer of filamentous (f-) actin attached to a layer of endoplasmic reticulum. It has been shown that the movement of spermatids together with the ectoplasmic specialization is mediated by a MT-based dynein transport, but the biological function of this translocation is still poorly understood (Guttman et al 2000).

Spermatogenesis is a cyclic process that allows a continuous production of sperm. It can be divided in 3 major phases: mitotic expansions of progenitors cells, meiotic division to form haploid cells, and the differentiation of spermatid cells into spermatozoa (Hess & Renato de Franca 2008).

The progenitor cells are named spermatogonia, and are divided into undifferentiated and differentiating one. The undifferentiated spermatogonia are the stem cells of the testis, called spermatogonial stem cells (SSC). After SSC division, it can either undergo stem cell renewal or begin the differentiation process. Those that undergo differentiation will enter a first mitotic division before entering meiosis. The cells that enter the meiotic phase are called spermatocytes. Through two meiotic divisions with a single round of DNA replication, spermatocytes will generate haploid cells, called spermatids. Finally, spermatids will be transformed into sperm cells through a complex cytodifferentiation process called spermiogenesis (Fig 6B).

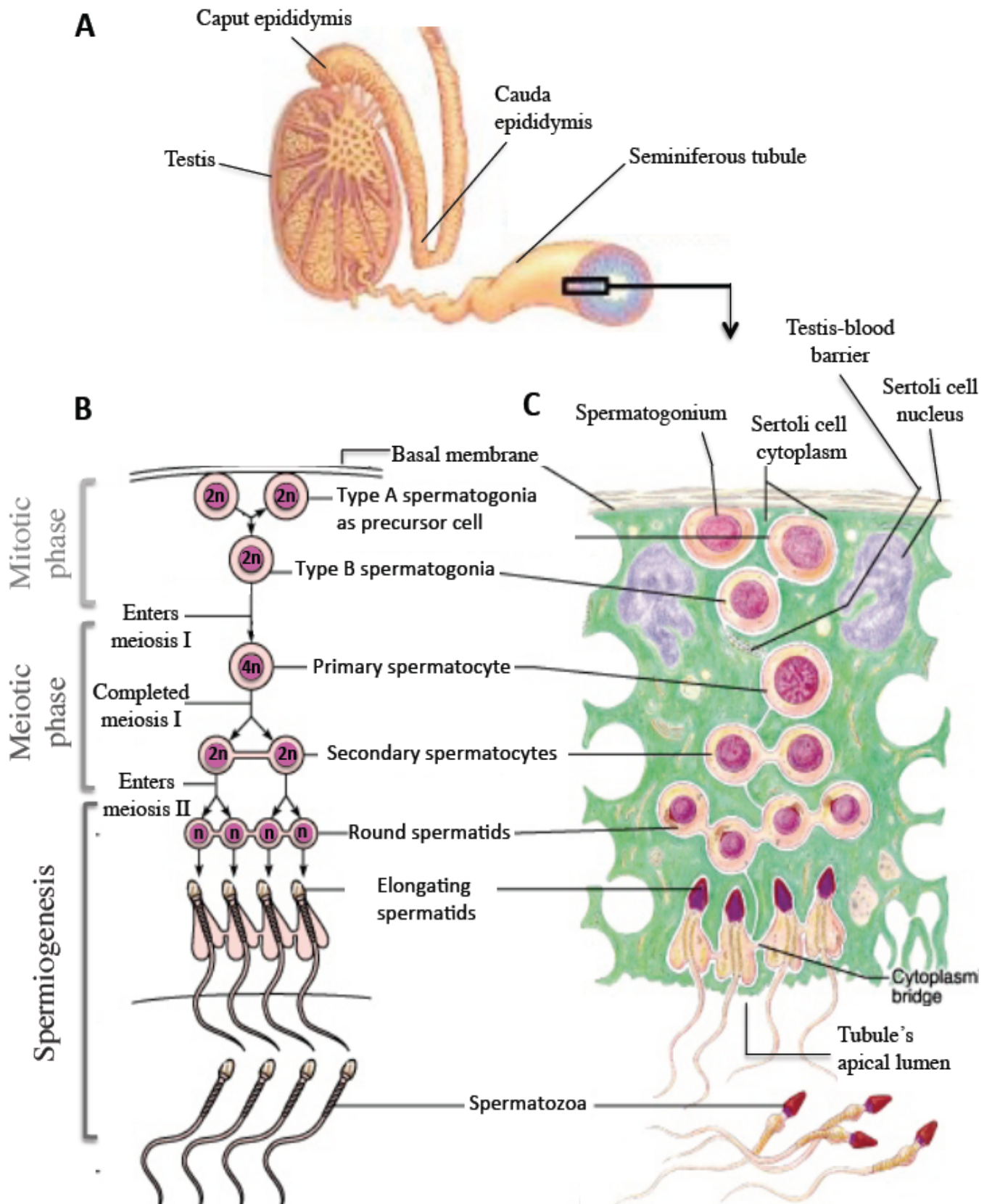


Figure 6: Schematic representation of mouse spermatogenesis. . (See figure legend at page 34)

Figure 6: Schematic representation of mouse spermatogenesis

A) Schematic diagram of a mouse testis and associated epididymis. Spermatogenesis takes place within the seminiferous epithelium of the seminiferous tubules. B) Schematic representation of male germ cell development into mature spermatozoa. Germ cell development is divided in three main phases: mitotic phase, meiotic phase and spermiogenesis. C) The seminiferous epithelium is represented. Note that each germ cell occupies a specific position accordingly to their developmental stage. Cytoplasmic bridges connect germ cells derived from the same stem cell. Adapted from: Copyright © 2001 Benjamin Cummings, an imprint of Addison Wesley Longman, Inc.

1.2.2 The mitotic phase: spermatogonial proliferation

In mice, spermatogonial proliferation lasts for approximately 9 days and consist of 9 to 11 mitotic divisions (de Rooij 2001). This first spermatogenic phase is important because it maintains both the pool of testicular stem cells and differentiating cells. Spermatogonia stem cells are also called type “A-single” spermatogonia (A_s). The cell division of A_s can either form another A_s cell, or can generate two connected type “A-paired” spermatogonia (A_{pr}). Once the A_{pr} spermatogonia are formed, the next cell divisions occur with incomplete cytokinesis giving rise to daughter cells that will be interconnected by cytoplasmic bridges until spermatogenesis is nearly complete (Fig. 6A, 6B) (de Rooij 2001). This divisions result in chains comprising of 4, 8 and 16 cells, called “A-aligned” spermatogonia (A_{al}). Then, at regular intervals, A_{al} cells are committed to transform into A_1 spermatogonia (A_1). This differentiation seems not to depend upon cell division, but is most likely due to expression of several differentiating factors by Sertoli cells and spermatogonia (de Rooij 2001). Each A_1 spermatogonia will divide 5 more times giving rise in turn to A_2 , A_3 , A_4 , Intermediate (In) and type B spermatogonia. These type B spermatogonia will enter the last mitotic division to give rise to primary spermatocytes that will enter the meiotic phase (de Rooij 2001).

During mitotic phase a correct balancing between stem cell renewal and spermatogonial differentiation has to be established. In healthy testis this ratio must be close to 1:1 because more self-renewal than differentiation would lead to an epithelium formed just by stem cells with a risk of a tumor formation. On the other hand, if differentiation prevails, then the seminiferous epithelium will end up with just the somatic Sertoli cells. One of the factors known to regulate this process is the Glial cell-derived neutrophic factor (GDNF) secreted by the Sertoli cells that will bind to its specific receptor expressed on the undifferentiated spermatogonia inducing self-renewal. Indeed, *gdnf* heterozygous mice

lose all the spermatogonial stem cells with age, whereas overexpression of the protein leads to the generation of only undifferentiating spermatogonia, leading to germ cells tumor formation in old mice (Jan et al 2012).

1.2.3 The meiotic phase: production of haploid germ cells

Meiosis is a germ-cell-specific division that involves two nuclear divisions without the duplication of DNA, giving rise to 4 haploid gametes, and resulting in germ cells with a single copy for each gene (Fig. 6B). The meiotic phase participates in the generation of a genetic diversity by promoting the shuffling of alleles. Moreover, during fertilization the male gamete combines with the female gamete, giving rise to offspring containing a mixture of genetic material from the two genitors. In mice, the whole meiotic phase lasts about 14 days (Hess & Renato de Franca 2008).

Once type-sB spermatogonia divide mitotically, pre-leptotene primary spermatocytes are formed. These cells are committed to enter the meiotic phase. First, pre-leptotene spermatocytes undergo DNA replication. After this event, the cell will enter the meiotic prophase and become a leptotene spermatocyte. The meiotic prophase is divided into 4 stages: leptotene, zygotene, pachytene and diplotene (Cooke & Saunders 2002). During leptotene, chromosomes start to condense, DNA double strand breaks are formed and recombination begins to occur. During this phase, the synaptonemal complex needed for the pairing of homologous chromosomes, starts to assemble as well. During the zygotene phase, spermatocytes are able to pass through the testis-blood barrier and go into the adluminal compartment of the epithelium (Yan et al 2008). Homologous chromosomes come together forming synapsis. Then spermatocytes enter in the pachytene phase during which DNA recombination occurs through crossing-over formation. Due to the lack of homology, the X and Y chromosome remain unsynapsed. Thus, the X and Y chromosomes form the XY-body, in which the two sexual chromosomes are marked by several proteins

that altogether cause the silencing of the two chromosomes in a process called meiotic sex chromosome inactivation (Jan et al 2012). During diplotene phase, when DNA recombination is over, synapsis are destroyed and homologous chromosomes start to separate.

The spermatocytes that go through the first meiotic prophase are tetraploid cells ($4n$), globally called primary spermatocytes (Fig 6B, 6C). Once the meiotic prophase I is over, each primary spermatocyte undergoes a first meiotic division, giving rise to two secondary spermatocytes that will be diploids ($2n$). Thereafter, a second rapid meiotic division will occur producing 4 haploid ($1n$) cells called round spermatids (Hess & Renato de Franca 2008). Those cells have a round nucleus and are devoid of cell division and protein synthesis. Interestingly, during the pachitene stage, traffic of material from the nucleus to chromatin body occurs. It has been hypothesized that this organelle serves as storage site for mRNA synthesized during meiotic prophase and will be utilized during late spermiogenesis, when RNA synthesis is over (Parvinen 1982). A meiotic checkpoint during prophase I defects if errors have occurred in homologous chromosome pairing or synapsis formation, and arrests the spermatocytes at meiotic prophase I (Jan et al 2012). Often, arrest of spermatogenesis at the stage of primary spermatocyte does not provoke massive changes in the cell morphology. However, it leads to apoptosis of the defective spermatocytes and as a consequence none or few spermatids will be produced (Holstein et al 2003).

1.2.4 Spermiogenesis: cytodifferentiation of round spermatids into spermatozoa

Spermiogenesis is the transformation of round spermatids into elongated, hydrodynamics spermatozoa that will be released into the lumen of the seminiferous tubules. Spermiogenesis can be divided in 4 main phases: the Golgi phase, the cap phase, the acrosome phase and the maturation phase (Fig 7). Round spermatids are transformed into sperm cells by partially concurrent processes; acrosome formation, centrioles migration, manchette development, flagellum assembly, nuclear condensation and reduction of the cytoplasm. Once cells are fully elongated and condensed, mature spermatids are released into the lumen of the seminiferous tubule. This process involves a specific actin-rich structure of the Sertoli cell, the ectoplasmic specialization (O'Donnell et al 2011). These different steps are described in the following sections with emphasis on the current knowledge on MT function and the role of MT PTMs during spermiogenesis. As the two major phenotypes detected in CCP5-Knockout spermatids are an unshaped head and abortive flagellum, mechanism involved in nuclear shaping and flagellum formation will be discussed in detail.

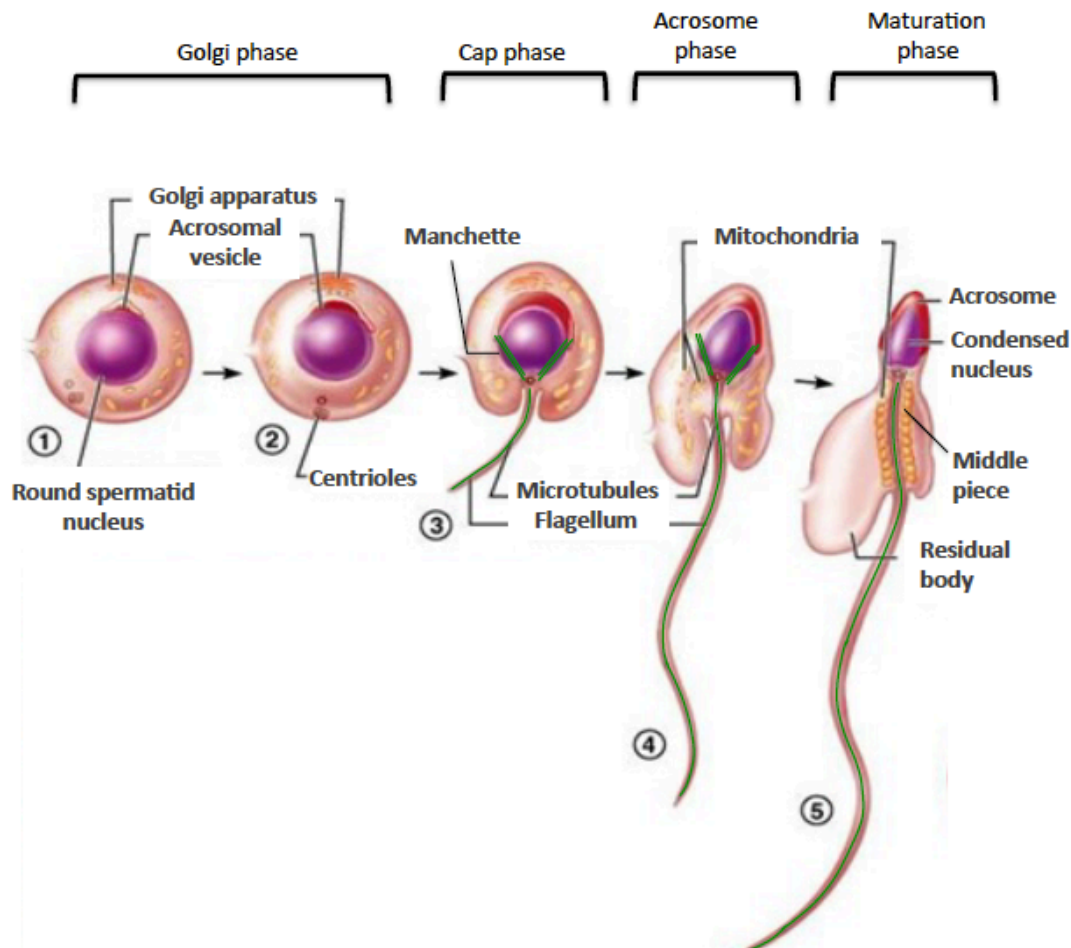


Figure 7: Schematic representation of spermiogenesis.

Spermiogenesis can be divided in 4 phases characterizes by partially concurrent processes. (1) A round spermatid is represented. During Golgi phase Golgi-derived vesicles fuse in the so-called acrosomal vesicle. (2) As acrosome biogenesis starts centrioles migrate to the opposite pole of the cell determining the polar axis of the spermatid. (3) An early elongating spermatid is represented. During the cap phase the acrosomal vesicle spread to form the acrosomal cap on the apical part of the nucleus. The Microtubule based manchette and the axoneme start to be assembled. Nucleus acquires an ovoidal shape. (4) An intermediate elongating spermatid is represented. During the acrosome phase the acrosome develops and covers two-tiers of the nucleus. Manchette moves caudally and participate in the nuclear shaping. Chromatin starts its condensation process as the histones acetylation results in replacement of histones with more basic transition proteins, and protamines. (5) During the maturation phase mitochondria align along the axoneme forming the midpiece of the flagellum. The distal centriole degenerate and the excess of the cytoplasm will be later released as residual body. At this step spermatid chromatin is fully condensed. (Figure downloaded from the web. Copyright © Benjamin Cummings, an imprint of Addison Wesley Longman. Inc.)

1.2.4.1 Acrosome, perinuclear theca and acroplaxome

One of the first events of spermiogenesis that will lead to the proper shaping of the spermatozoa is the acrosome formation. The acrosome is a Golgi-derived secretory granule, surrounded by an inner and an outer acrosomal membrane. It covers the anterior part of the spermatid nucleus and is composed of two parts: the anterior acrosome region and the posterior one, also called equatorial segment (Fig. 8). The acrosome contains hydrolytic enzymes required to penetrate the zona pellucida of the ovum during fertilization. The formation of this organelle takes place during the first of the four phases of spermiogenesis. During the Golgi phase, pre-acrosomal granules are shed from the trans-Golgi and fuse into the so-called acrosomal vesicle that associates with the nucleus. The zone of attachment defines the anterior part of the nucleus. During the cap phase, the acrosomal vesicle is enlarged by the addition of other newly synthesized acrosomal proteins from the Golgi apparatus. Thus, the acrosomic system grows and flattens over the nuclear surface forming the acrosomal cap, while the Golgi apparatus migrates to the posterior side of the cell. Then, during the acrosomal phase the nucleus start to elongate and the acrosome cap extends distally forming the equatorial segment (Fig. 7). Mutations linked to acrosome biogenesis such as acrosomal vesicles fusion or docking give rise to a formation of round sperm head, condition termed as globozoospermie (de Boer et al 2015).

It has been shown that MTs are involved in early phases of acrosome assembly (Huang & Ho 2006, Moreno et al 2006). Isolated round spermatids treated with the MT-depolymerizing agent Nocodazole show a cortical disorganized MTs network, associated with a Golgi network fragmentation and atopic acrosomal vesicle formation (Moreno et al 2006). As a consequence, the acrosome is fragmented, but still attached to the nuclear membrane. However, no acrosomal defects are detected in nocodazole-treated elongating spermatids, suggesting that MTs might only play a role in acrosome formation during the

Golgi and cap phase of spermiogenesis (Moreno et al 2006). Similar acrosomal defects are detected in colchicine-treated seminiferous tubules (Huang & Ho 2006). Furthermore, similar phenotypes were detected in round spermatid from the Abnormal Spermatozoon Head Shape (Azh) mouse model (Moreno et al 2006), in which the *hook1* gene is mutated (Mendoza-Lujambio et al 2002). Hook-family members are adaptor-like proteins involved in loading cargoes, including complexes and organelles (Liu et al 2015). The Hook1 protein is known to mediate the interaction between the Golgi apparatus and MTs (Moreno et al 2006). Interestingly a correlation between an altered MT network, defective shape and integrity of the Golgi apparatus, and acrosome fragmentation has been found in round spermatids of Azh mice (Moreno et al 2006). Altogether these results suggest that MTs play a role in acrosome formation specifically during the Golgi and cap phase of spermiogenesis.

The mechanism by which acrosomal vesicles bind to the nuclear envelope is not yet fully elucidated. The acrosome is connected to the spermatid nucleus via the perinuclear theca (PT). The PT is a detergent-insoluble capsule of cytoplasmic and nuclear proteins (Mujica et al 2003, Tovich et al 2004) that envelopes the whole spermatid nucleus, with the exception of the tail insertion zone (Okó & Sutovsky 2009). Located between the nuclear membrane and the inner acrosomal membrane (Fig. 8), the PT consists of two regions that are different in terms of localization and protein composition. The region situated between the inner acrosome membrane and the adjacent nuclear envelope is called subacrosomal layer (SAL) (Fig.8). In the caudal part of the nucleus the PT forms the post-acrosomal sheath (PAS) (Fig. 8) between the nuclear envelope and the plasma membrane of the developing spermatids. The PT seems to consist of a complex composition of proteins showing different localization pattern along the PT. Moreover, the protein composition varies between species (Okó & Maravei 1995). Investigations of the specific protein

composition and their biological functions are an emerging research field. A research group has suggested that PT biogenesis is concomitant with acrosome formation and is required for acrosome anchoring to the nucleus during bull spermatogenesis (Oko & Sutovsky 2009). It has been shown that proteins from the SAL get to their nuclear destination by coating the acrosomal vesicles during the Golgi and Cap phase of spermiogenesis (Oko & Sutovsky 2009). Interestingly, no SAL-related proteins are detected on the nuclear envelope before acrosomal vesicle-nucleus attachment, indicating that acrosome and SAL biogenesis are related processes (Oko & Sutovsky 2009).

Most of the proteins resident in the PAS, including some non-nuclear somatic histones, are transported through the manchette to their final position, and assemble in the PAS region while manchette descend caudally (Oko & Sutovsky 2009, Tovich et al 2004).

A cytoskeletal structure, the acroplaxome (Fig. 8), is important to maintain the acrosome anchored to the nucleus during its elongation (Kierszenbaum et al 2003). The acroplaxome is mainly composed of F-actin and keratin-5 intermediate filaments. It is anchored to the nuclear lamina and is bordered by a marginal ring (Fig 10). The latter is placed in a shallow circular nuclear indentation, and associated with the inner acrosomal membrane leading edge. So far, it is unclear whether acrosome biogenesis is dependent on perinuclear theca or acroplaxome formation or both (Kierszenbaum et al 2003, Oko & Sutovsky 2009). Further studies are needed to better understand the implications of these two cytoskeletal structures in acrosomal biogenesis. However, hypotonic and mild Triton X-100 treatment does not disrupt the acrosome-acroplaxome-nuclear lamina association (Kierszenbaum et al 2003), suggesting that acroplaxome may ensure the acrosome-nucleus attachment during spermatid elongation. During spermiogenesis the acroplaxome marginal ring guides the expansion of the acrosome caudally to the nucleus and acroplaxome seems to disassemble when nuclear elongation is over (Kierszenbaum et al 2003).

The acroplaxome is believed to play a role in the shaping of the spermatid nucleus by acting as a mechanical scaffold able to transmit forces to the nucleus (Fig. 10). Indeed, as spermatids start to elongate their nuclei, the acroplaxome is associated with the Sertoli cell apical ectoplasmic specialization (ES) (Lie et al 2010). The apical ES assembles as soon as spermatids polarize and become situated in apical Sertoli cell crypts. It is formed in the region juxtaposed to the elongating spermatids acrosome and is composed of a thin layer of Sertoli cell plasma membrane, a central layer of actin bundles, and endoplasmic reticulum cisternae (Vogl et al 2000). The actin hoops are proposed to exercise a clutching force on the attached spermatid and the acroplaxome is thought to transmit this force to the spermatid nucleus (Kierszenbaum et al 2003, Toshimori & Ito 2003) (Fig. 10).

Structure of mammalian sperm head

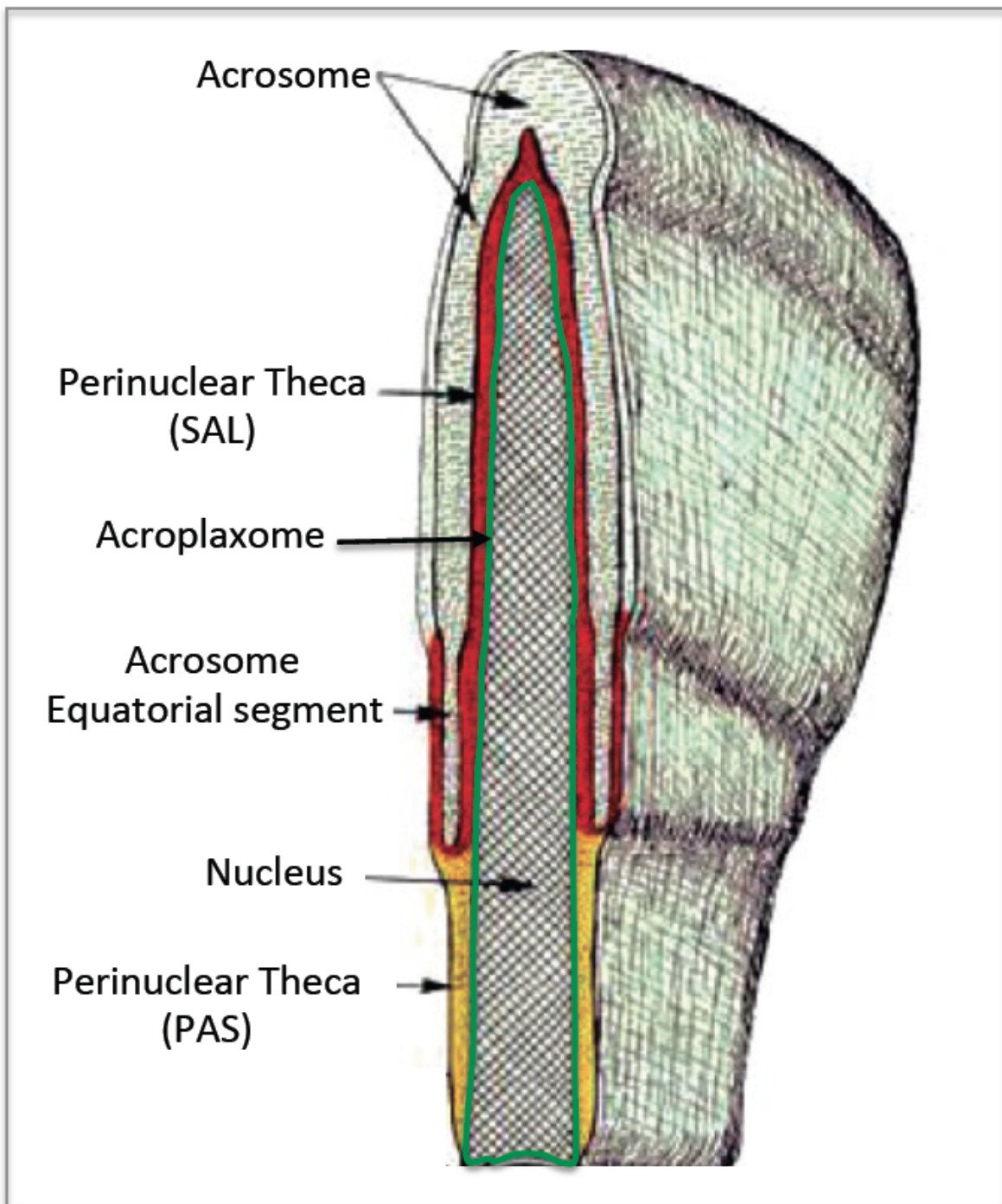


Figure 8: Schematic representation of the structural components of the mammalian sperm head. Representation of mid-sagittal section through the head of the spermatozoon. The acrosome and its equatorial segment are represented. In between the inner acrosomal membrane and the nuclear membrane is the Perinuclear Theca, composed by the Subacrosomal Layer (SAL) and the Postacrosomal Sheath (PAS). The acroplaxome is situated in between the nuclear membrane and the underlying nuclear lamina. (Figure modified from Journal of Human reproductive Sciences, downloaded from the web)

1.2.4.2 *The microtubule-based manchette*

The manchette is a MT-based structure that assembles as soon as the spermatid nucleus start to elongate, and disassembles when nuclear condensation is completed. The manchette is formed of up to 1000 MTs, bundled together by lateral interaction in a “skirt-like” fashion (Fig. 9D, Fig. 10). Manchette MTs seem to emanate from the perinuclear ring that is juxtaposed to the acroplaxome marginal ring, from which it is separated by a narrow-belt groove (Fig 9D, Fig 10). The perinuclear ring is mainly composed of δ - tubulin and keratin 9 (Hermo et al 2010a, Mochida et al 1999).

MTs run centro-distally towards the neck region and are oriented parallel to the long axis of the nucleus (Fig 9A). The emanation of the manchette MTs is currently under debate. It has been claimed the manchette MTs nucleate from the perinuclear ring (Moreno & Schatten 2000, Russell et al 1991). However, the perinuclear ring lacks γ -tubulin leading to the hypothesis that alternative MTOC proteins might exist in this structure (Lehti & Sironen 2016). Another hypothesis is that MTs are nucleated somewhere else in the cytoplasm of the germ cell and later captured by the perinuclear ring (Lehti & Sironen 2016). Indeed, short MTs are seen next to the centriolar adjunctions prior to manchette formation. The recent discovery that MTs can nucleate also from pre-existing MTs (Petry et al 2013) reinforces the hypothesis that the perinuclear ring sequesters those MTs and stabilizes them. To this day the manchette MTs have been found to be acetylated, detyrosinated as well as glutamylated (Fouquet JP. et al 1994, Hermo et al 1991, Mochida et al 1999).

Associations between the most external manchette MTs and vesicles of the endoplasmic reticulum are seen in spermatid transverse sections, caudally to the nucleus (Fig. 9C) (Fawcett et al 1971). During elongation, the manchette together with the perinuclear ring moves distally. During this movement the manchette participates in shaping the nucleus.

In mouse spermatids, showing a typical hook-like shape, the manchette appears to tilt as well as move caudally, thus creating a dorsal and ventral nuclear surface (Fig 10). This movement might be directed by the cytoplasmic dynein, that linked the most-inner manchette MTs to the nuclear envelope (Yoshida et al 1994).

Also, manchette movement seems to be affected by the activity of MT-severing enzymes (O'Donnell et al 2012). Indeed a mouse model lacking the regulatory subunit p80 of the MT-severing enzyme katanin develops a defective manchette (O'Donnell et al 2012). In this mouse model, the manchette fails to move caudally, but the progressive constriction of the perinuclear ring is unaltered leading to spermatids with an extra-long manchette with a longer and thin nucleus with a bulb shape in its apical part.

The hypothesis that manchette is implicated in shaping of spermatid nuclei is supported by the studies of several KO mice, in which an impaired manchette formation is correlated with a weird nuclear shape. The *azh* mutant mouse is characterized by spermatids with a nucleus that is long and enlarged in its apical portion and tapered in the posterior region (Mochida et al 1999). Mutant manchettes have a thinner, extra-long and conical shape compared to wild type ones that are shorter and cylindrical. In the *azh* mutant the *hook1* gene is mutated (Mendoza-Lujambio et al 2002). The Hook1 protein is believed to link manchette MTs to the nuclear envelope (Mendoza-Lujambio et al 2002). Hook1 co-localizes with the manchette and the perinuclear ring in wild type spermatids, and its localization follows a specific pattern during spermiogenesis. The loss of Hook1 leads to the disruption of the interaction between the manchette and the nuclear envelope, provoking an abnormal positioning of MTs within the manchette, and resulting in an abnormal shaped head (Mendoza-Lujambio et al 2002, Mochida et al 1999). Moreover, the *azh* mutant presents a bent and coiled mid-piece (Mochida et al 1999), characterized by a discontinuous mitochondrial sheath and accumulation of electron-dense material. Thus it suggests that the absence of Hook1 in the *azh* mouse lead to abnormal accumulation or

dislocation of material essential for the axonemal mid-piece assembly (Mendoza-Lujambio et al 2002). Another protein important for manchette function is the MT plus-end-tracking protein CLIP-170, a MAP that is known as a positive regulator of MTs growth that regulates the localization of dynactin complex to MTs plus ends (Akhmanova et al 2005). In wild type spermatids CLIP-170 localizes to the manchette and centrosome, and it has been hypothesized that the protein stabilizes the manchette MTs (Akhmanova et al 2005). CLIP-170 KO mice produce spermatozoa with a misshaped head due to formation of asymmetrical or mislocalized manchette and reduced cross-bridges between manchette MTs (Akhmanova et al 2005). Another protein that regulates manchette formation and function is E-MAP-115, also called MAP 7. This is a retinoic-acid-inducible gene encoding for a MAP involved in MTs stability. The ROSA 63 mice, in which the *E-MAP-115* gene has been mutated, are characterized by spermatids showing a detached or mislocalized manchette. Condensed mutant spermatids are characterized by highly unshaped nuclei and are phagocytized by Sertoli cells (Komada et al 2000). Interestingly, cross-sections of seminiferous tubules from 1 year-old mouse show tubules with just epithelial cells due to a progressive loss of all germ cells. The Sertoli cells of the mutant mouse show less MT bundles compared to the wild type, suggesting a potential role for E-MAP-115 in the regulation of the Sertoli cell cytoskeleton (Komada et al 2000). Nevertheless many agents that interfere with MTs dynamics have been shown to induce manchette abnormalities (Nakai et al 1997, Russell et al 1991). Testis administration of the MT-stabilizing agent Taxol is associated with the presence of manchette located at the caudal region of the spermatids nucleus and deeper indented into it (Russell et al 1991), causing nuclear invaginations. A similar phenotype was also observed in spermatids from testis treated with low dose of Carbendazim (Nakai et al 1997), a compound shown to be an effective inhibitor of MTs polymerization and depolymerization (Winder et al 2001). Altogether these data demonstrate how changes in MT stability and/or mutation in MAPs interfere with a

regular manchette assembly and positioning, that in turn cause defects in nuclear shaping
{(Komada et al 2000);Akhmanova, 2005 #316;Mendoza-Lujambio, 2002 #315;Mochida,
1999 #242;Russell, 1991 #381;Nakai, 1997 #382}.

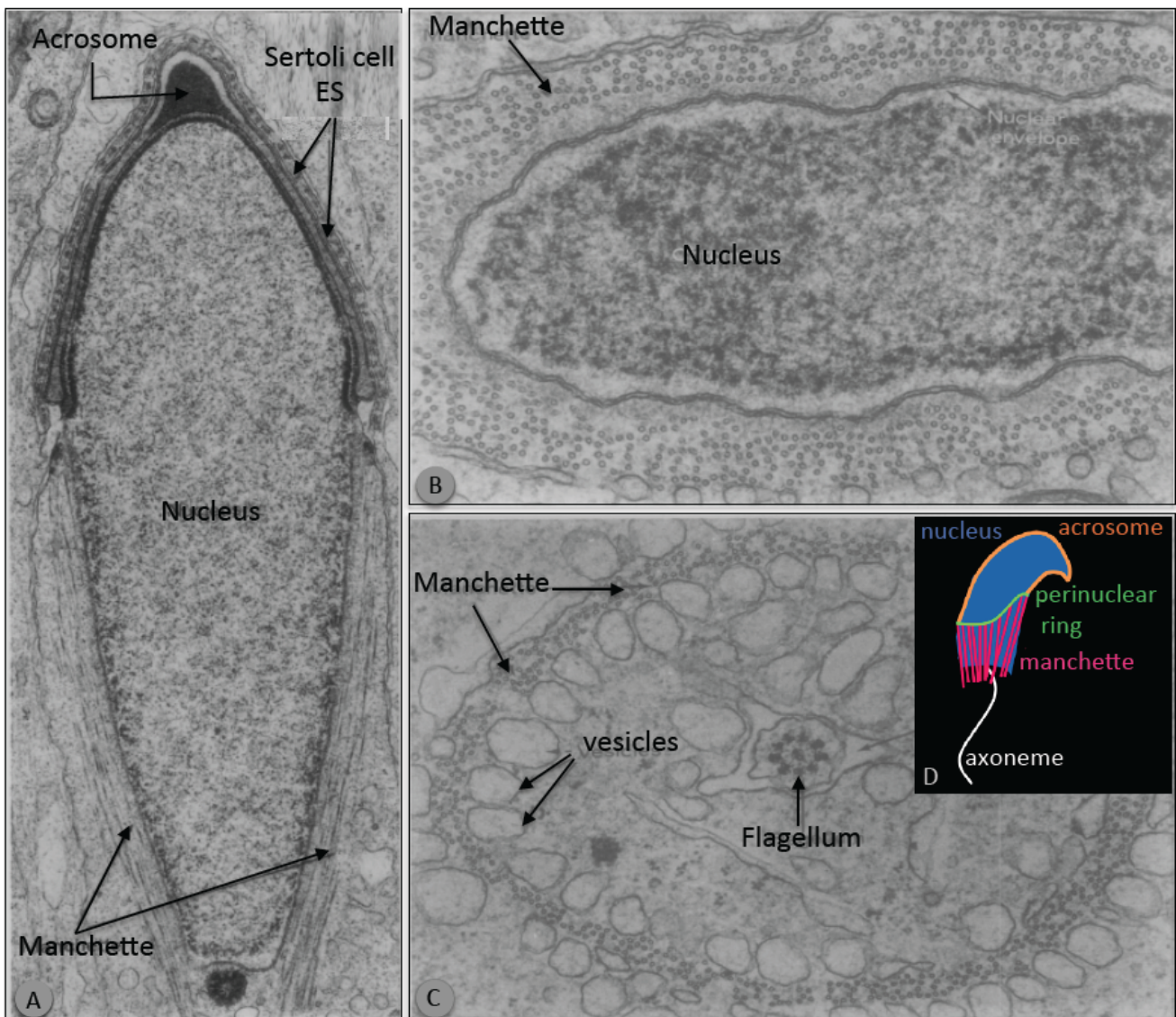


Figure 9: Ultrastructure of mammalian spermatid manchette

A) Sagittal section of an intermediate elongating rat spermatid visualized by electron microscopy. The acrosome covers the apical part of the nucleus. The Sertoli cell ectoplasmic specialization (ES) is represented. Microtubules of the developing manchette are tangential to the caudal half of the nucleus and converge to the flagellum. (Figure from Fawcett et al 1971a) B) Electron microscopy cross-section of the apical part of a hamster spermatid head. Manchette MTs appear to be uniformly spaced and organized. Manchette is symmetrically distributed around the nucleus. (Figure from Fawcett et al 1971a) C) Electron microscopy cross-section of the post-nuclear region of a hamster spermatid. Manchette MTs surrounding the flagellum are shown. Note that at their caudal position manchette MTs are associated with endoplasmic reticulum-derived vesicles. (Figure from Fawcett et al 1971a) D) Schematic representation of mouse spermatid head. Acrosome is represented in orange, the perinuclear ring is in green, manchette MTs are drawn in magenta whereas axoneme is in white. Nucleus is represented in blue. (Fawcett et al 1971, Jaworski et al 2008)

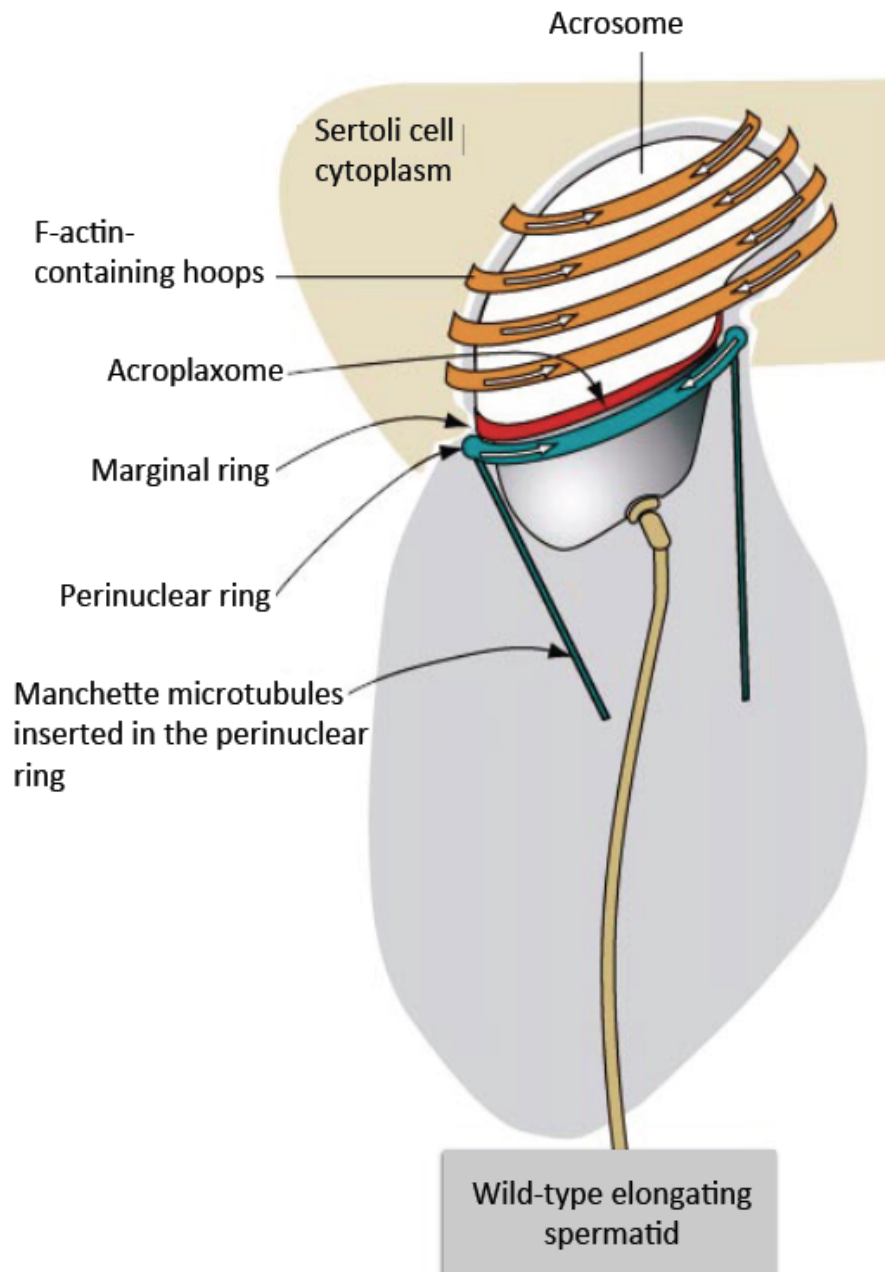


Figure 10. Subcellular structures involved in the shaping of the spermatid head

The acrosome is intimately in contact with the nucleus, which is ensured by underlying acroplaxome formed by a cytoskeletal plate and a marginal ring. F-actin-containing hoops, derived from the adjacent Sertoli cell, embrace the apical region of the elongating spermatid nucleus. At the caudal pole of the acrosome is the perinuclear ring from which MTs forming the manchette seems to emanate. During nuclear shaping and elongation, the perinuclear ring diminished its diameter and together with the manchette move caudally to elongate the nucleus. In the mean time the F-actin containing hoops from the adjacent Sertoli cell are believed to play a mechanical clutching forces that are transmitted to the nucleus via the stress-resistant acroplaxome. (Kierszenbaum & Tres 2004)

1.2.4.3 Spermatid nuclear condensation

Chromatin reorganization along with acroplaxome and manchette development (Kierszenbaum et al 2003, Kierszenbaum & Tres 2004), is contributing to spermatid nuclear shaping process. During mid-spermiogenesis, when manchette is formed, sperm chromatin undergoes an extensive reorganization starting from nucleosome-based structures to protamines based structures. The replacement of the canonical histones is mediated by testis-specific histones followed by transition proteins and protamines. The whole transition takes about 5 days in mice.

During mammalian spermiogenesis, round spermatids are highly transcriptionally active, but during spermatid elongation the transcriptional activity slowly reduces and is no more detected in late condensed spermatids. Thus, mRNA encoding transition proteins and protamines are synthesized early during spermiogenesis in round spermatids and stored in a transcriptionally repressed state.

Histone hyperacetylation appears to be a regulatory signal for chromatin remodeling (Rathke et al 2014). Histone H4 acetylation in elongating spermatids may cause an open chromatin structure that facilitates and induces histones removal. In mammals histones are not replaced directly by protamines. Transition proteins (TNP1 and TNP2) are basic nuclear proteins that are seen when histones are displaced and chromatin starts to elongate. The two proteins seems to have a redundant role as both TNP1- or TNP2-KO mice are fertile, although showing minor spermiogenesis defects (Sassone-Corsi 2002). In contrast concomitant TNP1 and TNP2 ablation causes infertility (Jan et al 2012). The displacement of transition protein is in turn regulated by their phosphorylation status (Sassone-Corsi 2002).

Protamines are arginine- and cysteine-rich proteins that constitute the most abundant chromatin component of mature sperm (Rathke et al 2014). The level of arginine mediates a strong DNA binding, whereas cysteines facilitate intra-protamine disulfide bonds, thus

contributing to the formation of a highly compacted chromatin. Most of mammalian species have only one type of protamine, whereas in human and mouse sperm two families of protamines have been found: protamine 1 and protamine 2 encoded by the *prm-1* and-2 genes. In mice, both types of protamines are essential for male fertility as even the deletion of a single copy of either *prm1* or *prm2* leads to infertility (Rathke et al 2014). It is known that protamines are highly phosphorylated just prior their binding to DNA leading to the hypothesis that protamine phosphorylation might regulates protamine-DNA binding (Oliva 2006).

Various hypotheses explain the functional significance of this specialized condensed chromatin structure. The condensation of sperm chromatin may help to the generation of a highly hydrodynamic shape and it may protect the paternal genome from physical and mechanical stress (Rathke et al 2014).

1.2.4.4 Sperm tail formation, structure and functions

Another MT-based structure that assembles early during the post-meiotic phase is the flagellum. Four main regions compose the sperm tail: the connecting piece (also called neck region), the midpiece, the principal- and the distal piece (Fig. 13A).

1.2.4.4.1 Axoneme structure and development

The core structure of the flagellum is called axoneme and is composed of nine outer MT doublets surrounding a MT central pair in a 9+2 conformation (Fawcett 1975) (Fig. 11). The MT-based axoneme has a very conserved structure that is also found in other motile cilia (Ishikawa & Marshall 2011). However, the sperm flagellum is structurally different from motile cilia because of the presence of peri-axonemal proteins that organize along the axoneme to form sperm-specific flagellar structures, such as the outer dense fibers (ODF), the mitochondria- and the fibrous sheaths (Fawcett 1975).

The outer MT doublets that assemble into the sperm axoneme are composed of a complete A-tubule made by 13 protofilaments and an incomplete B-tubule formed of 10 protofilaments (Hermo et al 2010b) (Fig. 11). The A-tubule anchors an inner- and an outer-dynein arm (Fig. 11), that project towards the adjacent doublet of the axoneme (Fawcett 1975). Each doublet is connected with the next ones by two elastic structures called nexin links that project from the A-tubule (Fig. 11). Finally, a radial spoke connects the MT doublet with the microtubules central pair. The central microtubules are called C1 and C2 (Fig. 11) and are connected to each other along their length by regularly spaced bridges (Fawcett 1975). The dynein motors on the A-tubules use ATP hydrolysis (Hermo et al 2010b) to generate forces to promote an antiparallel sliding of MT doublets relative to each other, producing the waveform required for sperm motility (Fawcett 1975).

The assembly of the flagellum starts in round spermatids. Soon after the acrosome biogenesis at the apical side of the cell, the paired centrioles migrate to the opposite pole,

where they initiate the formation of the axoneme (O'Donnell & O'Bryan 2014). Centrosomes are composed of a pair of barrel-shaped centrioles, which are built of nine triplets of MTs each (Hoyer-Fender 2010). During cell division, centrosomes ensure the proper orientation of mitotic spindles for alignment, duplication and segregation of chromosomes between daughter cells. When cells grow cilia or flagella, centrosomes migrate to the cell periphery, where distal centrioles dock to the cell membrane to become basal bodies, from which the axonemes are assembled (Bornens 2012). The spermatid centrosome is formed by a distal and a proximal centriole surrounded by pericentriolar material. The distal centriole is perpendicular to the cell surface, whereas the proximal centriole is oriented perpendicular to the long axis of the cell (Fawcett & Phillips 1969, Zamboni & Stefanini 1971) (Fig. 7). As round spermatids are non-cycling cells the centrosome undergo a functional shift (Chemes 2012), and the axoneme starts to be formed on the distal centriole that is now called basal body (Hermo et al 2010b). Thus, a new axoneme is assembled on round spermatids using centriolar MTs as template for axonemal MT nucleation. Once the axoneme is assembled the distal basal body-flagellum complex docks to the nuclear envelope in a concave invagination called implantation fossa (Fig. 12). Prior to nuclear docking the basal body links to the cell membrane via its distal and sub-distal appendages formation (O'Donnell & O'Bryan 2014, Tanos et al 2013). Following the initial assembly of the axoneme, secondary structures are added through the elongation phase to form the sperm tail mid-, principal- and distal-piece.

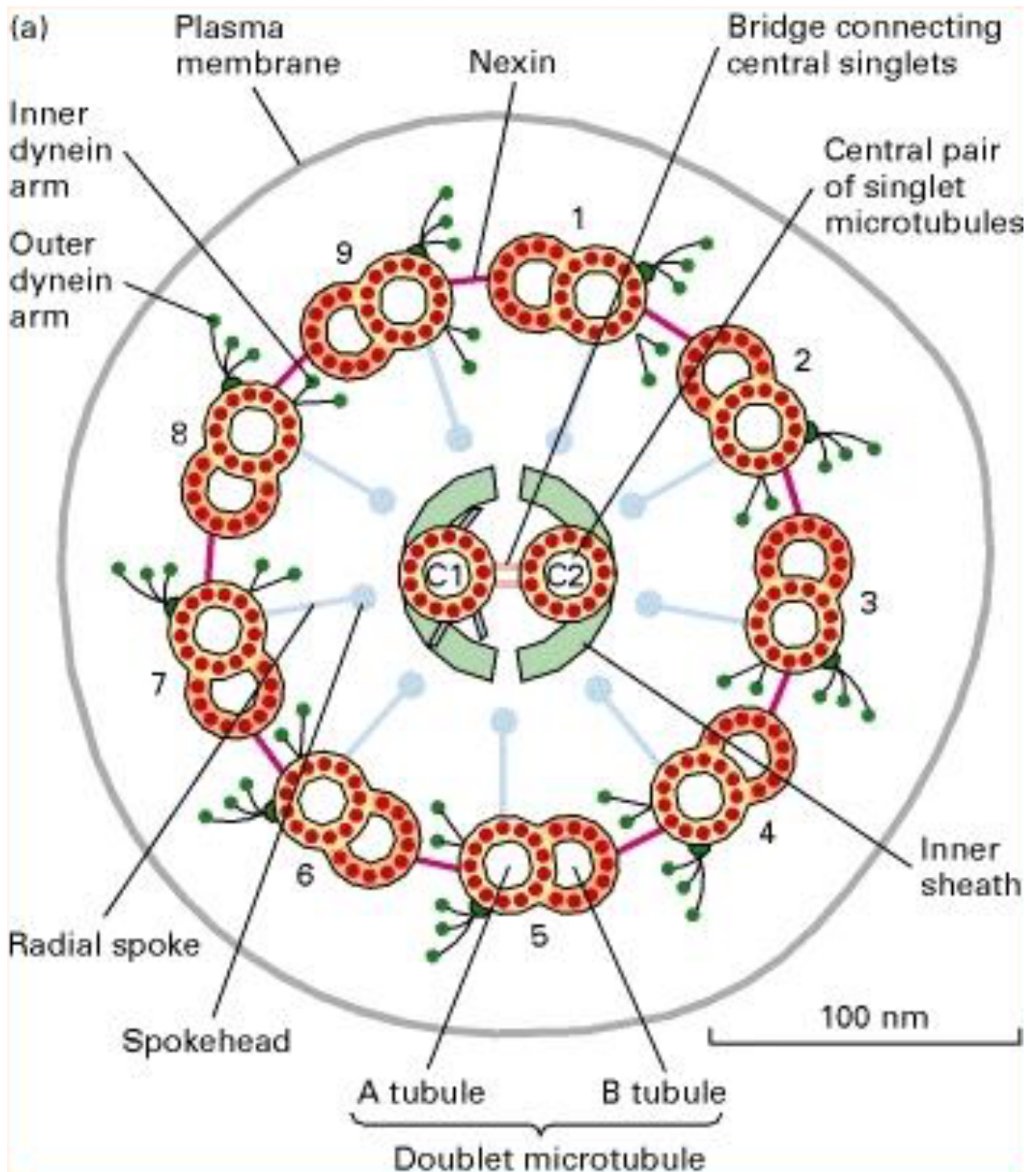


Figure 11: Cross section representation of the sperm central axoneme

The axoneme is formed by nine outer MTs doublets surrounding a MTs central pair (C1+C2). Each doublet is formed by a complete A tubule and an incomplete B tubule. Inner and outer dynein arms project from the A tubule. A Nexin link connects each outer MT with the adjacent one of the next doublet. Radial spokes connect the outer MTs doublets with the MTs central pair. Figure downloaded from <http://kc.njnu.edu.cn/>

1.2.4.4.2 The connecting piece

Early during sperm axoneme formation the PCM together with centrioles undergo complex morphological modifications, giving rise to the neck region of the future spermatozoa (Fig. 12). Briefly, proteins organize in nine longitudinal striated columns and the capitulum of the connecting piece (Fawcett & Phillips 1969, Zamboni & Stefanini 1971). Both, distal and proximal centrioles are believed to participate in the formation of those two structures (Hoyer-Fender 2012). The proximal centriole organizes the capitulum (Fig. 12), which will later be in contact with the implantation fossa, whereas both distal and proximal centrioles are involved in assembly of the striated columns. The striated columns are nine cylindrical structures (Fig. 12) that fuse cranially to form the capitulum, and are caudally connected to the 9 ODFs. The capitulum is in turn associated with a dense structure lining the outer nuclear membrane at the implantation fossa, called basal plate (Fig. 12) (Fawcett & Phillips 1969, Zamboni & Stefanini 1971). The association between striated columns, capitulum and basal plate is believed to maintain the flagellum linked to the spermatid head (Fawcett 1975). In most mammals, including humans, only the distal centriole disintegrates after axonemal assembly (Hoyer-Fender 2012). Thus, the proximal centriole is paternally inherited during fertilization (Manandhar et al 2000). However, in rodents centrosomes are exclusively maternally inherited, as both male centrioles degenerate during spermiogenesis. The first centriole is lost in the testicular phase, whereas the second one is degraded during sperm storage in the epididymis (Manandhar et al 1998). Thus, after fertilization the ovum will transmit both centrioles to the zygote.

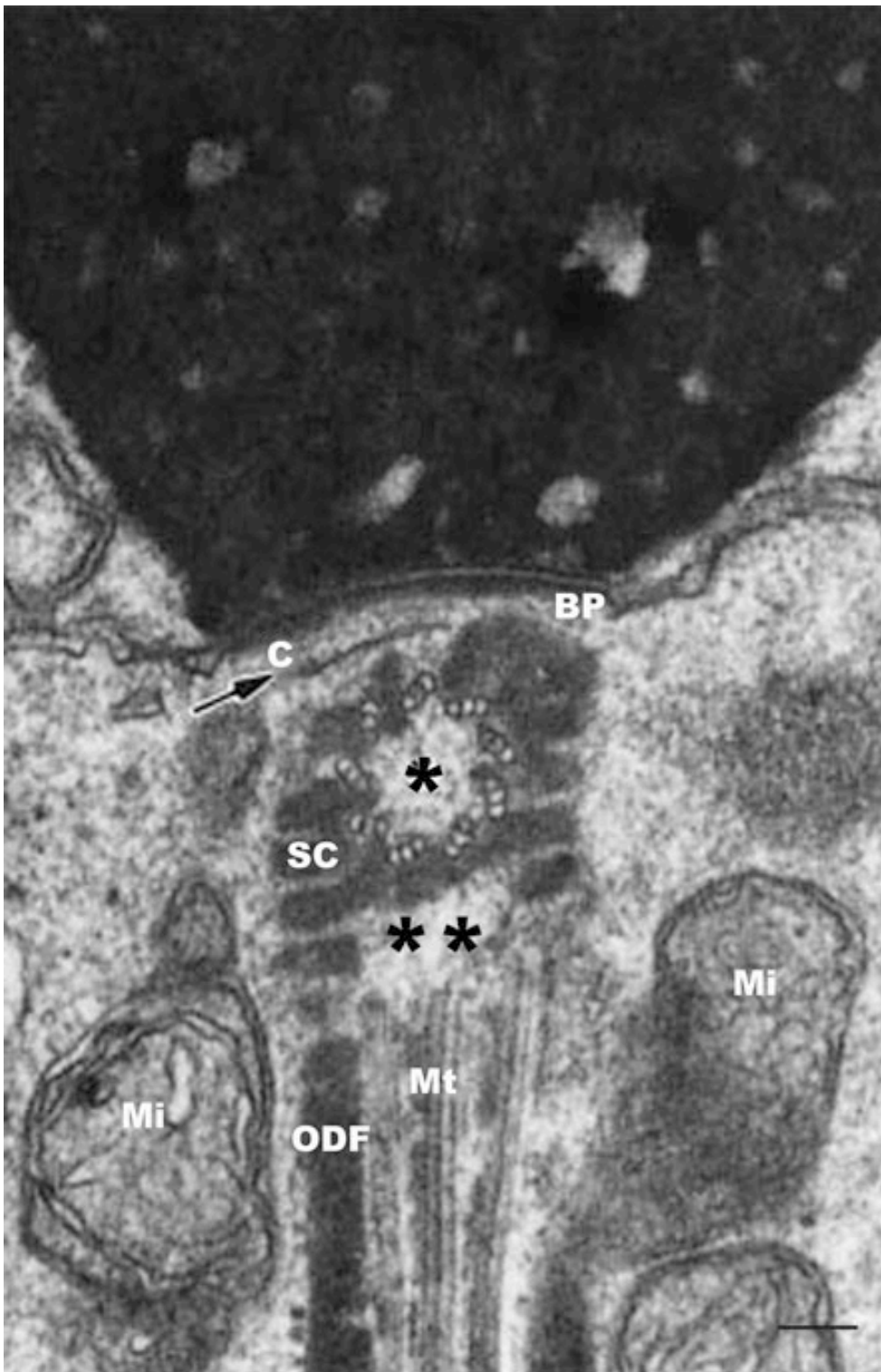


Figure 12: Electron micrograph of sperm connecting piece

The proximal centriole (*) is enclosed cranially by the capitulum (C) and the basal plate (BP) lining the implantation fossa on the spermatid nucleus. Proximal and distal (**) centrioles give rise to the striate columns (SC) that fuse caudally with the outer dense fibers (ODF) of the midpiece. Axonemal microtubules (MT) end cranially in the region occupied by the distal centriole from which they originate. MI is mitochondria. Scale bar is 0.1 μm . (Figure from (Chemes 2012))

1.2.4.4.3 The midpiece

The first section of the flagellum tail proximal to the connecting piece is the midpiece (Fig.13A, 13B), where ODFs and mitochondria sheath organize around the central axoneme. Nine ODFs arrange longitudinally to form a cylinder that encloses the central axoneme. The fibers are cranially fused with the striated columns of the neck region and extend in the principal piece (Fawcett 1975, Hermo et al 2010b). At the annulus, a sperm structure that marks the delimitation between mid-piece and principal piece, two of the nine ODFs terminate and are replaced by the two longitudinal columns of the fibrous sheath (Petersen et al 2002). Each ODF is associated with a specific MT doublet and is distinguishable in cross sections because of its proper size and morphology (Fig. 13B). The outer dense fibers are rich in intermediate filaments-like and keratin-like proteins (Petersen et al 2002), and are believed to impact rigidity to the flagellum to overcome shear forces during epididymal transit, ejaculation and in the female reproductive tract (O'Donnell 2014). This hypothesis is reinforced by the observation that ODFs are found to be components of sperm flagella only in organisms with external fertilization (Petersen et al 2002). Despite the fact that ODFs are conserved among organisms, a deep understanding of their protein composition and function is yet to be achieved (Petersen et al 1999). To date only few ODF proteins are known: ODF1, ODF2 and ODF3 (Inaba 2011). Sperm-associated antigens (SPAGs) are chaperone-like proteins known to drive ODF proteins to their final destination (Kierszenbaum 2002b).

The ODF-based cylinder is enclosed by a discontinuous helix of individual elongated mitochondria that extends from the connecting piece to the annulus, forming the mitochondria sheath (Fig. 13A, 13B) (Fawcett 1975). The main role of the mitochondria sheath is to provide ATP molecules needed to promote sperm motility. Little is known about the mechanism leading to mitochondria alignment around the ODF in the midpiece (Zhang et al 2012). The Kinesin light chain 3 (KLC3), a component of the kinesin-1 motor

protein, has been shown to link mitochondria and outer dense fibers. Interestingly, the association of KLC3 with mitochondria in rat spermatid coincides with the mid-piece formation step (Zhang et al 2012). In round spermatids, mitochondria are located near the cell membrane and are retained in place most probably by the mitochondrial-binding Kinesin KIF1B (Zhang et al 2012). At the moment of midpiece assembly, KLC3 could dislodge mitochondria from KIF1B and mediate the translocation of mitochondria toward the center of the cell most probably via cytoplasmic dynein association (Martin et al 1999). Once the KLC3-associated mitochondria have moved to the midpiece region, KLC3 is believed to function as a scaffold protein that links together ODFs and mitochondria, thus ensuring mid-piece integrity (Zhang et al 2012). This model is supported by the analysis of a mouse mutant expressing a defective KLC3 protein, able to bind mitochondria but not ODFs. Mutant spermatozoa present sperm motility defects, as well as defects in mid-piece assembly and mitochondria organization (Zhang et al 2012).

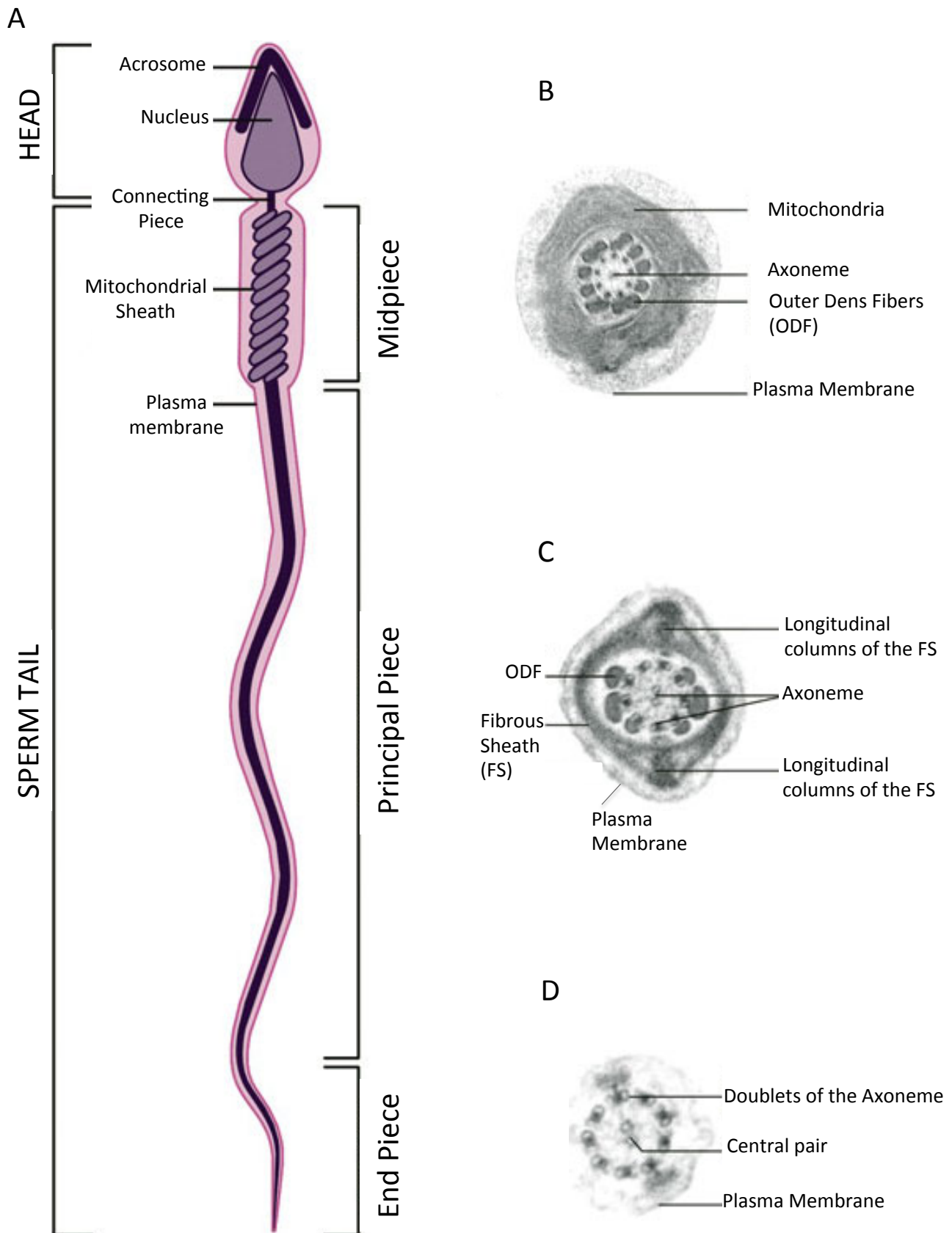


Figure 13: Architecture of mammalian sperm flagellum. (See figure legend at page 61)

Figure 13: Architecture of mammalian sperm flagellum.

A) Schematic representation of mouse sperm flagellum. The sperm head is composed by a nucleus capped by the acrosome. The sperm flagellum is composed of four elements. The connecting piece that anchors the flagellum to the sperm head, the midpiece in which the mitochondria sheath is formed, the principal piece and the distal piece. B) Electron microscopy cross-section of flagellum midpiece. C) Electron micrograph of principal piece cross section. Note that the two longitudinal columns of the fibrous sheath replace two of the nine ODFs. D) Electron microscopy cross-section of the distal piece of the flagellum. No sperm accessory structures are present in this region. (Figure modified from: <https://embryology.med.unsw.edu.au>)

1.2.4.4 The principal and distal piece

Following the midpiece is the principal piece of the flagellum, which in humans is ten times longer than the midpiece (Hermo et al 2010b). In the principal piece (Fig. 13A), a fibrous sheath replaces the mitochondria sheath. The fibrous sheath is placed between the flagellar plasma membrane and the ODFs. It is composed of two longitudinal columns that replace two of the nine ODFs (Hermo et al 2010b) becoming associated with the outer MTs doublet n°3 and n°8 (Fig. 13C) (Eddy et al 2003). Circumferential ribs connect the two columns. The fibrous sheath assembles from the distal end of the flagellum, whereas the ODFs are known to assemble in a postero-distal direction indicating that at least two different transport mechanisms regulate ODFs and fibrous sheath formation (Lehti & Sironen 2016). The fibrous sheath is important to confer rigidity to the flagellum, and is believed to regulate the plane and shape of the flagellar beat (Eddy et al 2003). It acts as a scaffold for glycolytic enzymes, thus appearing to be important as well for ATP production. The fibrous sheath is also the docking site for key components in signal transduction pathway regulating sperm functions (Eddy et al 2003). In spermatozoa phosphorylation of proteins through c-AMP mediated Protein Kinase A (PKA) activation is known to regulate sperm motility (Hermo et al 2010b). Interestingly, the majority of protein components of the fibrous sheath belong to the Protein Kinase A Anchoring Protein family (AKAPs). AKAP proteins are known to bind PKA thus participating in the PKA-mediated phosphorylation of proteins leading to sperm motility regulation (Hermo et al 2010b).

At the level of the end piece, the flagellum is formed by the MT-based axoneme surrounded by the plasma membrane. No ODF and fibrous sheath are founded in this region of the flagellum (Fig. 13D).

1.2.4.5 Importance of intraflagellar and intramanchette based transport in spermatid development

During flagellar growth, the axoneme is assembled by the addition of new axonemal subunits to its distal tip. As the flagellum is devoid of machinery necessary for protein synthesis, axonemal proteins are synthesized in the cell cytoplasm, far away from the site of flagellum assembly. The intraflagellar transport (IFT) is the mechanism that assures the delivery of the new axonemal building blocks to their site of assembly (Rosenbaum & Witman 2002). IFT is a highly conserved mechanism, that regulates both cilia and flagella assembly (Rosenbaum & Witman 2002).

During axonemal anterograde transport, IFT particles are moved along the axonemal doublets MTs from the base to the tip of the flagellum, thus contributing to axonemal growth. At the tip of the flagellum, axonemal proteins are transported back to the base by the retrograde transport that assures the turnover of IFT particles (Rosenbaum & Witman 2002). IFT particles are composed of two large protein complexes called IFT complex A and IFT complex B that globally contain at least 20 proteins (Ishikawa & Marshall 2011). IFT complex B participates in the anterograde transport, whereas IFT complex A is required for retrograde transport. Whether IFT A and B carry distinct sets of cargo proteins and the specific roles of most IFT particles is still not known (Ishikawa & Marshall 2011).

Two motor proteins mediate the movement of the IFT particles along MTs: Kinesin-2 and Cytoplasmic dynein 2. Kinesin-2 is a heterotrimeric complex consisting of two motor subunits (KIF3A and KIF3B) and a non-motor subunit (KAP) (Lehti et al 2013). The kinesin-2 complex mediates the anterograde IFT transport. The retrograde transport is instead mediated by the cytoplasmic dynein 2 motor protein (Rosenbaum & Witman 2002). Interestingly, kinesin motors as well as cytoplasmic dynein have been found along the MTs of the manchette. Indeed, another protein transport mechanism exists within the manchette: the Intramanchette Transport (IMT) (Kierszenbaum 2002a). This is a MT- and

actin-based transport that allows the movement of molecules from the acrosomal region to the caudal pole of the cell and *vice versa* (Fig. 14). It has been suggested that actin motor proteins mediate the short distance transport, while MTs are responsible for the long one (Goode et al 2000). IMT and IFT share molecular homology as several IFT particles have been found within the manchette (Lehti et al 2013, Lehti & Sironen 2016). Indications for the existence of the IMT originate from the observation that several proteins with functional requirement for spermatogenesis are transported through the manchette to the basal body region and sperm tail (Kierszenbaum 2001, Kierszenbaum 2002a, Kierszenbaum et al 2002). SAK 57 is a keratin 5-like protein that has been found to change its localization during spermatid development. First, it is seen within the acroplaxome and then it localizes with manchette MTs. During late phases of spermiogenesis, it associates with ODFs and the longitudinal columns of the fibrous sheath, but is not detected anymore in the spermatid head (Tres et al 1996).

Another protein that has been implicated in the IMT mechanism is the intra flagellar transport protein of 88 kDa (IFT88). This protein is part of the IFT B complex and has been associated with the development of acrosome-acroplaxome system, head-tail coupling apparatus and flagellum formation (Kierszenbaum et al 2011b, San Agustin et al 2015). Interestingly, in round spermatid IFT88 is first seen to co-localize with the Golgi MT-associated protein 210 (GMAP210) in proacrosomal vesicles and later in the acrosomal cap (Infante et al 1999, Kierszenbaum et al 2011b). During later developmental stages, when manchette is present, GMAP210 together with IFT88 are seen within this structure and in the acroplaxome. However, after manchette clearance, GMAP210 is no more detected on the acroplaxome. During later stages, the two proteins are associated with the basal body region, the so-called head-tail coupling apparatus (Kierszenbaum et al 2011b) and developing tail. Thus, these two proteins seem to participate in acrosome-acroplaxome formation and tail development via the IMT and IFT. This hypothesis was

confirmed by the study of the *Ift88*-hypomorphic mutant mouse (Kierszenbaum et al 2011b, San Agustin et al 2015). In this mouse model a reduced amount of a truncated form of IFT88 is expressed in order to avoid mouse embryonic lethality (San Agustin et al 2015). *Ift88*-mutant spermatids show defective shaped head and abortive flagellum development. Interestingly, cytoplasm of elongating mutant spermatids was characterized by the presence of multiple basal bodies; disorganized ODFs together with mitochondria that associate with disperse atopic MTs (Kierszenbaum et al 2011b).

Moreover, mutations of motor proteins also interfere with IMT and IFT functions leading to development of highly defective spermatids. In developing spermatids the kinesin-2-related motor subunit KIF3A localizes to the manchette, basal body and the forming axoneme. However, in mature spermatozoa KIF3A localization is restricted to the flagellum midpiece (Lehti et al 2013). The conditional germ cells-specific *kif3A*-KO mouse model is sterile and shows, in addition to a delayed manchette disassembling, impairment in flagellum development (Lehti et al 2013). In conditional *KIF3A* KO mice, the lacking of the motor protein KIF3A leads to mislocalization of axonemal MTs and flagellar associated structures (ODFs, mitochondria and fibrous sheath) that fail to correctly assemble in the flagellum, but form disorganized complexes in the caudal cytoplasm of the spermatid (Lehti et al 2013). Interestingly, sperm tail defects have been associated with a delayed translocation within the manchette of the Meiosis-Specific Nuclear Structural protein 1 (MNS1). MNS1 is a coiled-coil protein of about 60 kDa that is expressed in high levels during the post-meiotic phase of spermatogenesis, when it has been shown to regulate flagellum assembly (Zhou et al 2012). In differentiating wild type spermatids, MNS1 co-localizes with KIF3A in the acrosomal region. Following manchette formation the two proteins are localized in the perinuclear ring and manchette, while they are restricted to the principal piece in mature, epididymal sperm. In *kif3A*-KO spermatids, MNS1 seems to be stuck within the manchette as well as in the acrosomal region. Thus, a failure in MNS1

delivery to the flagellum is most likely responsible for the anomalies observed in the sperm flagella of *kif3A*-KO mice (Lehti et al 2013, Zhou et al 2012).

Altogether these results demonstrate the importance of the IMT together with IFT in spermatid development (Fig. 14). Several proteins have been shown to dynamically translocate from the acrosome-acroplaxome region to the spermatid tail using the manchette MTs as transport tracks. Thus, a fine-tuning regulation of the MT-based transport appears to be essential during the whole spermiogenesis process. This regulation might in part come from the generation of MTs carrying specific PTM patterns.

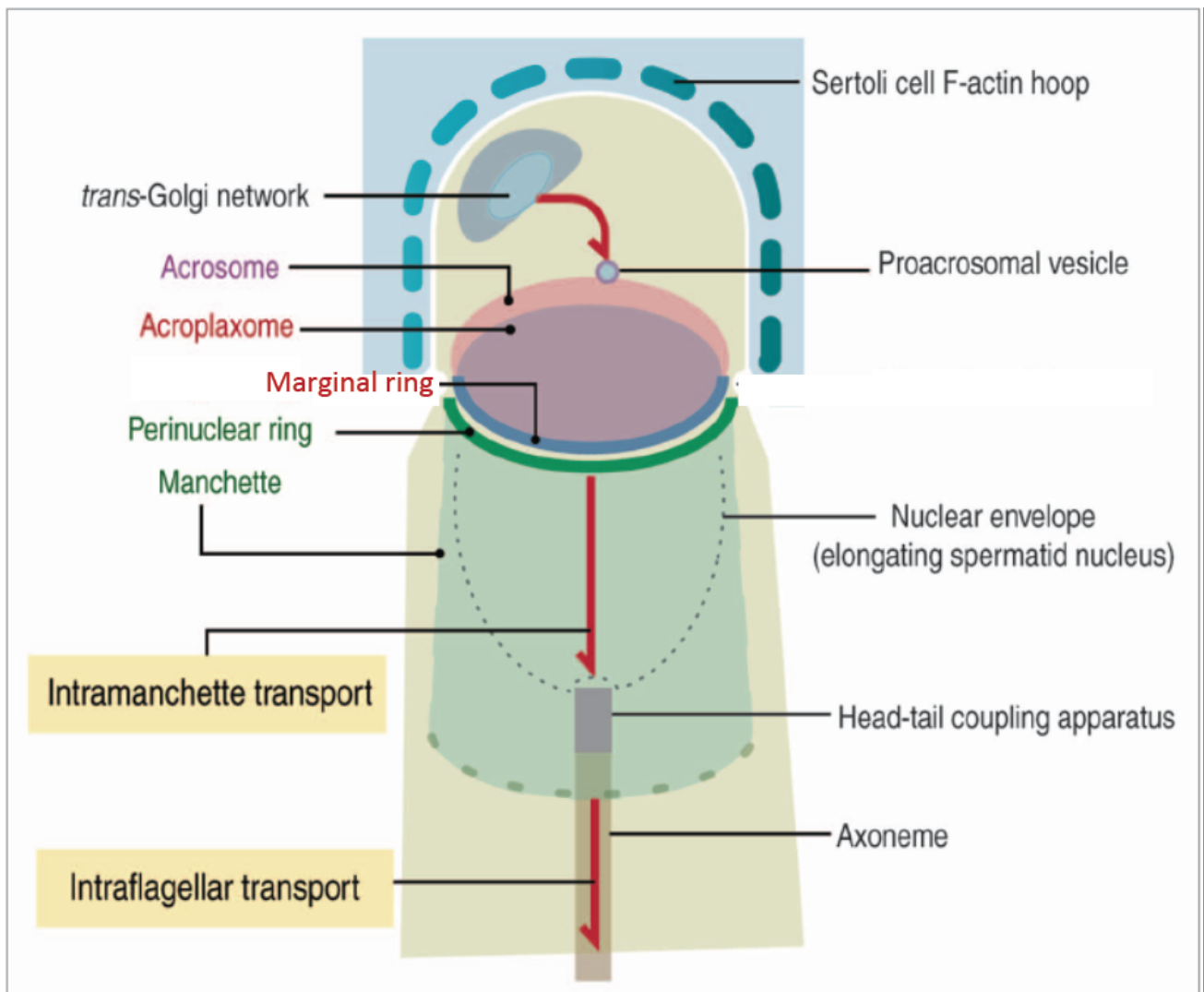


Figure 14: Role of microtubule-based transport in spermatid development.

Diagram of the cargo transport pathways involved in spermatid differentiation. Red arrows represent MTs based transport. During acrosome formation, Golgi derived pro-acrosomal vesicles are transported from the Golgi apparatus to the spermatid nucleus via MTs and F-actin based transport. Acrosome is linked to the nucleus by the acroplaxome and its marginal ring. Proteins first seen in the acrosome and acroplaxome as well as flagellar structural proteins are directed towards the head-tail apparatus (basal body region) via Intramanchette transport. Sperm tail formation depends on intraflagellar transport that assures the movement of cargo from the distal side of the flagellum to its tip and *vice versa*. (Kierszenbaum et al 2011a)

1.2.4.6 Microtubule polyglutamylation in flagella

Since many years the mammalian sperm axoneme is considered a good model to study tubulin PTMs functions because of the high degree of tubulin modification in spermatozoa. For the last two decades, several research groups have tried to characterize the biological function of glutamylation in axoneme assembly and functions (Bre et al 1996, Fouquet et al 1997, Fouquet et al 1996, Fouquet JP. et al 1994, Kann et al 2003, Mary et al 1997, Plessman U & Weber K 1997, Pringent Y. et al 1996, Redeker et al 1994) The presence of glutamylated tubulin at sperm axonemes of different mammalian species, such as rabbit, dog, monkey, hamster, rodents and human, suggest a conserved role for this PTM in regulating spermatozoa functions (Fouquet JP. et al 1994).

Several studies using the GT335 antibody have contributed to the analysis of the distribution of glutamylation along the axoneme and within the axonemal sub-structures. GT335 is a monoclonal antibody that recognizes glutamate short and long side chains. It was originally raised against a bi-glutamylated peptide mimicking the α -tubulin CTT modified on glutamate 445; however it detects also glutamylation on β -tubulin tails (Fouquet JP. et al 1994, Wolff et al 1992). Glutamylation is first detected in all MTs of growing axonemes in round spermatids (Kann et al 2003). During spermatid maturation, axonemal tubulin shows a gradient of GT335 labeling, with a strong signal in the midpiece, and a decreased labeling from the distal to the end piece (Fouquet et al 1997). Moreover, it has been shown that the central MT pair and the outer MT doublets present a heterogeneous distribution of glutamylated tubulin doublets (Fouquet et al 1996, Kann et al 2003, Pringent Y. et al 1996). In mouse, the outer MTs are more glutamylated than the central pairs. The doublets n°1, n°5 and n°6 show an increased polyglutamylation level compared to other outer MTs doublets (Fouquet et al 1996, Kann et al 2003, Pringent Y. et al 1996). Interestingly, the plane of the flagellar wave passes through the doublet 1 and

between doublets 5 and 6 (Pringent Y. et al 1996). As these doublets are the ones showing a stronger glutamylation levels, it has been suggested that tubulin glutamylation play a major role in the regulation of sperm motility. Indeed, blocking of glutamylation sites by incubation of permeabilized sea urchin and human sperm axonemes with GT335 provokes a decrease in the flagellar beat amplitude (Gagnon et al 1996). Moreover, sodium-azide immobilized spermatozoa present a decrease glutamylation level in the axonemal proximal tract as well as a uniform labeling for glutamylation on the outer MTs doublets (Fouquet et al 1997). The same changes in the glutamylation profile was found in immotile human spermatozoa lacking dynein arms (Fouquet et al 1997).

In the past decade, the discovery of the glutamylase and deglutamylase enzymes has lead to the generation of knockout mouse models for several enzymes of these two families, allowing for a deeper understanding of the importance of tubulin glutamylation in spermatogenesis, focusing on axoneme formation and maintenance. The first mouse model for glutamylation that has been linked to male infertility is the PCD mouse, a well-known model characterized by cerebellar ataxia caused by Purkinje cell degeneration (Mullen et al 1976). The mutation in PCD mice invalidates the *AGTPBP1* gene that encodes the tubulin deglutamylase CCP1 and leads to tubulin hyperglutamylation in some regions of the brain (Rogowski et al 2010). PCD mice show a significantly reduced sperm count compared to wild type littermates (Handel & Dawson M. 1981, Kim et al 2011). Sperm of the mutant mouse is immotile and is characterized by unshaped bulbous head and coiled flagella with supernumerary and disorganized ODFs (Handel & Dawson M. 1981). A further examination of the mutant mouse demonstrates that the lower sperm count was due to an increase in the apoptotic index of spermatocytes and spermatids, the two cell types in which CCP1 is more strongly expressed (Kim et al 2011).

Interestingly, an upregulation of the Cyclin B3 protein has been found in PCD testis (Kim et al 2011). Cyclin B3 is a meiosis-specific cyclin highly expressed in leptotene and

zygotene spermatocytes, but not in pachitene ones (Refik-Rogers et al 2006). Interestingly, it has previously been reported that a prolonged expression of cyclin B3 through the pachitene and later meiotic stages leads to increased non specific-germ cell apoptosis and reduced sperm count in transgenic Cyclin B3 mice (Refik-Rogers et al 2006). This data suggests that cyclin B3 expression from pachitene stage to the end of meiosis impairs the normal development of spermatogenesis (Refik-Rogers et al 2006). Defects in early or late meiotic checkpoints result in a premature arrest of the spermatogenic process at a particular germ cell developmental stage. However, in the PCD mouse (Kim et al 2011), germ cells at all developmental stages were detected (Refik-Rogers et al 2006), similar to cyclin B3 transgenic mice (Refik-Rogers et al 2006). Another common phenotype in these two mouse models is the presence of multinucleated and degenerating spermatids in the lumen of seminiferous tubules (Kim et al 2011, Refik-Rogers et al 2006) that reflects the defects in later meiotic phases such as anaphase and cytokinesis. The PCD mouse is characterized by an extensive degeneration of cerebellar cells that has been linked to an augmented tubulin glutamylation level in this brain region (Rogowski et al 2010). Thus, it has been suggested that CCP1 might be responsible for a common mechanism regulating cell survival and maintenance in several tissues, including testis (Kim et al 2011, Rogowski et al 2010). However, further studies are needed to fully understand the infertility phenotype of the PCD mouse.

Another tubulin-modifying enzyme that has been shown to be involved in the regulation of spermatogenesis is the glutamylase TTLL1 (Campbell et al 2002, Vogel et al 2010). Two mouse models have been analyzed, the ROSA22 mouse model (Campbell et al 2002), in which PGs1 a subunit of the TTLL1-enzyme complex (Janke et al 2005, Regnard et al 2003) is mutated, and the *ttl1*-KO mouse (Ikegami et al 2010, Vogel et al 2010).

The ROSA 22 mouse model shows reduced level of alpha-tubulin glutamylation (Ikegami et al 2007). Microscopic analysis of mutant testis revealed various defects in axoneme assembly (Campbell et al 2002). Interestingly the severity of the phenotype correlates with the stage of spermatid development. No axonemal defects are detected in round spermatid at early steps of axoneme assembly, whereas at later developmental stages several axonemal anomalies were observed in elongating spermatid. Axonemal defects appear to be heterogeneous varying from missing of one particular MT doublet or central pair to complete axonemal disorganization. Spermatids that managed to assemble a flagellum show a truncated axoneme and a poor connection with the distal centriole. Moreover, prior to sperm release a lot of decapitated spermatozoa were seen in the testis. Disorganized ODF-like structures were detected in the cytoplasm of certain elongating spermatids (Campbell et al 2002).

In 2011, another study confirmed the importance of TTLL1 in sperm flagellum formation (Vogel et al 2010). The *ttll1*-KO mouse was generated by introducing a trap mutation in the ATP-binding domain of the TTLL1 enzyme, leading to protein inactivation (Vogel et al 2010). *Ttll1*-KO males present a similar infertility-related phenotype described for the ROSA22 mice (Campbell et al 2002, Vogel et al 2010). Histological analysis of *ttll1*-KO testis reveals no defects in the pre-meiotic germ cells, however epididymal spermatozoa were immotile and characterized by truncated or absent flagella and thickened midpiece (Vogel et al 2010). However an ultrastructural analysis of *ttll1*-KO spermatids would be useful to better compare and understand the PGs1 and TTLL1 related phenotypes. Interestingly, an analysis of the respiratory cilia of the *ttll1*-KO mouse model reveals reduced cilia motility, but not ultrastructural axonemal defects (Vogel et al 2010). Interestingly, no ultrastructural defects were detected in the 9+2 organization of axonemes from tracheal motile cilia either (Ikegami et al 2010, Vogel et al 2010), suggesting that TTLL1 seems to play a specific role in the regulation of sperm flagellum assembly.

TTLL5 is another glutamylase that has been shown to be important for sperm flagellum formation (Lee et al 2013). TTLL5 is the only initiating glutamylase with substrate preference for α -tubulin (van Dijk et al 2008b). *Tll5/stamp targeted mutant* mice are subfertile and produce 30% less sperm cells compared to *wild type* littermates (Lee et al 2013). Epididymal sperm is characterized by the presence of detached heads, and often by coiled tails. No decrease in sperm viability was detected *tll5*-KO mice compared to wild type mice. However, sperm lacking TTLL5 show a reduced progressive motility (Lee et al 2013). Sperm immunostaining against tubulin glutamylation showed no differences in glutamylation level in the midpiece, but the intensity of the staining was decreased in the principal and distal piece of the mutant flagellum (Lee et al 2013). An ultrastructural studies of epididymal sperm reveals that in almost 95% of analyzed axonemes the MT doublet n°4 with the associated ODF was missing (Lee et al 2013). Interestingly, the overall level of sperm tubulin glutamylation is reduced by 40% in the mutant mouse. In the *wild type* doublet n°4 is one of the MTs doublets showing a lower amount of tubulin glutamylation (Fouquet et al 1996). Thus it has been suggested that the lower level of polyglutamylation in the MT doublet n°4 could make it more sensitive to subtle changes in the glutamylation levels. Moreover as the doublet n°4 is close to the plane of flagellar beating (doublets 1, 5, 6) it has been suggested that it could be responsible for the reduced sperm motility of the TTLL5 mutant mice (Lee et al 2013). No morphological defects were detected in mutant spermatogonia and spermatocytes. Moreover, the level of tubulin glutamylation from testis extracts was similar between mutant and control mice and no changes in the expression level of other TTLLs were detected in the mutant testis (Lee et al 2013). Moreover, no axonemal ultrastructural defects were detected in other ciliated organs (Lee et al 2013). Thus TTLL5 seems to be specifically important for sperm axoneme maintenance and formation.

A recent work has suggested that the glutamylating enzyme TTLL9 might be involved in the mechanism regulating the switching of bending direction during flagellar beating (Konno et al 2016). Cilia and flagellar beating consist in the propagation of bends that originates from the base of the axoneme. In mouse, the bend occurring in the direction of the sperm hook is called pro-hook bend, whereas bending toward the opposite direction is referred as anti-hook bending. Thus, sperm beating consist in successive anti-hook and pro-hook bending along the axoneme (Ishijima et al 2002) Spermatozoa collected from the epididymis of TTLL9 mutant mice show frequent flagellar stalls after the anti-hook bending (Konno et al 2016). *Ttll9*-KO male produce a less amount of sperm cells compared to wild type animals. Mutant spermatozoa appear to have normal gross morphology, with a hook-like shaped head and an elongated flagellum (Konno et al 2016). However, electron microscopy analysis of epididymal sperm reveals some ultrastructural defects in the flagellum of mutant spermatozoa. Around 50% of mutant sperm cells have a shortened outer MT doublet n°7. As such defect was never detected in testicular spermatozoa, which is why it was suggested that TTLL9 is not likely to regulate axoneme assembly. A possible explanation for the generation of a shorter MT doublet could be induced by MTs severing, or MT depolymerization. The missing of the doublet n°7 was always observed posteriorly to the region where its associated ODF terminate. This observation leads to the hypothesis that ODF might protect doublet n°7 from depolymerization and/or severing (Konno et al 2016). To assess the consequence of the lacking of TTLL9 in tubulin glutamylation heterogeneity among axonemal doublets, electron immune gold analysis of polyglutamylated tubulin was performed on axonemal doublets and central pair from mutant and *wild type* midpiece axonemal cross sections. The doublet MTs n°5 showed reduced glutamylation levels in mutant axonemes compared to *wild type* ones. As mentioned before, the majority of mutant spermatozoa display flagellar stalls after anti-

hook bending, most likely due to failures of bend switching after anti-hook bending (Konno et al 2016). Pro-hook bend is directed toward doublet 5 and 6 through the action of dyneins on doublets 6-9 (Ishijima et al 2002, Konno et al 2016). Anti-hook bend is directed toward doublets n°1 through the activity of dynein arms on doublets n°1-4 (Ishijima et al 2002, Konno et al 2016). Flagellar beating arises from the coordinated activation of axonemal dyneins and inter-doublets sliding (Satir 1985, Satir P. 1979). It has been suggested that reduced polyglutamylation weakens the interaction between dynein and MTs (Kubo et al 2010). Thus, it has been hypothesized that the reduction of glutamylation due to the lacking of TTLL9 is likely to be the cause of the flagellar stalls (Konno et al 2016).

2. AIM OF THE STUDY

Spermatogenesis is a complex biological process during which stem cells of the testis differentiate into mature haploid spermatozoa. Spermatogenesis consists of three sequential phases called amplification-, meiotic- and spermiogenesis phase. These events are associated with drastic changes in cells shape and cell movement across the seminiferous epithelium, and it has been shown that the MT cytoskeleton participates in these cellular processes (Lie et al 2010, O'Donnell & O'Bryan 2014). MTs are modified by a large range of posttranslational modifications, which are believed to control their functions and biophysical behavior. While recent works have underlined the importance of tubulin glutamylation in sperm axoneme assembly and/or maintenance (Campbell et al 2002, Handel & Dawson M. 1981, Kim et al 2011, Konno et al 2016, Lee et al 2013, Vogel et al 2010), nothing is so far known on the functions of this posttranslational modification on earlier steps of spermatogenesis.

My purpose is to investigate the role of CCP5 in mouse spermatogenesis. CCP5 is a deglutamylase with the unique activity to remove the glutamate branching point of posttranslationally generated glutamate side chains from tubulin (Rogowski et al 2010). RT-PCR results had revealed that CCP5 is particularly highly expressed in murine adult testis compared to others organs (Fig. 3.1). Moreover, during the establishment of the CCP5-KO mouse colony the laboratory realized that the CCP5-KO males were most likely infertile because they failed to give pups, even with wild type females. Altogether these preliminary observations suggested a potential role for CCP5 in mouse spermatogenesis.

The goal of my PhD project was to understand by which mechanisms CCP5 controls spermatogenesis, and how its biochemical role as a deglutamylase affects the MT cytoskeleton and its posttranslational modifications during mouse spermatogenesis.

The main objectives of my thesis projects are:

- To characterize the posttranslational modification patterns in wild type testicular germ cells at different developmental stages.
- To define which phase of spermatogenesis is affected in the CCP5-KO mouse.
- To investigate the impact of CCP5-KO on Sertoli cells, and to investigate the role of these cells in the infertility phenotype observed in CCP5-KO mice by generating and analyzing a conditional, germ cell-specific CCP5-KO mouse model.
- To assess the mechanism underlying the role of CCP5 in mouse spermatogenesis.

3. MATERIAL AND METHODS

Animal experimentation

During my thesis project two mouse strains were analysed. The main part of the project was carried out on the BL/6N-CCP5^{-/-} mouse model, whereas key experiments were performed on the CCP5^{f/f}-STRA8-icre mouse model. The latter was obtained by crossing BL/6N-CCP5^{f/f} animals with STRA8-icre 1Reb/J mice obtained by the Jackson laboratory. The transgenic STRA8-icre mice expresses a variant of Cre recombinase (icre) that is under the control of the stimulated by Retinoic Acid gene 8 (STRA8) promoter. When Stra8-cre transgenic male are crossed with CCP5 Flox female carrying the lox-P flanked sequence, a icre-mediate recombination gives rise to the excision of the CCP5 floxed sequence. STRA8 mediated icre expression is detected from early spermatogonia stage (PN3) to pre-leptotene spermatocytes stage and is not detected in other tissues or in male or female embryos (Sadate-Ngatchou et al 2008). Thus, *CCP5 flox* alleles are defloxed just in male premeiotic germ cells, but not in the somatic cells of the testis.

Mice were housed under Specific Pathogen Free (SPF) conditions in the animal facility of the Institut Curie. Animals were maintained with access to food and water *ad libitum* in a colony room kept at constant temperature (19-22°) and humidity (40-50%) at 12-h light/dark cycles. All experimental procedures were performed in strict accordance with the guidelines of the European Community (2010/63/EU) and the French National Committee (87/848) for care and use of laboratory animals.

Genomic DNA isolated from mouse tail snip was analysed by PCR. Mice were genotyped by polymerase chain reaction (PCR) according to MCI (Mouse Clinical Institute -MCI, Illkirch, France) protocols using GoTag polymerase (Promega) and 33 amplification cycles.

The primer pairs listed below were used to define genotypes for CCP5 wildtype, flox and knockout alleles.

(1) CCP5_Ef_4243_5'-CCAGGCCTCTTGTACCCTAACCAGGG-3' and

CCP5_Er_4244_5'-GCGGTCATGCCACCATAGTCCACG-3'

(2) CCP5_Lf_4241_5'-TTCCCAGCACCCACACTGTGCC-3' and

CCP5_Lr_4242_5'-CCCTGGGGTACAAGATAAACCGGGTCC-3'

(3) CCP5_Lf_4241_5'-TTCCCAGCACCCACACTGTGCC-3' and

CCP5_Er_4244_5'-GCGGTCATGCCACCATAGTCCACG-3'

To genotype the *STRA8-iCre* gene the following primer combinations were used:

(1) oIMR7338_5'-CTAGGCCACAGAATTGAAAGATCT-3' and oIMR7339_5'-

GTAGGTGGAAATTCTAGCATCATCC-3' and oIMR9266_5'-

AGATGCCAGGACATCAGGAACCTG-3' and oIMR9267_5'-

ATCAGCCACACCAGACACAGAGATC-3'

For each experiment I choose mutant and a control littermates having the same age. To minimize the number of animals needed for our experiments I tried to maximise the number of manipulation doable on a single mouse. For each type of experiment I performed at least 3 replicates (N=3). Exceptions are indicated in the results section.

Testicular germ cell dissociation.

Adult mice (>8 weeks-old) were killed by cervical dislocation. Testes were surgically removed and placed in Dulbecco's phosphate-buffered saline (PBS). Testes were decapsulated from the tunica albuginea and incubated in 3 ml of dissociation solution (2 mM CaCl₂, 12.1 mM Glucose, 10 mM HEPES, 5 mM KCl, 1 mM MgCl₂, 6 mM Na-Lactate, 150 mM NaCl, 1 mM NaH₂PO₄, 12 mM NaHCO₃ (pH = 7) containing 1 mg/ml collagenase (SIGMA G9023) and incubated under horizontal agitation for 30 minutes at

room temperature. The dispersed seminiferous tubules were washed in PBS and thinly cut. Cells were dissociated by gentle pipetting, filtered with a 70 µm nylon mesh and centrifuged at 500 g for 10 minutes. Cell pellet was suspended in 1 ml of PBS and fixed for 5 minutes at room temperature with 4% PFA. Cells were washed with PBS and plated on 12 mm microscope cover glasses. Cells were stored at -20°C prior to immunostaining analysis.

BSA density gradient-based testicular germ cell fractionation

Decapsulated testes were incubated in 3 ml of the above-mentioned dissociation solution containing 1 mg/ml of collagenase for 30 minutes. Seminiferous tubules were washed with PBS and then were incubated for 15 minutes in 8 ml of PBS containing 2 mg/ml of trypsin (GIBCO) and 1 µg/ml DNase. Trypsin reaction was stopped by adding 8 ml of High Glucose DMEM medium (DUTCHER) containing 50% BSA (SIGMA). Tubules were mechanically dissociated by gentle pipetting, and pelleted down by centrifugation at 500 g for 10 minutes at 4° C. Finally pellet was carefully resuspended in 18 ml of 50% BSA-DMEM High Glucose medium, filtered with a 70 µm nylon mesh and loaded in the sedimentation chamber.

The Sedimentation chamber was kindly provided by Christophe Arnault (University of Grenoble) and sedimentation procedure was performed at 4° C. Sedimentation chamber set up was done by replacing the previously filled 260 ml of FC77 Fluorinert™ Liquid (Chemical Group, European Business center, Belgium) by adding 360 ml of a mixed solution of 2%- and 4% BSA- High Glucose DMEM (10 ml/min). The 18 ml cell suspension was carefully added to the sedimentation chamber (18 ml/1 min) followed by 25 ml of PBS. Cells were allowed to seat in the sedimentation chamber according to their density for 1.5 hour. Cells were collected in thirty-15 ml fractions within 5 minutes and pelleted by

centrifugation (500 g, 10 minutes, 4° C). Cell composition of each resuspended fraction was observed under light microscopy. Fractions containing germ cells at the same developmental stage were pooled together and pelleted by centrifugation, whereas the ones containing a mixed population of cells were discarded. Spermatocytes-, round spermatids-, elongating spermatids- and condensed spermatids-containing pellets were snap frozen in liquid nitrogen and stored at -80° C for immunoblot or RT-qPCR analysis.

Computer-assisted motility analysis

Sperm suspension was placed onto an analysis chamber (100 µm depth, Leja Products B.V., Nieuw-Vennep, Netherlands) and kept at 37°C for microscopic quantitative study of sperm movement. Sperm motility parameters were measured at 37°C using a sperm analyzer (Hamilton Thorn Research Inc, Beverly MA). The settings employed for analysis were as follows: acquisition rate: 60 Hz; number of frames: 100; minimum contrast: 25; minimum cell size: 10; low static-size gate: 2.4; high static-size gate: 2.4; low static-intensity gate: 1.02; high static-intensity gate: 1.37; minimum elongation gate: 12; maximum elongation gate: 100; magnification factor: 0.70. The motility parameters measured were curvilinear velocity (VCL), average path velocity (VAP) and amplitude of lateral head displacement (ALH). At least, 200 motile sperm were analyzed for each assay. CCP5^{+/+} (N=2), CCP5^{+/-} (N=1). The experiment was performed in collaboration with Christophe Arnault Lab. (University of Grenoble).

Sperm counting

Sperm was obtained by placing cauda epididymis in 1 ml of PBS. After epididymis laceration using 0.5 x 16 mm needles, sperm cells were allowed swim out from the epididymis by 15 minutes incubation at 37° C. To perform sperm counting, sperm suspension from control animal was diluted 1:100 in distilled water. Sperm dilution was adjusted for mutant samples accordingly to the experimental conditions. A 10 µl drop of

diluted sperm suspension was loaded into a cell counting chamber (KOVA Glasstic Slide10 with Grid Chamber. KOVA INTERNATIONAL). Sperm cells situated within one quadrant of the grids were counted. Spermatozoa touching the right and bottom side of each sub-quadrant were not counted. For control animals sperm counting was performed on 3 quadrants and the average of the obtained values was considered. For the mutants, the counting was performed in the 9 quadrants forming the chamber. The mean of the obtained values was considered to calculate final sperm cells concentration

Sample preparation for electron microscopy analysis

Testes were decapsulated from the tunica albuginea and seminiferous tubules were divided into three pieces using a razor blade (Gillette Super Silver). When possible spermatozoa were collected by swim out technique and pelleted by centrifugation at 400 g for 10 minutes. Samples were placed in a 1,5 ml eppendorf tube and fixed in 0.1 M HEPES, 4 mM CaCl₂, 2,5% Glutaraldehyde, 2% formaldehyde at pH 7.4 by a first 20 minutes-incubation at room temperature, followed by 4 washes of 40 minutes each at 4°C in the fixation solution. Samples were processed for transmission electron microscopy analysis in collaboration with Stefan Geimer (University of Bayreuth). Briefly samples were washed in 0,1 M HEPES (4mM CaCl₂, pH 7,4) After treatment with osmium tetroxide the samples were embedded in 2% (w/v) agar noble. The epon embedding was done according to McFadden and Melkonian (1986). Single sections were cut at a thickness of 60 - 80 nm, serial sections were cut at a thickness of 80 - 85 nm. The contrasting was done according to Reynolds (1963). The electron microscope JEM-2100 (JEOL, Tokyo, JP) was used for the analysis of the sections. It was used at an accelerating voltage of 80 kV.

Germ cells depletion from mouse testis seminiferous tubules

Busulfan (SIGMA) was dissolved to a final concentration of 4 mg/ml in 50% dimethyl sulfoxide (DMSO). Mice were injected peritoneally with a dose of 30 mg/KG as suggested in (Wang et al 2010). Untreated control animals were injected with 50% DMSO. 1-month post injection mice were sacrificed by cervical dislocation and testes were processed for immunoblot analysis.

Histology and Immunofluorescence

Upon sacrifice by cervical dislocation testis were harvested from the abdominal cavity of the mouse and fixed overnight in Bouin's solution (SIGMA). Samples were carefully washed with 70% ethanol and embedded in paraffin after dehydration procedure. Histological examination was performed on 5 µm testis cross-sections. Slides were deparaffinised with two-10 minutes washes using the xylene-substitute Microclearing (DIAPATH, X0026) and rehydrated.

Testis cytoarchitecture was analysed using the Periodic Acid-Schiff (PAS) staining system (SIGMA). Briefly, paraffin embedded testis cross sections were incubated in Periodic Acid Solution for 5 minutes at room temperature (RT), washed in distilled water and then incubated in Schiff reagent for 15 minutes at RT. After a wash with tap water, slides were counterstained for 1 minute and 30 seconds with Hematoxyline Gill solution. Slides were finally washed in tap water, dehydrated and mounted using Entellan mounting medium. Alternatively, standard Hematoxylin and Eosin staining protocol was performed on testis and epididymis cross-sections.

For Immunofluorescence analysis, PFA-fixed testicular dissociated cells were plated onto poly-L-lysine (SIGMA, P4832) coated 18 mm-coverslips. Slides were incubated at least 1 hour in blocking solution (PBS, 10% Normal Goat Serum, 0.3% Triton(TX)-100) and then incubated for 2 hours with primary antibody. Next, cells were washed 3 times in PBS-0.1%

TX-100 and incubated for 45 minutes with anti-mouse and/or anti-rabbit Alexa fluorophore-conjugated secondary antibody 488 (green) and/ or 568 (red). Primary and secondary antibodies were diluted in blocking solution. DNA was visualised by staining with 20 µg/ml 4',6'-diamidino-2-phénylindole (DAPI). Coverslips were mounted using Prolong Gold antifade reagent (Life technology, P36930).

Microscopy and Imaging

Testis and epididymal cross-sections treated for histological analysis were scanned using the Metafer system (Metasystem) using a 63X oil immersion objective. Slide scanning was performed with Metafer5 software. Images were visualised using Metaviewer software (all softwares provided by Metasystem).

For fluorescent labelling, images were acquired on Structured Illumination Microscope (SIM) (Optigrid/Leica systems) with a 63 X (N.A. 1.40) oil immersion objective. Images were acquired using the ORCA-Flash4.0 camera (Hamamatsu) and Leica MM AF imaging software.

Quantification of CCP5 KO-related phenotypes

Testicular dissociated cells from CCP5^{-/-} and control testis were probed with GT335 antibody to detect tubulin glutamylation and DAPI to visualise the nucleus. Multiple images were taken in order to cover the whole coverslip with the care not to image cells twice. Each counting procedure was performed in CCP5^{+/+} and CCP5^{-/-} testicular dissociated cells by 3 replicate experiments (N=3). Only one counting experiment was performed in conditional CCP5^{-/-} and control testicular dissociated cells (N=1).

The percentage of hyperglutamylated round spermatids was determined by counting round spermatids showing more than two GT335-positive microtubules in the analysed image.

The percentage of early elongating spermatids bearing a glutamylated MT hair-like structure was obtained by counting the number of early elongating spermatids showing ectopic glutamylated microtubules located caudally to the manchette. Only cells with an ovoidal nuclear shape were considered as early round spermatids.

The presence of MTs-hair like structures was also quantified in intermediate elongating spermatids showing a nucleus not yet fully condensed with a “hook-like shape”. As nuclear shape was highly defective in the mutant spermatids I also considered the intensity of the DAPI signal to recognize this cell stage basing on nuclear condensation.

The percentage of defective flagella on late condensed spermatids was assessed as well. The analyzed flagella were subdivided in four main categories: normal, coiled, malformed flagella. Multiple flagella were considered as malformed. The number of cells for each category was counted.

The number of defective shaped nuclei was analyzed by visualizing DAPI staining. Nuclei were divided in three classes: normal shaped nuclei, longer and/or curved- and wider nuclei. A cell nucleus showing a thin elongate shape, with a bulb-like formation in its apical part was considered as a longer and thinner nucleus. Nuclei shorter than normal with a larger distal part were classified in the “wider nucleus” group. To perform this analysis elongating spermatids (early, intermediate and condensed) were counted for each category.

Quantification of elongating spermatids showing supernumerary centrioles was done on γ -tubulin labelled testicular dissociated cells to visualise basal bodies. Images were taken in order to cover the whole γ -tubulin labelled coverslip field. Elongating spermatids were divided into 3 categories: cells showing 1 or 2 γ -tubulin-positive spots (1-2 basal bodies

(bb)), cells with more than 2 positive spots (>2 bb) and spermatids with a single but larger γ -tubulin-positive spot (clustered bb). Cells belonging to each class were counted in each genotype. CCP5^{+/+}: N=3. CCP5^{-/-}: N=3;

Western Blot

Samples were lysed by incubation in PBS containing 25 mM HEPES pH 7.5, 200 mM NaCl, 5% Glycerol, 1 mM DTT, 0.5% NP40 for 20 minutes. After sonication and centrifugation, concentrations of the samples were obtained by Bradford assay. Lysates were diluted at a final given concentration into protein sample buffer containing 450 mM DTT, 10% SDS, 400 mM Tris-HCl pH 6.8, 50% glycerol 100, and 30 μ g/ml of 0.2% bromophenol blue and boiled for 5 minutes at 95°C. Samples were separated by polyacrylamide gel electrophoresis (SDS-PAGE) using running buffer containing 50 mM Tris, 384 mM Glycine, 0.1% SDS (L5750 Sigma), pH 8.3. Proteins were transferred to nitrocellulose membranes (Millipore) using the Trans-Blot^R TurboTM Transfer System (BIORAD) and immunoblots were performed by overnight primary antibody incubation.

Antibodies used for immunoblots are listed in table 1

RNA extraction

Fractionated germ cell pellets were resuspended and incubated in 200 μ l of TRIzol reagent (Life technology) for 5 minutes. Chloroform (40 μ l/ 200 μ l of TRIzol) was added to homogenised suspension and samples were vigorously vortexed for 15 seconds and then incubated for 3 minutes at room temperature. Upon sample centrifugation (15 minutes, 12000 g at 4°C), the aqueous phase was transferred to new tubes containing 100 μ l of isopropanol. After 15 minutes incubation at room temperature, samples were centrifuged for 10 minutes at 12000 g at 4°C. Pellet was washed with 200 μ l of 75%

ethanol. RNA was dissolved in 6 µl of sterile, RNAase-free water. RNA concentration was determined by absorbance at 260 nm using Nanodrop Spectrophotometer (Thermo Fisher). RNA quality was analysed by comparing the quality and relative quantities of the 18S and 28S rRNA bands after agarose-gel electrophoresis, staining with ethidium bromide and visualisation with UV light.

Real-Time Quantitative Reverse Transcription PCR

cDNA was synthesized with First-Strand cDNA Synthesis kit according to the manufacturers' instructions (27-9261-01, GE Health care). Quantitative PCR experiments were performed in 25-µl reactions using 96-well plates. SYBR GREEN (Power Syber Green PCR Master Mix, Applied Biosystem) was used as marker for DNA amplification. Primers for murine TTLLs and CCPs genes are shown in table 2. The TATA binding protein (TBP) housekeeping gene was used for value normalization.

Statistical analysis

Statistical analysis was performed by Two-tailed unpaired test, or ANOVA using GraphPad Prism version 5. P-values <0.05 were considered statistically significant. The asterisks mark the significant levels (**P<0,005, ***P< 0,0005).

Table1: Antibodies

Antibody	Reactivity	Dilutions WB	Dilutions IF	Company
α - tubulin (12G10)	mouse	1:500	1:250	from J. Frankel, E.M. Nelson, University of Iowa, USA
β - tubulin (Tub2.1)	mouse	/	1:250	Sigma # T4026
β - tubulin (AXO45)	mouse	1:250	/	
β 3- tubulin (SDL3D10)	mouse	/	1:250	Sigma # T8660
Monoglutamylolation (mono-glut-tub)	rabbit	/	1:4000	T. Surrey, CRUK
Glutamylolation (GT335)	mouse	1:2000	1:2000	our own production
Polyglutamylolation (Poly E)	rabbit	1:2000	1:2000	our own production
Monoglycylation (GlyPep1)	rabbit	1:8000	1:4000	PSL
Polyglycylation (Poly G)	rabbit	1:2000	1:2000	our own production
anti detyrosinted tubulin (anti-deTyr tubulin)	rabbit	1:1000	/	Millipore #AB3201
anti Δ 2 tubulin	rabbit	/	1:2000	our own production
Acetylated tubulin (6-11 B-1)	mouse	1:1000	1:5000	Sigma #T6793
Acetylated tubulin (ac-a-tub-III 1H8)	mouse	1:1000	/	our own production
γ tubulin	rabbit	/	1:5000	Sigma # T3320
Acrosome (mouse sperm protein sp56)	mouse	/	1:2000	Gentaur #55101

Table 2: Primers for qPCR

Gene	Forward	Reverse
TTL	CAGCCGGTGCCAAAGGTGAA	CAAGCAGCAGAGGGTGCTCAAGA
TTLL1	CCCTGGCTGATCGAGGTGAA	GTTGAGGGTGTCATTAATCAGGTTGT
TTLL2	ATCCGAGGCAAACCACACTGA	CAAATGAGGTTTTTTCTTCTTCTCCA
TTLL3	GATGCTGGACCGCAACTGTGA	GCTTCTTGATGGTGAAGCCCTCT
TTLL4	CTCTGATTCTGCTCCAGTGTGGTCT	CTCTGATTTGCTGAAGGCATTGAGTA
TTLL5	CGCCTCTTCCAGGACAGAATGACT	CCAGAGACAGGAGCTTCCTCTCGTA
TTLL6	AGGAGTATGCCCCGGCAACTGA	ATTCCCCCTGCATCTCTACCTTCT
TTLL7	TGGAGCAATGTGAAATTGATGATGA	GGCATAGAACACAGAGGCTTTGGT
TTLL8	ACTCCCTCGTTCATGGCGAT	TGAGGGTTCACAGACGTGATTCTA
TTLL9	CAAAGGGAAAAGAGCGAGAGCA	TTCGTCCTTCACTTCCACCCAT
TTLL10	GCGGGTGGTGCAGAGGTACAT	GCAGGTAGGAGCGCACGTCA
TTLL11	TCAGCATCCGCCAGCTCAAG	GTGAAATGAACTCCATGCCAGTAGA
TTLL12	TGACCCGGATGTGGTGCTGAA	CCCGGAAGATCTCAGCCTGGA
TTLL13	CTAGCCCGTTTTGCCACCA	GCATGCAGACATTGTCCAGGTT
CCP1	ATCCCGATTATTTTGGTCACATTC	ATCTTGAGCAATTTTGTCTTTGTA
CCP2	AAACATAGCAGATGAGCTGACTCAGA	ATACTGCTCATTTTCGCTGTTTCCT
CCP3	TCCTTCTTGTCCTGAGCCAGTGTA	AAAACAGGGCTCTTTGTAAGCATCT
CCP4	GAAAATGTGGAGTCCAAAGGATCA	GCAAAGGCCAAGGCTCATCTA
CCP5	CGAGGCCTAAGCAGCACTCTGA	GGAGACAGGCAACCCATTGTGA
CCP6	GCTCCTCTGCCAGAATGCTGA	CGACGGCCAGTTCCTGCTT

4. RESULTS

4.1 Infertility phenotype in CCP5^{-/-} mice is mainly due to defects in haploid post meiotic germ cells.

In order to understand whether the CCP5 enzyme is necessary for mouse male fertility, semen was analyzed to assess the morphology and sperm count. Spermatozoa were collected from cauda epididymis of sexually mature and isolated CCP5^{-/-}, CCP5^{+/-} and their wild type littermates by the swim-out technique (N=3). To assess the sperm morphology, semen smears were stained with 0.22% Coomassie Brilliant Blue. A condensed, hook-shaped head and a long flagellum characterize the wild type murine sperm cells (Figure 4.1 A). Heterozygous sperm cells did not show major morphological defects, in contrast to CCP5^{-/-} semen that is mainly composed of immature germ cells (short arrows, Fig 4.1 A), cytoplasmic debris and very few mature sperm cells (long arrow, Fig. 4.1 A). These results were confirmed by histological analysis of cauda epididymis. As expected, Hematoxyline Eosine staining of paraffin-embedded epididymal cross sections reveals that tubules from wild type and heterozygous animals are rich in spermatozoa, whereas epididymis from the mutant was mainly filled with immature round cells, elongating spermatids and cytoplasmic debris (Fig 4.1 C).

Caudal epididymal sperm concentration from CCP5^{+/+} (n= 3), CCP5^{+/-} (n=3) and CCP5^{-/-} (n=5) was analyzed to understand the degree of CCP5^{-/-} male infertility (Fig 4.1 B). Statistical analysis reveals a significant difference between CCP5^{+/+} and CCP5^{-/-} sperm concentration (respectively $30.6 \times 10^6 \pm 5.5 \times 10^6$ vs. $14.8 \times 10^4 \pm 2 \times 10^4$), with 100 fold-less produced mutant sperm cells compared to wild type. In contrast, no significant differences in sperm cell numbers were detected between CCP5^{+/+} and CCP5^{+/-} (respectively $30.6 \times 10^6 \pm 5.5 \times 10^6$ vs. $21.7 \times 10^6 \pm 8.4 \times 10^6$).

To detect possible causes of male infertility, I compared the gross-morphology of the testis between genotypes. No defects in gross organ morphology and size were observed in 3 month-old mutant testis compared to wild type despite the significantly lower sperm count (Fig 4.2 A). To detect subtle changes in the organ size, testis weight from the mice was compared. The average weight of testes (mg) was normalized to the body weight (g) of the animal. No significant differences were observed between CCP5^{-/-}, CCP5^{+/-} and control testes. As CCP5 mutant mice produce a low number of sperm cells compared to wild type animals, I decided to compare the weight of cauda epididymides as well (Fig 4.2 C). Interestingly, cauda epididymides from CCP5^{-/-} animals are slightly heavier than control, although the difference is not statistically significant (P=0.0721). Despite a small sperm production, this augmentation could be explained by the presence in the semen of immature germ cells that, because of their DNA content, are heavier than sperm cells.

I next analyzed whether intercrossing CCP5 heterozygous mice generate wild type, heterozygous and homozygous F2 progeny that reflect the WT:HT:KO expected Mendelian ratio (25%:50%:25%). Interestingly, the CCP5 KO homozygous allele is not distributed at the expected Mendelian frequency (** P=0.009 calculated with CHI-SQUARE test). Indeed I observed the following frequency of offspring genotypes for WT, HT, KO loci: 31.7%: 56.3%: 11.9% (Fig 4.2 D). This data suggest that lack of CCP5 might affect mouse embryonic and/or post-embryonic development. However, in my project I do not further investigate on the potential role of CCP5 in embryogenesis and rather focus on understanding the mechanisms leading to male infertility in CCP5^{-/-} mice.

To understand whether sperm differentiation is impaired at early or late steps of spermatogenesis, histological analysis was performed on Hematoxylin Eosine and/or Periodic acid-Schiff (PAS) stained paraffin-embedded testis cross-sections.

A healthy seminiferous epithelium is characterized by a well-ordered and organized architecture. Spermatogenesis is a cycling process as the spermatogonial stem cells continually differentiate to produce spermatozoa. Spermatogonial differentiation is not synchronous, leading to the generation of new waves of spermatogenesis each time that a stem cell differentiates. To reflect this cycling it is possible to identify seminiferous tubules at different stages accordingly to their germ cell composition at a particular steps (Hess & Renato de Franca 2008). While we did not precisely stage the tubules, I compared tubules with similar cell compositions, such as the ones in which sperm cells are going to be released in the lumen (tubules in spermiation, Fig 4.3 B), or tubules at slightly later stages to observe spermatogonia, spermatocyte (arrow, Fig 4.3 C) and early elongating spermatids (arrowhead, Fig 4.3 C).

Histological analysis revealed that seminiferous tubules from 4-month-old CCP5^{+/+} and CCP5^{+/-} mice were filled with spermatozoa (arrows, FIG 4.3 A, D), whereas in CCP5^{-/-} testis the seminiferous tubules were empty (asterisk, Fig. 4.3 G and H). To understand which steps of spermatogenesis is impaired in CCP5^{-/-} animals, the germ cell composition was analyzed to check if a particular germ cell type was missing in CCP5^{-/-} testis. I thus performed histological sections of a tubule in spermiation to identify various germ cell types (Fig. 4.3 B). From the base to the apex of the seminiferous tubule, it is possible to recognize spermatogonia (SPG), spermatocytes (SPC), round spermatids (RS), elongating spermatids (ES) and spermatozoa (spz). No differences in germ cell type composition and spatial organization were detected in CCP5^{+/-} tubules (Fig. 4.3 E and F) as compared to wild type. In contrast, CCP5^{-/-} testicular tissue was characterized by several histological alterations. Although I observed germ cells at all the different developmental stages (Fig 4.3 H), cellular organization was slightly disorganized compared to control animals with ectopically located elongating spermatids (long arrows, Fig 4.3 I and M). Moreover multinucleated cells, which appear to be haploid cells, were often observed near the

luminal edge of the seminiferous tubules (dashed boxes, Fig 4.3 L and M). In general, the overall cytoarchitecture of $CCP5^{-/-}$ seminiferous tubules were characterized by a larger amount of cytoplasm compared to control and $CCP5^{+/-}$ testes (bracket, Fig 4.3 N).

To check whether spermatogenic failures worsened over time I compared histological sections from one-year-old $CCP5^{-/-}$ and control littermates (Fig 4.4). Interestingly, I did not observe a more severe phenotype in 1-year-old mutant testes compared to 4 month-old ones.

Considering that none of the germ cell types is missing in the mutant seminiferous epithelium, it is possible to presume that infertility in $CCP5^{-/-}$ males might be due to defects in post-meiotic cells. The presence of immature germ cells in the mutant semen suggests that the lower sperm production is a consequence of a defective differentiation of round spermatids into spermatozoa during spermiogenesis. However, the observation of multinucleated cells suggests a possible failure in late phases of round spermatids cytokinesis and/or spindle orientation as well. For my PhD project, I decided to focus my interest on the causes leading to defects in the spermiogenesis phase, rather than on the meiotic phase.

To verify whether heterozygous sperm cells show flagellar motility defects I analyzed sperm motility parameters by computer aided sperm analysis (CASA) on at least 200 $CCP5^{+/+}$ (N=2 mice) and $CCP5^{+/-}$ (N=1 mouse) epididymal spermatozoa. No differences were detected in all analyzed parameters (Fig 4.5), suggesting that one copy of $CCP5$ allele is sufficient to guarantee normal sperm functions. As I did not observe major defects in heterozygous spermatozoa and testes, for the rest of the study we focused on $CCP5^{+/+}$ and $CCP5^{-/-}$ mice. However, it would be important to consolidate the CASA analysis by studying a higher number of $CCP5^{+/-}$ mice in order to better exclude the presence of an intermediate motility phenotype

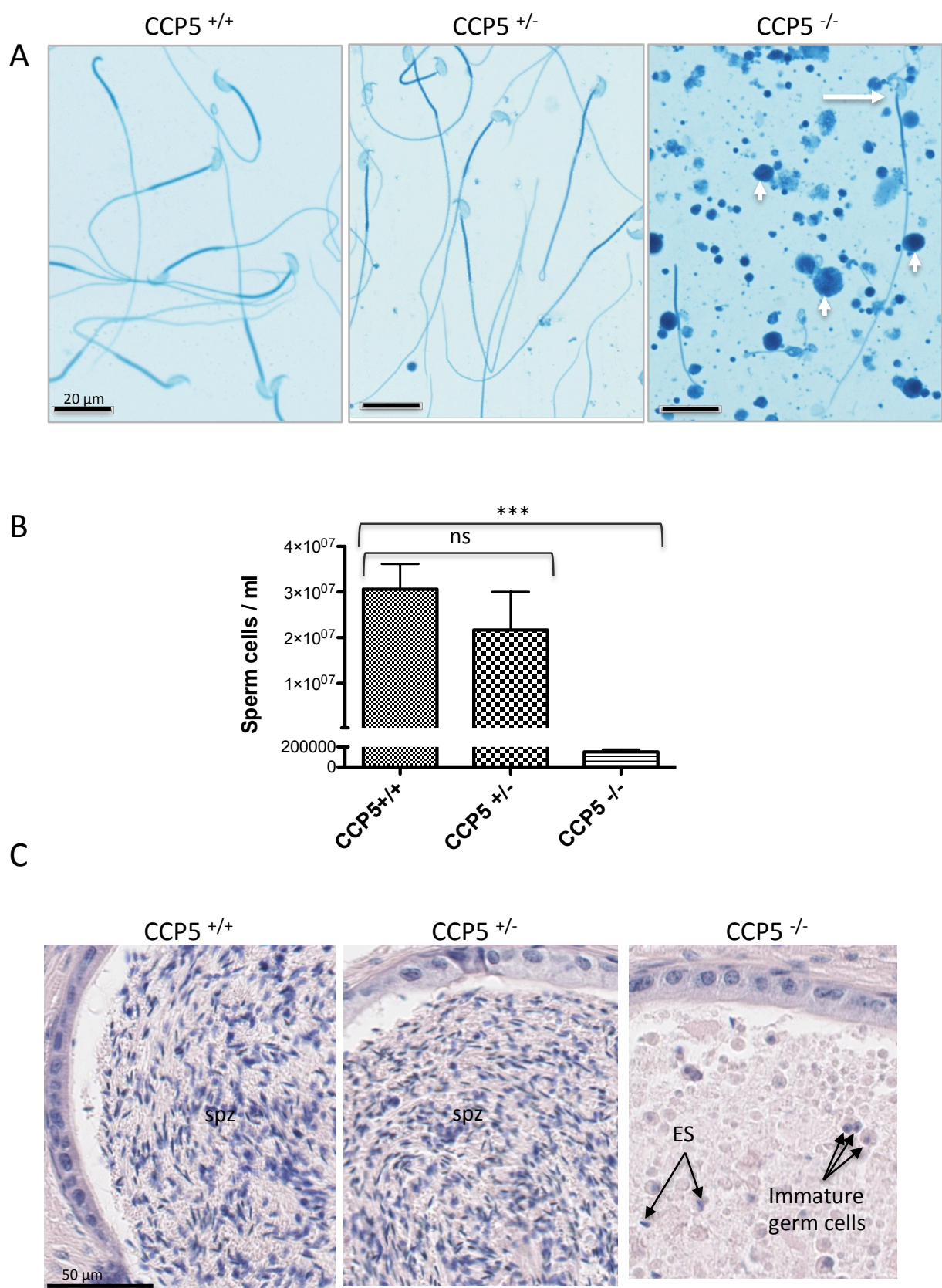
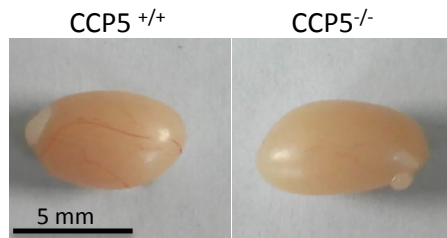
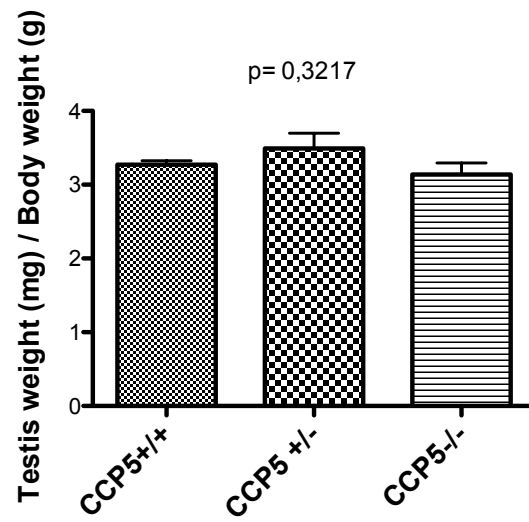


Figure 4.1: Poor sperm production in CCP5 $^{-/-}$ mice. (See figure legend at page 94)

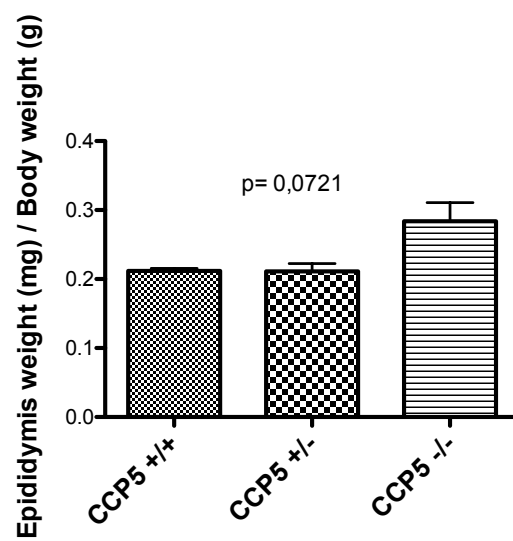
A



B



C



D

Freq. observed/genotype (%)

(**)

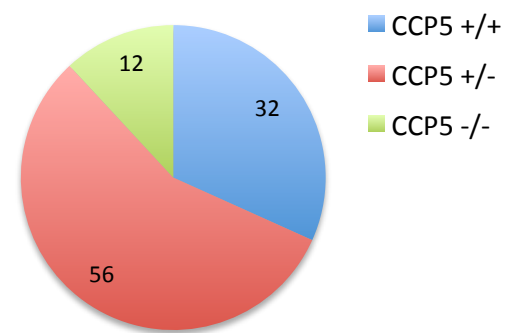


Figure 4.2: Infertility in CCP5^{-/-} mice. (See figure legend at page 94)

Figure 4.1: Poor sperm production in CCP5^{-/-} mice.

A) Coomassie-blue stained epididymal sperm smears from CCP5^{+/+}, CCP5^{+/-} and CCP5^{-/-} animals (n=3). While CCP5^{+/+} and CCP5^{+/-} males show normal-looking sperm, almost no sperm is found in CCP5^{-/-}. The long white arrow indicates a rare spermatozoon. Short white arrows indicate immature germ cells. Scale bars, 20 μ m. (B) Sperm cells concentration (n° sperm cells/ml) in semen of adult CCP5^{-/-} (n=5), CCP5^{+/-} (n=3) and CCP5^{+/+} (n=3) male littermates. Values are expressed as the means \pm SEM. Unpaired two-tailed t-test revealed statistically significant differences in sperm concentration between control and CCP5^{-/-} (***) P=0,0003), whereas no significant differences were obtained between control and CCP5^{+/-} mice (ns, P=0,4244). (C) Hematoxylin and Eosin staining of epididymal cross-sections. Note the presence of immature spermatozoa (Spz= spermatozoa, ES= elongating spermatids). Scale bars, 50 μ m

Figure 4.2: Infertility in CCP5^{-/-} mice. (A) Gross appearance of dissected wild type and CCP5^{-/-} testis. Scale bar, 5 mm. (B) Relative testis weight (value of the mean of two testes) to body weight of CCP5^{+/+} (n=3), CCP5^{+/-} (n=3) and CCP5^{-/-} (n=4) animals. Numbers are expressed as mean \pm SEM. One-Way ANOVA revealed no statistically significant differences between the three genotypes (P=0.3217, ns). (C) Relative epididymis weight (value of the sum of two cauda epididymis) to body weight of CCP5^{+/+} (n=3), CCP5^{+/-} (n=3) and CCP5^{-/-} (n=5) animals. One-Way ANOVA revealed no statistically significant differences between the three genotypes (p=0.07). (D) Observed frequency of offspring genotypes in CCP5^{-/-} mouse line. The observed frequencies were calculated on 378 mice from the CCP5 KO colony. Only mice born from crossing between heterozygous mice were considered in this study. CHI-SQUARE test revealed a non-Mendelian genotype ratio (**, P=0.009; df=2).

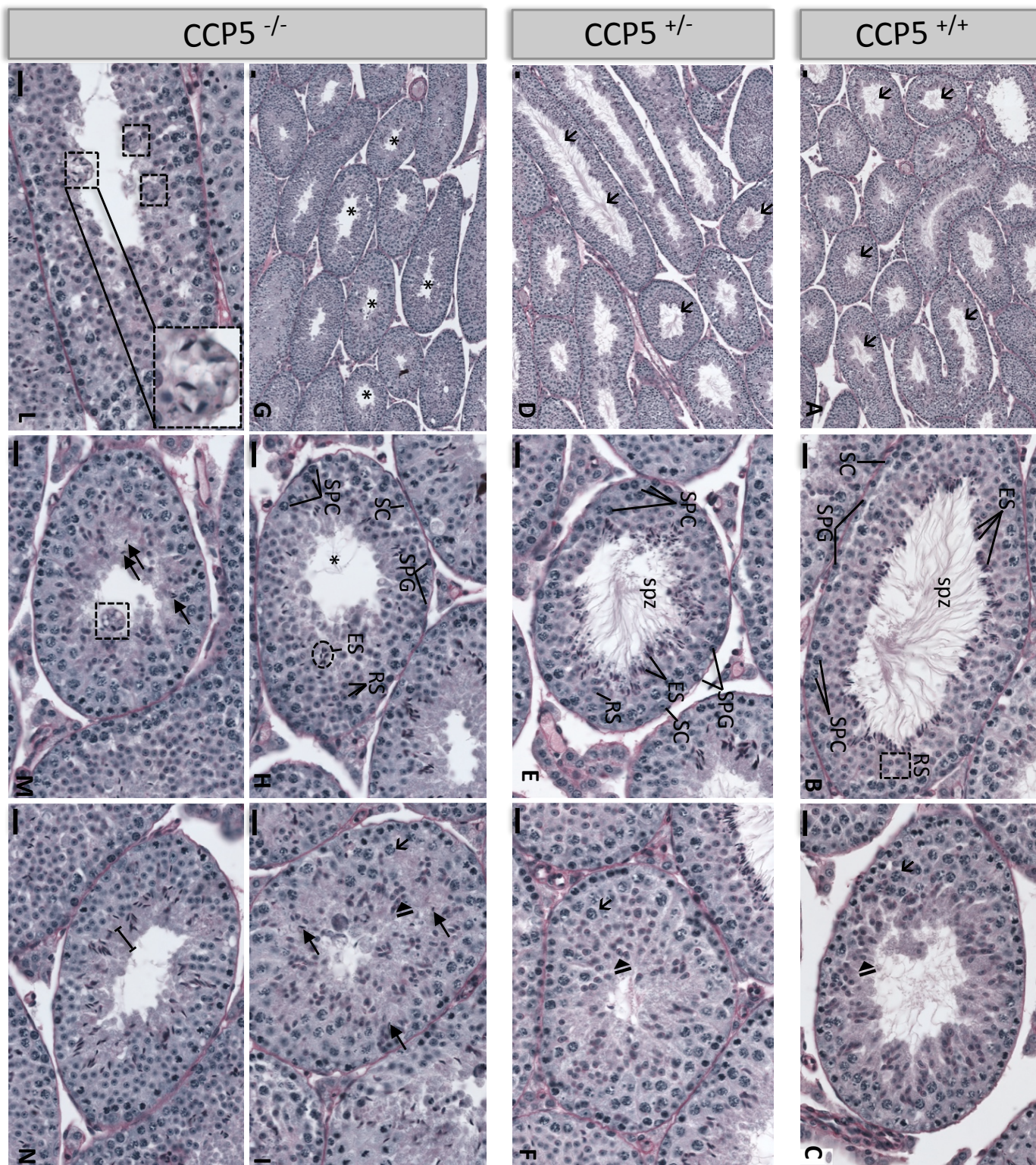


Figure 4.3: Disorganized testis cytoarchitecture in 4-months-old CCP5 ^{-/-} mice. (See figure legend at page 97)

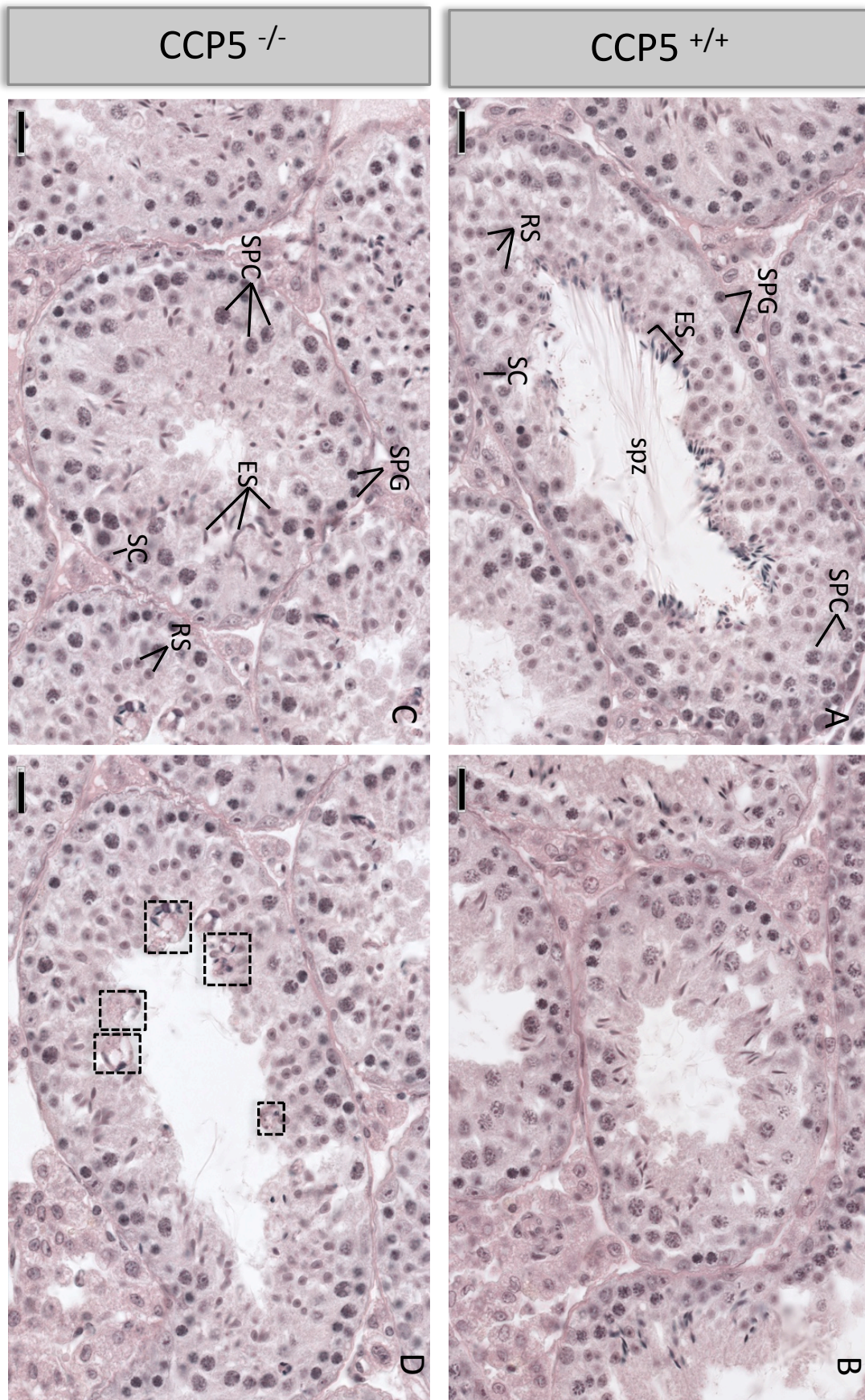


Figure 4.4: Histological examination of 1-year-old CCP5 ^{-/-} testis: Absence of age-related pejorative phenotype. (See figure legend at page 97)

Figure 4.3: Disorganized testis cytoarchitecture in 4-months-old CCP5 ^{-/-} mice. Periodic acid-Schiff (PAS) staining of paraffin-embedded testis cross-sections. SPC= spermatocytes, SPG= spermatogonia, RS= round spermatids, ES= elongating spermatids, SC= Sertoli cells, spz= spermatozoa. Scale bar is 20 μ m. (A) Lower magnification of CCP5^{+/+} seminiferous epithelium showing tubules containing a great amount of sperm cells (arrows). (B) Control tubule in spermiation composed of all different germ cell types. From the base to the apex: Sertoli cell and spermatogonia, spermatocytes, round spermatids, elongating spermatids and spermatozoa. (C) Control tubule at later stages showing early elongating spermatids (arrowhead) and spermatocytes (arrow). (D) CCP5^{+/+} seminiferous tubules are filled of spermatozoa (arrows). (E-F) No differences are found in the cell composition and organization between CCP5^{+/+} and control tubules. Arrowhead indicates early elongating spermatids; spermatocytes are marked with an arrow. (G) Lower magnification of CCP5^{-/-} seminiferous tubules showing empty tubules (asterisks). (H-I): No differences in cell composition but slight disorganized cytoarchitecture is found in CCP5^{-/-} seminiferous tubules. The asterisk indicates few sperm cells in the lumen, arrowheads show early elongating spermatids; the short arrow indicates spermatocytes and long arrows illustrate mislocated elongating spermatids. (L-M) Presence of multinucleated cells in CCP5^{-/-} testis (dashed box). Note the presence of ectopic elongating spermatids in (M) (arrows). (N) CCP5^{-/-} seminiferous tubules are characterized by a greater amount of cytoplasm (bracket) compared to wild type

Figure 4.4: Histological examination of 1-year-old CCP5 ^{-/-} testis: Absence of age-related pejorative phenotype. Hematoxylin Eosin staining of paraffin-embedded testis cross-sections. SPC= spermatocytes, SPG= spermatogonia, RS= round spermatids, ES= elongating spermatids, SC= Sertoli cells, spz= spermatozoa. Scale bar is 20 μ m. (A, B): control seminiferous tubules showing germ cells at different developmental stages. (C) None of the different germ cell types is lost in aged CCP5^{-/-} mice compared to control (A). (D) Presence of multinucleated germ cells in CCP5^{-/-} testis (dashed boxes).

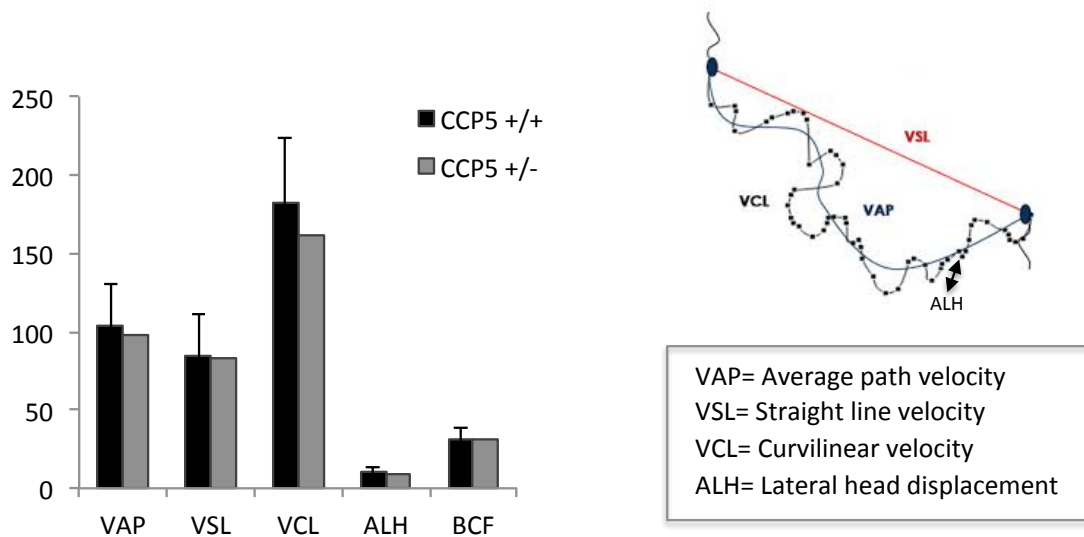


Figure 4.5 Motility analysis of CCP5^{+/-} spermatozoa. Computer Assisted Sperm Analysis (CASA) was conducted at least on 200 sperm cells per sample. CCP5^{+/+}: N=2, CCP5^{+/-}: N=1. Data are shown as means \pm SD. No differences in any of the analyzed parameter was detected between CCP5^{+/+} and CCP5^{+/-} spermatozoa.

4.2 High CCP5 expression levels in wild type testicular tissue

Before analyzing the posttranslational modification pattern profile of CCP5^{-/-} testicular germ cells, I decided to perform an extensive study of the expression pattern profile of genes for deglutamylases, glutamylases and glycyllases in testes, as well as in the different type of testicular germ cells from wild type animals.

Expression levels of CCPs and some TTLLs in several murine tissues were previously studied in our lab using qPCR analysis. Interestingly, although CCP5 is a broadly expressed enzyme, its expression level appears to be particularly high in testis compared to the other organs (Fig 4.6). This already suggests a particularly important role of this deglutamylase in spermatogenesis. Among the other analyzed enzymes, CCP1 and TTLL5 show a high expression level in the testis (Fig 4.7) accordingly to their importance in spermatogenesis that has been proved by the analysis of CCP1-mutant *pcd* mouse (Handel & Dawson M. 1981, Kim et al 2011) and TTLL5 KO (Lee et al 2013) mice. However, it is important to note the relatively low expression level of TTLL1 in the testis (Fig 4.7), an enzyme that has been shown to be important for sperm formation (Campbell et al 2002, Vogel et al 2010).

To study TTLLs and CCPs expression level during the different steps of spermatogenesis, I performed qPCR analysis in wildtype spermatocytes (N=4 mice), round spermatid (N=5 mice), elongating (N=3 mice) and condensed spermatids (N=4 mice). The different cell populations were obtained by cell fractionation using a BSA-based density gradient. In general, the overall expression levels of glutamylases, deglutamylases and glycyllases increase during germ cell development with relatively lower expression in spermatocytes and round spermatids and maximal relative expression in elongating condensed spermatids (Fig 4.8, blue histogram). Among CCP enzymes, CCP5 appears to be highly

expressed starting from spermatocytes and its expression increases in elongating and condensed spermatids (Fig 4.8, blue histograms).

To check whether lack of CCP5 could lead to up/down regulation of other CCPs and/or TTLLs enzyme, I performed qPCR from testicular fractionated cells obtained from CCP5^{-/-} testis (N=1). As I did not observe any evident difference in expression levels of CCPs and TTLLs between CCP5^{+/+} and CCP5^{-/-} germ cell (Fig 4.8), we decided to not repeat the experiment considering the very low probability of finding different results, and the limited number of CCP5^{-/-} animals available for other experiments.

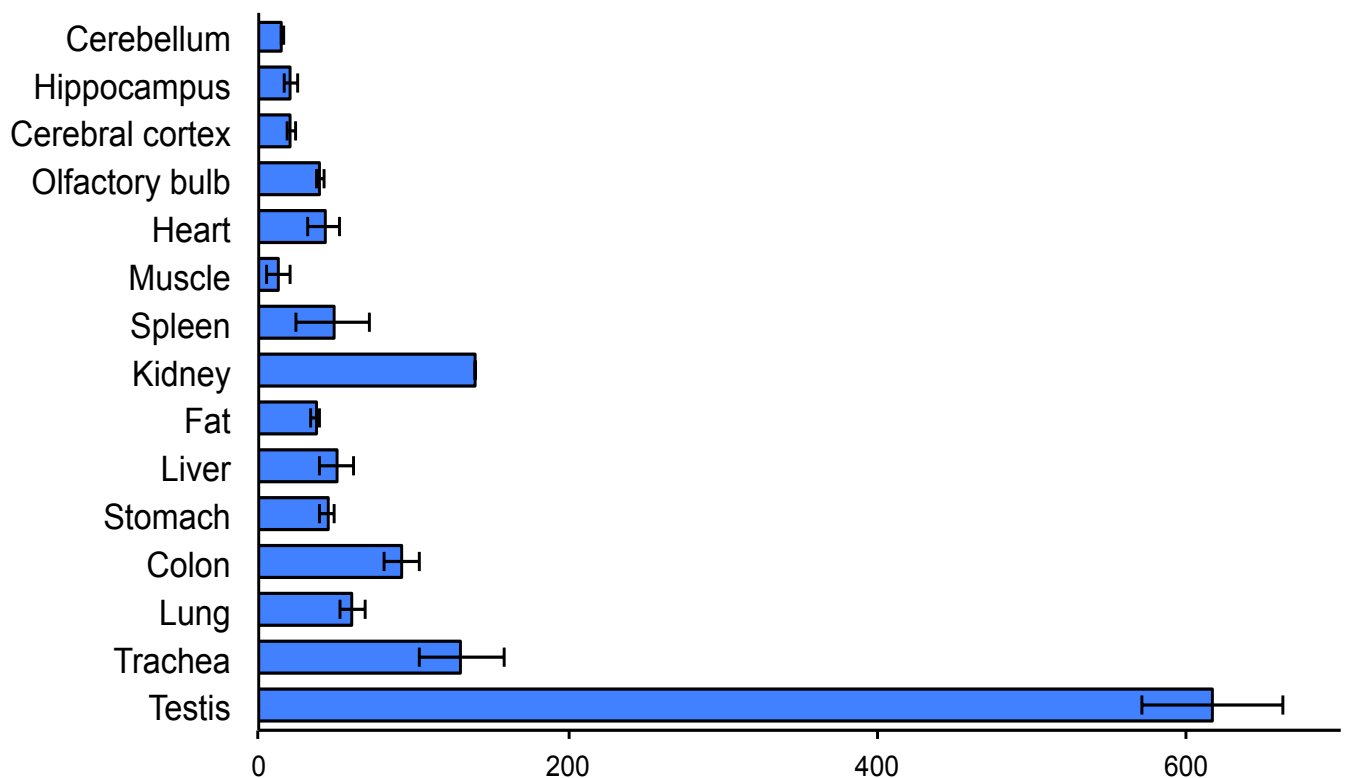


Figure 4.6: Relative expression levels of CCP5 in wild type adult murine tissues.

Expression levels of CCP5 were analyzed with quantitative RT-PCR (qPCR). The values were standardized to the expression levels of TATA binding protein (TBP) gene, N=5. Values indicate means \pm SDV

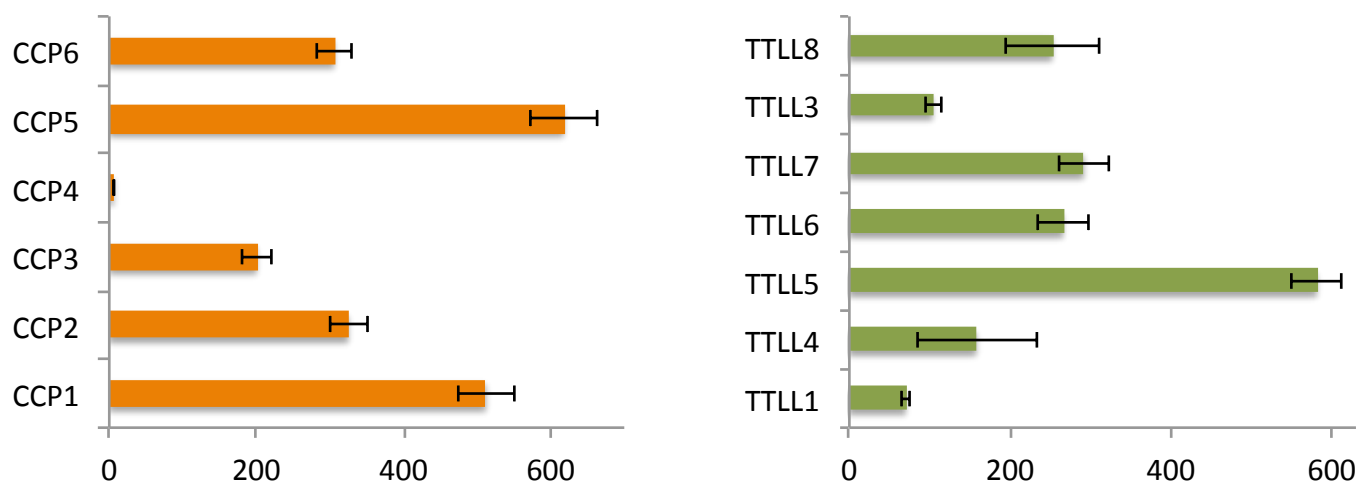


Figure 4.7: Expression levels of selected CCPs and TTLLs in wild type mouse testis. Expression levels of different CCP and TTLL genes were determined by qPCR, and standardized to the expression levels of the TATA binding protein (TBP) gene. Data are expressed as mean \pm SDV (N=4).

4.5 CCP5^{-/-} elongating spermatids are characterized by supernumerary basal bodies.

The observation that MTs forming the hair-like structure were never detected with anti-tubulin antibody in wild type elongating spermatids suggest that those MTs are either specifically nucleated in the CCP5^{-/-} either not disassembled. To check this hypothesis, I performed γ -tubulin immunostaining on testicular dissociated cells to visualize basal bodies in elongating spermatids. Interestingly I observed multiple γ -tubulin-positive spots in CCP5^{-/-} elongating spermatids, whereas only one or two γ -tubulin positive spots were detected in control cells (Fig 4.14). In both samples, I sometimes observed a single, but larger positive spot, most probably due to the presence of clustered centrioles (data not shown).

I next confirmed the presence of multiple basal bodies by electron microscopy analysis of serial sections from CCP5^{-/-} testis (Fig 4.14 B). Quantification of elongating spermatids bearing supernumerary basal bodies revealed a statistically significant difference in the percentage of positive cells between control and CCP5^{-/-} elongating spermatids (Fig 4.14 C). Indeed, while only about 5% of control spermatids have more than two γ -tubulin-positive spots, I counted about 63% of CCP5^{-/-} elongating spermatids bearing multiple basal bodies (*** P=0.004). No statistically significant difference was detected in spermatids with bigger γ -tubulin-positive spots, which are presumably clustered basal bodies.

Taken together these results suggest that CCP5 is important for the regulation of generation and/or repartition of centrioles during spermatogenesis. Moreover, MTs forming the hair-like structures could be a direct consequence of the presence of multiple basal bodies in the cell.

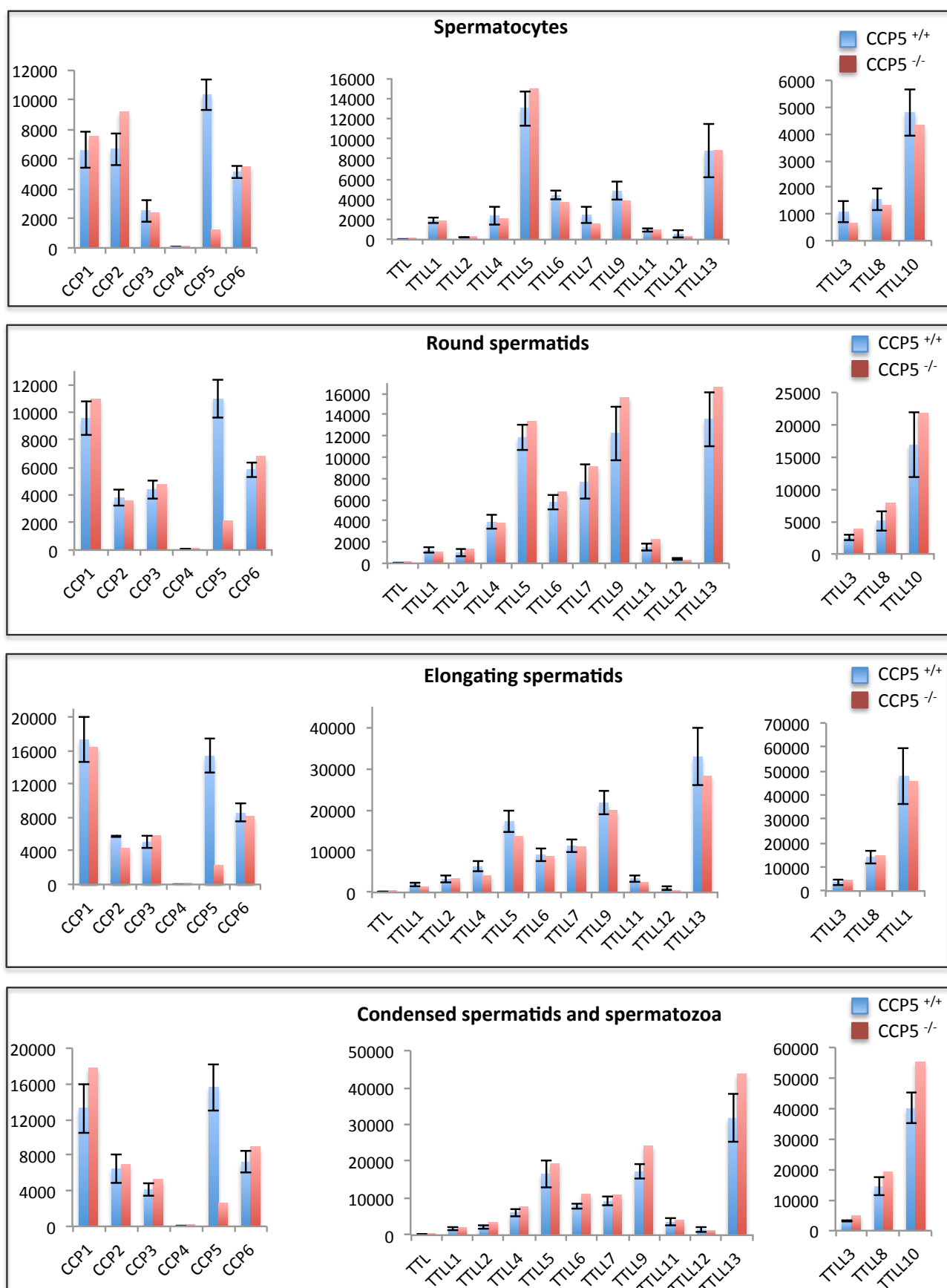


Figure 4.8 Absence of up- or down-regulation of expression levels TLLs and CCPs in CCP5^{-/-} testicular germ cells. (See figure legend at page 104)

Figure 4.8 Absence of up- or down-regulation of expression levels TTLLs and CCPs in CCP5^{-/-} testicular germ cells. Testicular germ cells were fractionated using a BSA density gradient in order to obtain cell population of CCP5^{-/-} (N=1) and CCP5^{+/+} spermatocytes (N=4), round spermatids (N=5), elongating spermatids (N=3) and condensed spermatids together with spermatozoa (N=4). Expression levels of all genes were analyzed by qPCR and standardized to the TATA binding protein gene. Data indicate that no major changes in expression level of CCPs and TTLLs occurs in CCP5^{-/-} cells. Values indicate means \pm SDV Deglutamylases are shown in the left histograms, glutamylases in the center and glycyases in the right histograms

4.3 CCP5^{-/-} testicular germ cells present increased tubulin PTMs levels.

To understand how tubulin glutamylation regulates spermatogenesis, I analyzed the evolution of posttranslational modifications of wild type and CCP5^{-/-} germ cells during germ-cell development (Fig 4.9A). Glutamylation was analyzed by immunoblot using GT335 and poly E antibody. In the wild type, glutamylation is first detected by GT335 antibody at α -tubulin of elongating spermatids, and an even stronger signal in condensed spermatids. The presence of a faint polyE-positive α -tubulin band suggests that round spermatids are weakly polyglutamylated. Interestingly, a non-tubulin substrate appears to be glutamylated in elongating and condensed wild type spermatids (*, Fig 4.9A). Similar to glutamylation, monoglycylation also appears first in elongating spermatids, and is detected on both α - and β - tubulin as well as in the non-tubulin substrate (*, Fig 4.9A). In condensed spermatids, monoglycylation is no more detected in α -tubulin. There is a possibility that monoglycylation gets converted to polyglycylation at this step. However unfortunately I was not able to obtain a readable immunoblot for polyglycylation, thus will be necessary to repeat the experiment in the future. Interestingly, CCP5^{-/-} testicular germ cells appear to be strongly glutamylated as well as glycylation at earlier developmental stages (Fig 4.9 A). Both GT335 and polyE detect α -tubulin as well as the non-tubulin substrate throughout the whole germ cell development in these mice (*, Fig 4.9A). Strikingly, the GT335 signal in CCP5^{-/-} elongating spermatids is stronger than in controls, whereas the polyE signal does not increase significantly. Monoglycylation is also first detected in spermatocytes, with an overall increased signal thorough development. Moreover, the non tubulin-substrate, which is glycylation in wild-type elongating spermatids, is not anymore detectable with pep1G antibody in CCP5^{-/-} elongating spermatids. To verify that the new observed non-tubulin substrate is not a version of α -tubulin migrating slower on the SDS-PAGE, I performed a “1-band Immuno-blot assay” in wild type and CCP5^{-/-} round spermatids

extract (Fig 4.9 B). This confirmed that the anti α -tubulin antibody does not detect the extra protein band, which is thus most likely another substrate of glutamylation and glycylation. It is important to point out that GT335 antibody recognizes glutamate side chains regardless their length, whereas polyE detects specifically long glutamate chains of three and more glutamates. Thus, I concluded from the immunoblot analyses that in CCP5^{-/-} mice, germ cells are getting strongly glutamylated at earlier developmental stages and present an increased level of short glutamate side chains compared to control. Despite tubulin glutamylation and glycylation have been so far considered as inversely correlated, here I show an overall increase in both modification levels. Moreover, the observed changes of modification pattern profiles of the non –tubulin substrate protein suggest that other proteins might regulate spermatogenesis via their glutamylation/glycylation status.

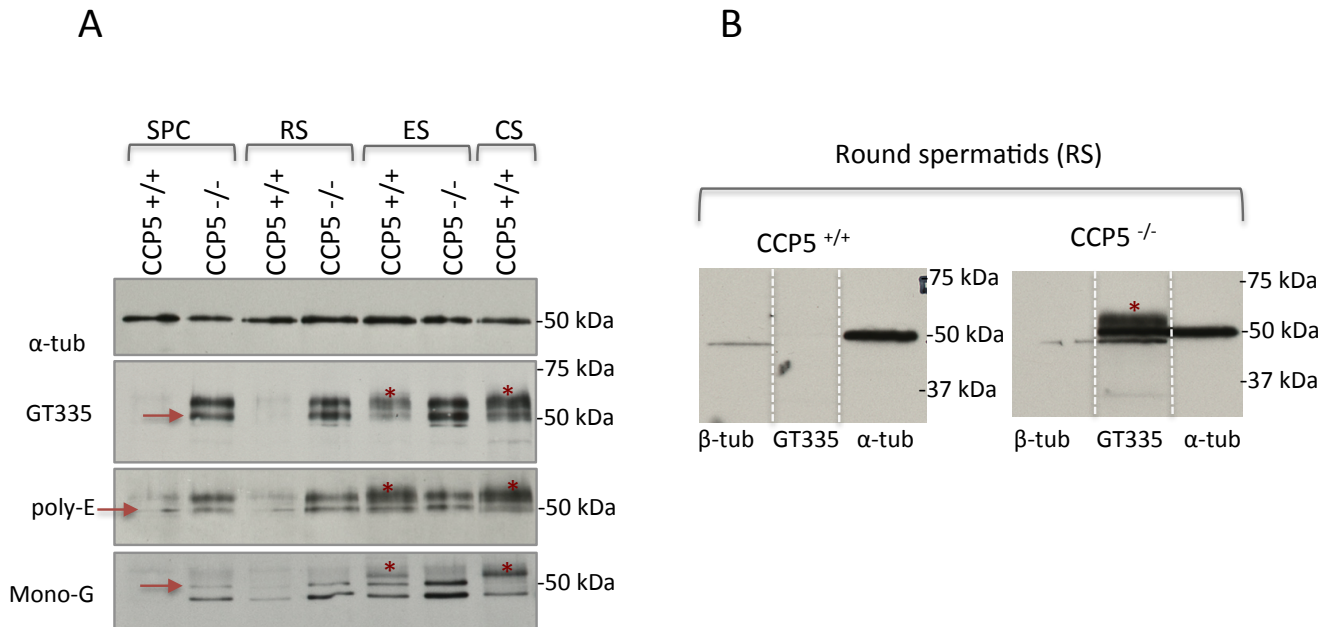


FIG 4.9: Analyses of tubulin PTMs in testicular fractionated cells. (A) Immunoblot analysis of extract from fractionated spermatocytes (SPC), round spermatids (RS), elongating spermatids (ES) and condensed spermatids (CS) from CCP5^{+/+} and CCP5^{-/-} testes. GT335 antibody detects glutamylation regardless the glutamate side chain length. PolyE antibody is specific for long glutamate side chains. Mono-G is monoglycylation, and polyG polyglycylation. Arrows indicate α-tubulin; asterisks indicate a non-tubulin substrate. (B) Immunoblot analysis of wild type and CCP5^{-/-} round spermatid extracts confirming the presence of a glutamylated non-tubulin substrate. Samples were loaded into 2,5-cm large wells, separated on a 10-cm SDS-PAGE, and transferred to nitrocellulose membrane. Each lane was separated into 3 stripes, which were incubated respectively with anti β-tubulin, anti glutamylation (GT335) and anti α-tubulin antibody. Before visualizing of the antibody signals, the original lanes were reconstituted by re-assembling the membranes. Note that in the CCP5^{-/-} spermatids, the lower GT335-positive band is identical with the alpha-tubulin band, whereas the upper band (asterisk) is not alpha-tubulin. Note also that the beta-tubulin antibody did not work very well in these conditions

4.4 CCP5^{-/-} spermatids are characterized by several morphological defects and overall increased level of tubulin PTMs

I next wanted understand which subcellular structures are glutamylated in wild type germ cells and whether changes in tubulin glutamylation might interfere with germ cells morphology. Thus I performed an immunofluorescence analysis of glutamylation on testicular dissociated cells using GT335 antibody (Fig 4.10). Pachitene cells do not show a distinct glutamylation signal, and no difference in their morphology and modification signal were detected between CCP5^{-/-} and control cells. However, immunoblot analysis of fractionated CCP5^{-/-} spermatocytes revealed an increase in glutamylation (Fig 4.9 A). In this regard is important to point out that germ cell fractionation does not allow to obtain a 100% pure population of cells. Indeed spermatocytes-fraction contains also some contaminating round spermatids. Thus, as I never observed by immunofluorescence such glutamylation positive signal and because of the important increase of glutamylation in CCP5^{-/-} round spermatids fraction, I conclude that the observed increased glutamylation signal observed in CCP5^{-/-} spermatocytes by western blot analysis is most-likely due to the presence of contaminating CCP5^{-/-} round spermatids in the fraction.

The first obvious differences appear at the state of round spermatids. Wild type round spermatids are not glutamylated, except for the axoneme that is detectable in some cells. Interestingly, CCP5^{-/-} round spermatids are characterized by a cortical array of glutamylated MTs that was rarely observed in control cells (Fig 4.10). As expected manchette of elongating spermatid is glutamylated in both, wild type and CCP5^{-/-} mice, however a group of MTs located caudally to the manchette is specifically modified specifically in the mutant cells, whereas similar arrays are not found in wild type cells. These MTs form a “hair-like” structure at the caudal pole of the nucleus, where the axoneme is supposed to assemble (Fig 4.10). When present, the developing axoneme is

modified but subjected to several aberrations such as tail coiling (Fig 4.10) and / or organization in multiple flagella (data not shown). Moreover, the immunofluorescence analysis of testicular dissociated cells reveals the presence of aberrant shaped nuclei in CCP5^{-/-} spermatids that do not show the typical nuclear hook-like shape of CCP5^{+/+} spermatids (Fig 4.10).

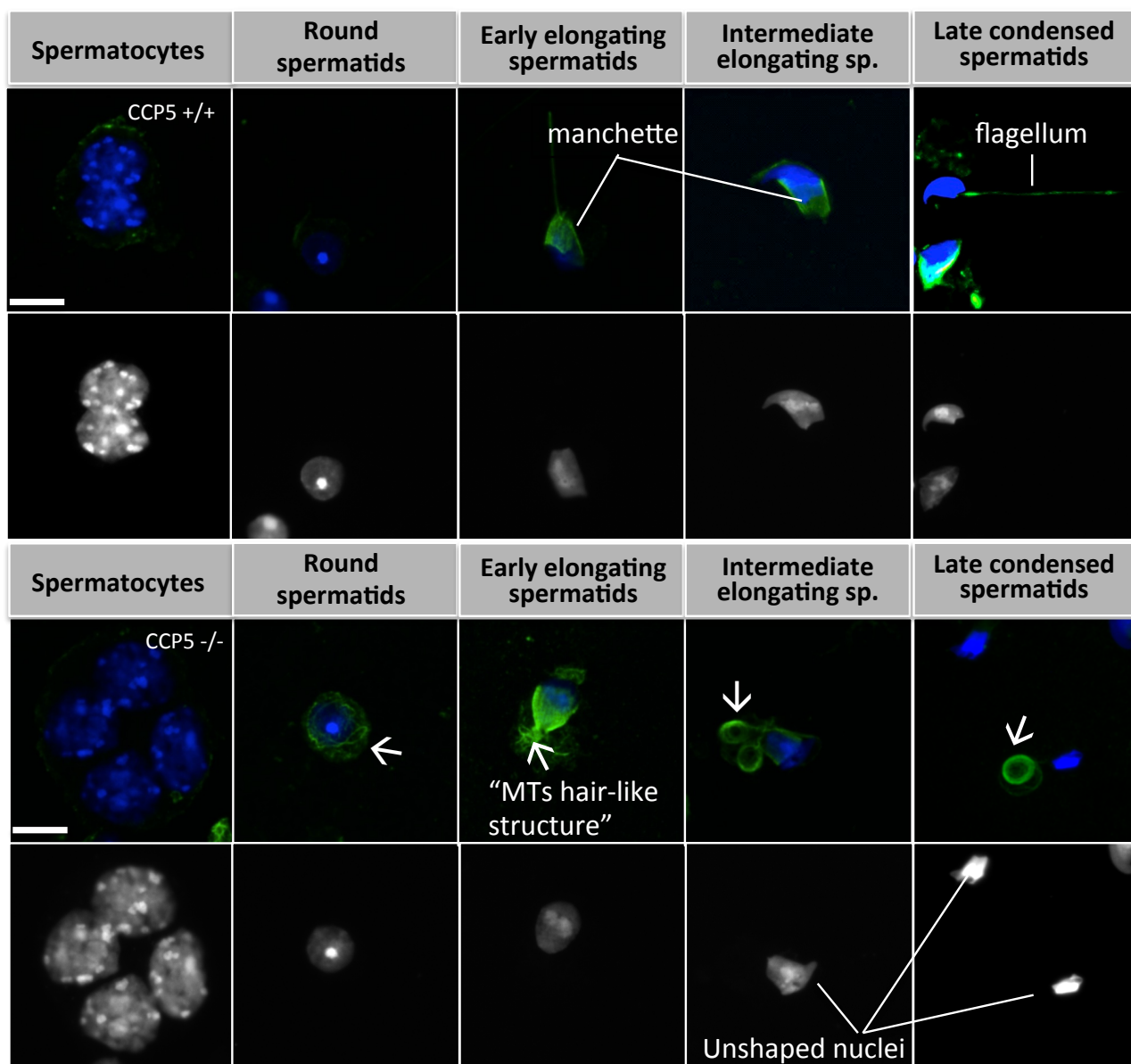


FIG 4.9: Localisation of glutamylated tubulin in CCP5^{+/+} and CCP5^{-/-} testicular dissociated cells. Wild type testicular cells are imaged in the top panel. CCP5^{-/-} cells are shown in the bottom panel. The first range in each panel shows merge images; GT335 antibody was used to detect glutamylation (green). Nuclei were stained with DAPI (blue), and are shown separately in the second range to better visualize the nuclear shapes of the spermatids. Scales bar are 10 μ m. In the CCP5^{+/+}, glutamylation is first detected in elongating spermatids at the manchette and flagellum. In CCP5^{-/-}, glutamylation is detected at earlier step of spermatogenesis (arrow, round spermatids). There is an ectopic presence of extra MTs located basally to the manchette forming hair-like structures (arrow in CCP5^{-/-} early elongating spermatids). Coiled flagella were observed in CCP5^{-/-} intermediate elongating and condensed spermatids (arrows). Moreover, the nuclear shape is abnormal in CCP5^{-/-} spermatids

Next, I wanted to investigate if the modified MTs observed in CCP5^{-/-} round and elongating spermatids are specifically generated in the mutant cells, or whether these MTs are also present in CCP5^{+/+} cells, but not glutamylated. To assess this question I performed immunostaining on testicular dissociated cells using anti-tubulin antibodies together with the polyE antibody. As several tubulin populations coexist within a single cell I analyzed the expression profile of tubulin glutamylation and α -, β 2- or β 3- tubulin in order to understand which specific tubulin population characterize the modified MTs observed in the mutant spermatids. CCP5^{+/+} and CCP5^{-/-} round spermatids are characterized by α - and β 2-tubulin positive cortical array of MTs (respectively Fig. 4.11 A, B). β 3-tubulin was slightly detected in CCP5^{-/-} round spermatids, but not in controls (Fig 4.C). As expected, tubulin glutamylation was detected only on CCP5^{-/-} round spermatids (Fig 4.11 A, B, C). In wild type spermatids α - and β 2-tubulin stain manchette MTs through their entire length (Fig 4.11 A, B), whereas the β 3-tubulin signal is not detected in manchette MTs situated caudally to the base of the nucleus (Fig 4.11 C). Interestingly glutamylated MTs forming the hair-like structure are exclusively detected by α - and β 2-tubulin antibodies in CCP5^{-/-} elongating spermatids (Fig 4.11 A, B). As those MTs have been never detected in the CCP5^{+/+} I concluded that MTs forming the hair like structure are a typical features of CCP5^{-/-} spermatids. Altogether these data suggest that while in mutant round spermatids cortical MTs are getting glutamylated, mutant elongating spermatids are characterized by a CCP5^{-/-}-specific subpopulation of glutamylated MTs organizing a MT-hair like structure at the base of the nucleus.

In conclusion, the study of glutamylation pattern in dissociated testicular germ cells of CCP5^{-/-} mice revealed several exciting phenotypes:

- Cortical MTs are strongly glutamylated in round spermatids

- Extra MTs are organized in hair-like structure at the base of the nucleus in elongating spermatids
- Malformed/coiled flagella are found in condensed spermatids
- Aberrant nuclear shape in elongating spermatids is prevalent in CCP5^{-/-} mice

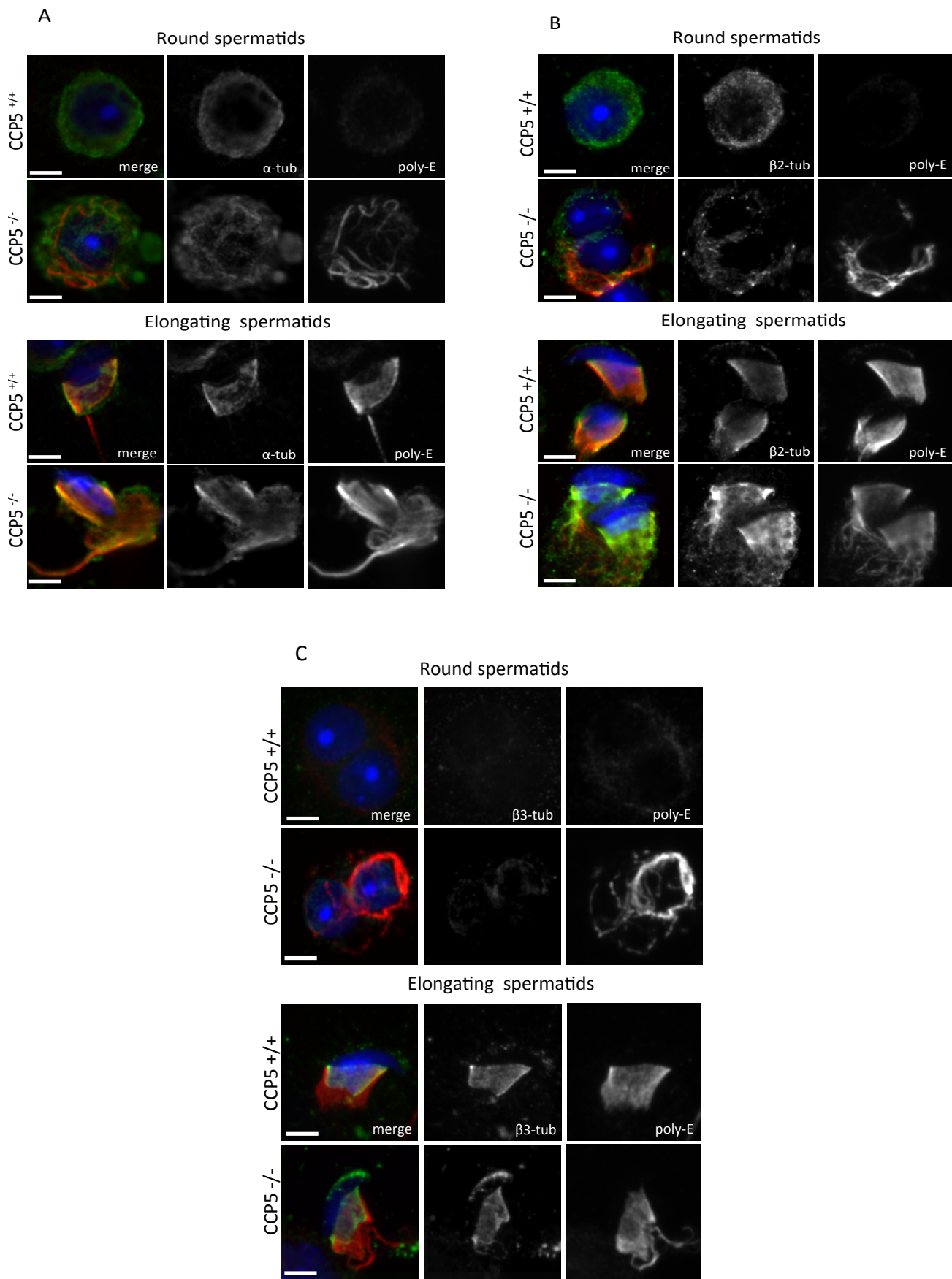


Figure 4.10: Tubulin and polyglutamylation signals in round and elongating spermatids in CCP5^{+/+} and CCP5^{-/-} mice. (See figure legend at page 114)

Figure 4.10: Tubulin and polyglutamylation signals in round and elongating spermatids in CCP5^{+/+} and CCP5^{-/-} mice. Signal for polyglutamylation (detected with polyE antibody) is in red, tubulin is shown in green and DAPI is in blue. Scale bar is 5 μ m. (A) α -tubulin and polyglutamylation localization in round and elongating spermatids from wild type and CCP5^{-/-} testicular dissociated cells. (B) Immunolocalisation of β -2-tubulin and polyglutamylation in round and elongating spermatids from CCP5^{+/+} and CCP5^{-/-} testicular dissociated cells. (C) Immunolocalisation of β -3-tubulin and polyglutamylation in round and elongating spermatids from control and CCP5^{-/-} testicular dissociated cells. Note that β 3 tubulin staining is restricted to manchette MTs, whereas α - and β 2-tubulin stain round spermatids cortical MTs and manchette in wild type and CCP5^{-/-} spermatids. None of the utilized tubulin antibodies reveals the presence of ectopic MTs located caudally to the manchette of wild type spermatids

I next decided to quantify the above-described phenotypes for CCP5^{-/-} and CCP5^{+/+} testicular germ cells (Fig 4.12). Testicular dissociated cells from control and CCP5^{-/-} mice were stained with DAPI to distinguish elongating spermatids nuclear shape, and with GT335 antibody to visualize the other phenotypes to be analyzed.

I observed that in CCP5^{-/-} mouse about 70% of round spermatids are glutamylated, whereas I counted only about 13% of positive cells in the control (Fig 4.12 A).

Among CCP5^{-/-} early and intermediate elongating spermatids, I observed respectively about 70 % and 65% of cells showing the MTs hair-like structure. In the control I counted respectively only about 6% and 1.6 % of defective early and intermediate elongating spermatids (Fig 4.12B, C).

For the analysis of flagellar phenotype I decided to divide condensed spermatids in 3 categories based on their flagellar morphology: cell with a normal flagellum, cells with a coiled flagellum and cells with malformed flagella. In the latter category, I considered all cells with multiple or malformed flagella (Scheme- Fig 4.12 D). Only about 8% of coiled flagella and 6% of malformed flagella were detected in CCP5^{+/+} condensed spermatids, whereas in the CCP5^{-/-} I observed 35% of coiled- and about 60% of malformed flagella (Fig 4.12 D).

Finally, to assess the frequency of aberrantly shaped nuclei, I divided elongating spermatids based on their nuclear morphology: normal nuclei (with typical hook-like shape), wider nuclei and longer and/or curved nuclei presenting a bulb-like shape in their apical pole (Fig 4.12E). While almost 90% of the analyzed CCP5^{-/-} cells had aberrant nuclear shape (respectively 50% and about 40% of wider and longer/curved nuclei), only about 11% of wider nuclei and 8% of longer one were detected in control spermatids.

Globally, the low penetrance of the analyzed phenotypes in control germ cells compared to CCP5^{-/-} suggests that the absence of CCP5, and the resulting changes in MT

glutamylation are most likely the cause of the observed phenotypes in the $CCP5^{-/-}$ testicular germ cells.

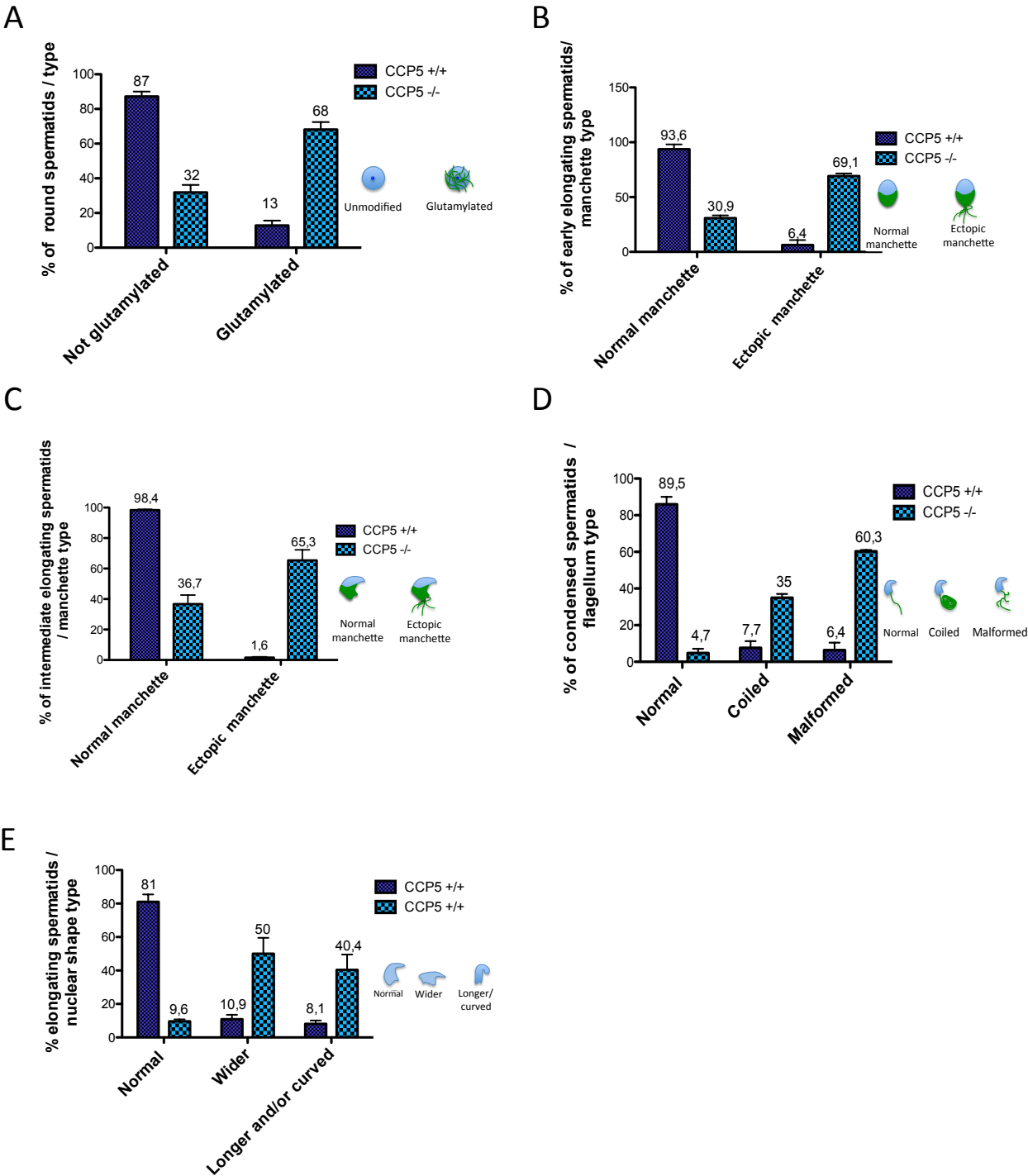


Figure 4.12: Augmented frequency of defective germ cells in $CCP5^{-/-}$ mice. (See figure legend at page 117)

Figure 4.12: Augmented frequency of defective germ cells in CCP5^{-/-} mice.

(A) Premature glutamylation of round spermatids in CCP5^{-/-} mice. Percentage of observed glutamylated and unmodified round spermatids in wild type and CCP5^{-/-} mice (N=3). Data are expressed as means \pm SEM. (B-C) Higher frequency of elongating spermatids showing a MT hair-like structure caudally to the manchette (indicated as ectopic manchette). Percentage of early (B) and intermediate (C) elongating spermatids showing an ectopic manchette in CCP5^{+/+} (N=3) and CCP5^{-/-} (N=3) mice. Data are expressed as means \pm SEM. (D) Higher incidence of coiled and malformed flagella in CCP5^{-/-} condensed spermatids compared to wild type spermatids. Data are shown as means \pm SEM (N=3). (E) Presence of a high frequency of misshaped nuclei in CCP5^{+/+} and CCP5^{-/-} elongating spermatids. Data are shown as means \pm SEM (N=3).

As I had observed changes both in tubulin glutamylation levels and glutamylation cellular localization in $CCP5^{-/-}$ round and elongating spermatids, I decided to perform a more extensive analysis of tubulin PTMs in order to see whether the lacking of CCP5 might indirectly cause changes in others PTMs. The following PTMs were analyzed by immunofluorescence in testicular dissociated cells from $CCP5^{-/-}$ mice and control littermates: mono- and polyglutamylation, mono- and polyglycylation, $\Delta 2$ -tubulin modification and acetylation (Fig 4.13) with specific antibodies.

None of the analyzed modifications stained wild type round spermatids, except for $\Delta 2$ -tubulin and acetylation showing signal on cortical MTs. $CCP5^{-/-}$ round spermatids are negative for monoglutamylation, but positive for polyglutamylation. Analysis of glycylation in $CCP5^{-/-}$ round spermatids demonstrates an increase in monoglycylation levels, but no changes were detected in the polyglycylation status compared to control cells. Finally, $CCP5^{-/-}$ round spermatids are stained with $\Delta 2$ -tubulin and acetylation antibodies as well.

PTM analysis in $CCP5^{+/+}$ and $CCP5^{-/-}$ elongating spermatids revealed that manchette MTs are subjected to all the analyzed PTMs except for monoglutamylation. Interestingly, the typical MT hair-like structures in $CCP5^{-/-}$ spermatids are also modified by all the analyzed PTMs, except for monoglutamylation.

Altogether these results demonstrate that $CCP5^{-/-}$ spermatids present overall increasing levels of MT PTMs. Interestingly, atopic MTs located caudally to the manchette are not just glutamylated, but also glycylation, acetylated and subjected to $\Delta 2$ -tubulin modification.

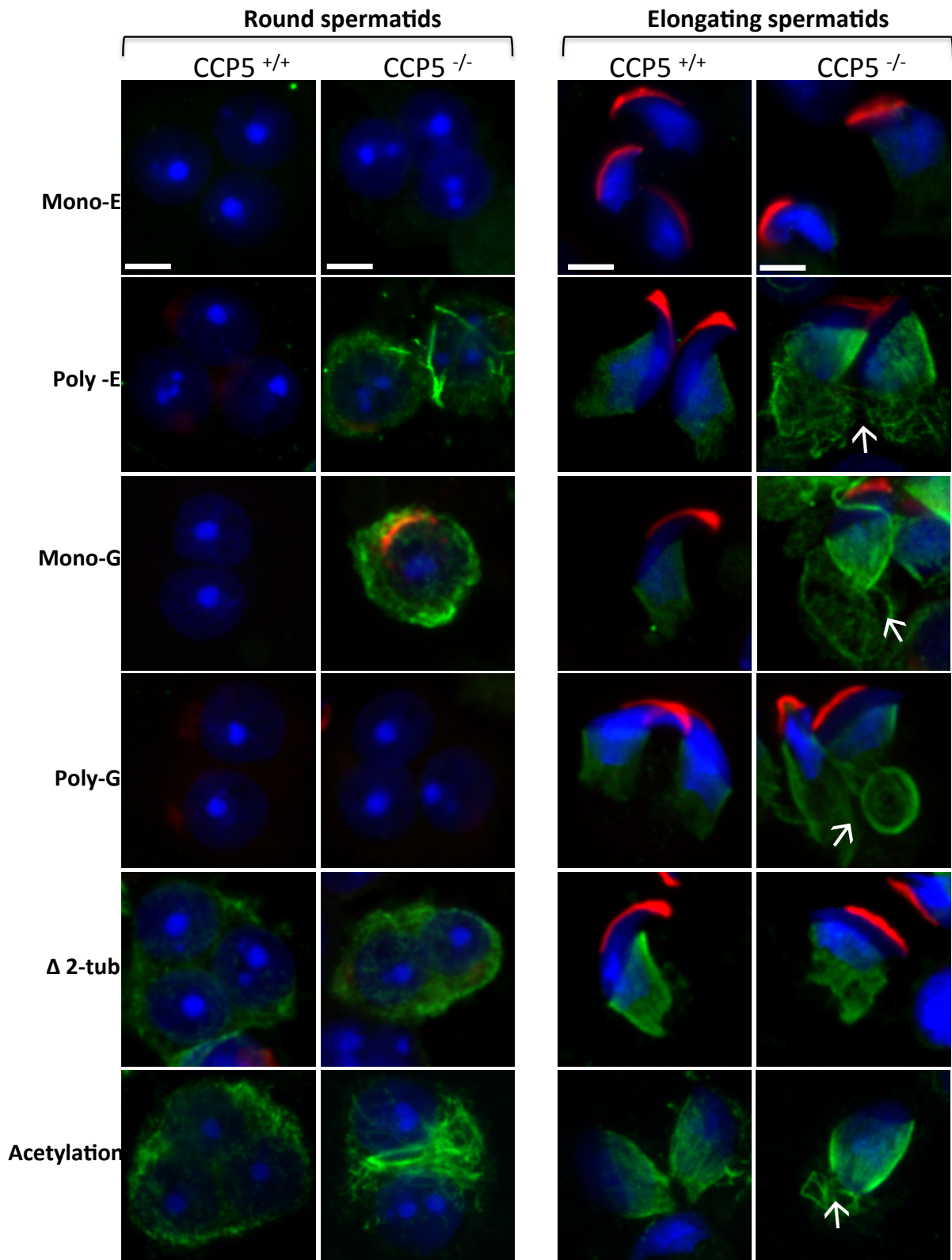


Figure 4.13 Immunodetection of a range of tubulin posttranslational modifications in round and elongating spermatids. Testicular dissociated cells from CCP5^{+/+} and CCP5^{-/-} mice were analyzed with antibodies for different posttranslational modifications (green). The acrosome was co-stained in red (sp56 antibody), and DAPI was used to stain nuclei (blue). Scale bar is 5 μ m. From the top to the bottom: tubulin monoglutamylation (Mono-E), polyglutamylation (PolyE), monoglycylation (Mono-G), polyglycylation (PolyG), Δ 2 modification (Δ 2-tub) and acetylation. Arrows indicate MTs hair-like structure in CCP5^{-/-} cells.

4.5 CCP5^{-/-} elongating spermatids are characterized by supernumerary basal bodies.

The observation that MTs forming the hair-like structure were never detected with anti-tubulin antibody in wild type elongating spermatids suggest that those MTs are either specifically nucleated in the CCP5^{-/-} either not disassembled. To check this hypothesis, I performed γ -tubulin immunostaining on testicular dissociated cells to visualize basal bodies in elongating spermatids. Interestingly I observed multiple γ -tubulin-positive spots in CCP5^{-/-} elongating spermatids, whereas only one or two γ -tubulin positive spots were detected in control cells (Fig 4.14). In both samples, I sometimes observed a single, but larger positive spot, most probably due to the presence of clustered centrioles (data not shown).

I next confirmed the presence of multiple basal bodies by electron microscopy analysis of serial sections from CCP5^{-/-} testis (Fig 4.14 B). Quantification of elongating spermatids bearing supernumerary basal bodies revealed a statistically significant difference in the percentage of positive cells between control and CCP5^{-/-} elongating spermatids (Fig 4.14 C). Indeed, while only about 5% of control spermatids have more than two γ -tubulin-positive spots, I counted about 63% of CCP5^{-/-} elongating spermatids bearing multiple basal bodies (***P*=0.004). No statistically significant difference was detected in spermatids with bigger γ -tubulin-positive spots, which are presumably clustered basal bodies.

Taken together these results suggest that CCP5 is important for the regulation of generation and/or repartition of centrioles during spermatogenesis. Moreover, MTs forming the hair-like structures could be a direct consequence of the presence of multiple basal bodies in the cell.

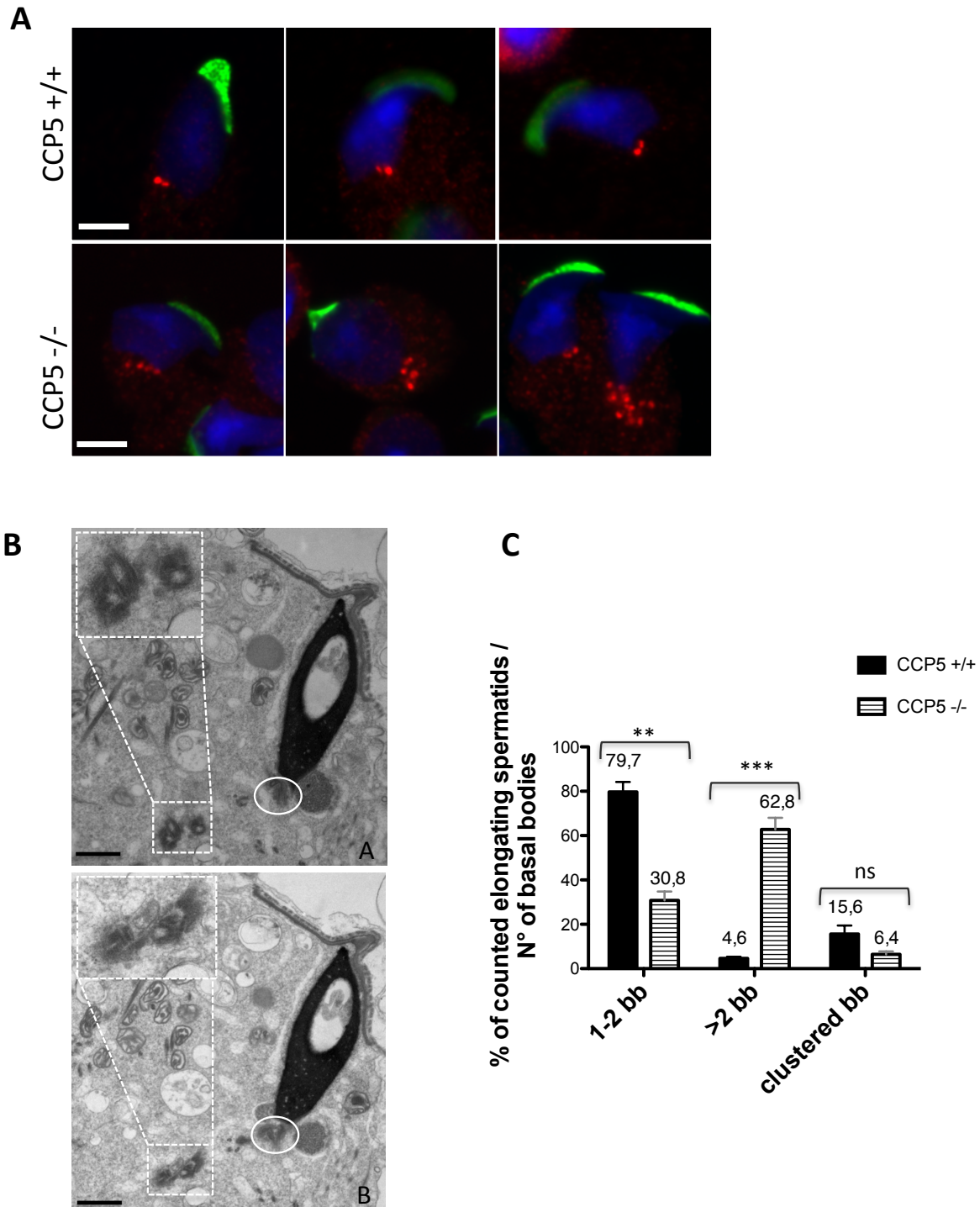


Figure 4.14: Presence of supernumerary centrioles/basal bodies in CCP5^{-/-} elongating spermatids. (A) Centrioles were immunodetection with anti- γ -tubulin antibody (red). The acrosome is in labeled in green and nuclei were stained with DAPI (blue). Note the presence multiple γ -tubulin positive spots in CCP5^{-/-} spermatids. Scale bar is 5 μ m. (B) Micrographs of serial sections of a CCP5^{-/-} spermatid showing multiple basal bodies. Note the presence of one basal body next to the cell nucleus (white circle) and three extra centrioles located in the cell cytoplasm (insert). Scale bar is 1 μ m. (C) Quantification of elongating spermatids showing supernumerary basal bodies. Elongating spermatids from wild type and CCP5^{-/-} testes were immunostained with γ -tubulin, and phenotypes were classified into three categories: cells showing one or two γ -tubulin positive spots (1-2 bb), cells with more than two γ -tubulin positive spots (>2 bb), and cells showing a single but larger γ -tubulin-positive spot (clustered bb). Percentages of counted elongating spermatids/category/genotype obtained in 3 individual experiments (N=3) were plotted into a histogram. Data express means \pm SEM. ** P= 0,0013, *** P= 0,0004 by unpaired two tailed t-test.

4.6 CCP5^{-/-} spermatids are characterized by ultrastructural defects on acrosomes, manchettes and flagella

To better understand the consequences of the lacking of CCP5 on spermatids differentiation, we decided to analyze testis cross-sections from CCP5^{+/+} and CCP5^{-/-} mice by electron microscopy focusing on elongating spermatids.

Wild type elongating spermatids are characterized by an acrosome that is intimately attached to the nuclear membrane, thus covering the apical part of the nucleus (Fig 4.15 A, D, C). Next to the caudal edge of the acrosome is the manchette, formed of MTs emanating from the perinuclear ring (arrows, Fig 4.15A). The manchette is formed from a parallel and symmetric array of MTs that extend toward the caudal germ cell cytoplasm (Fig 4.15 A; arrows and arrowheads Fig 4.15 B, E). At the base of the nucleus, the basal apparatus forms the connecting piece of the flagellum (CP, Fig 4.15 B). At later developmental stages, when chromatin is fully condensed (asterisks, Fig 4.15 C), the manchette is already disassembled and flagellum is fully developed (Fig 4.15 C, F). Strikingly, I observed defects in all of those structures in CCP5^{-/-} spermatids.

First, acrosomes observed in CCP5^{-/-} elongating spermatid show a range of heterogeneous defects such as asymmetric elongation (arrows Fig 4.15 G) and an unusual shape (insert, Fig 4.15 I). Moreover, I frequently observed acrosomes that are detached from the nuclear membrane (arrow, Fig 4.15 N). Interestingly detached acrosomes were detected especially in condensed spermatids showing a high degree of cytoplasm vacuolization and disorganization (Fig 4. 16 A-D), suggesting a possible correlation between elongating spermatids degeneration and acrosome- nucleus detaching.

Second, the emanation of manchette MTs does not appear to be always symmetric (arrows, Fig 4.15 G). Moreover, manchette MTs seem not be organized in parallel arrays,

since it is possible to observe both longitudinally (long arrows, Fig 4.15 L) and coronally-cut MTs (short arrows, Fig 4.15L) in manchettes of longitudinally sectioned CCP5^{-/-} elongating spermatids. Furthermore, manchette MTs appear to be quite disorganized in CCP5^{-/-} mice (Fig 4.15-M, P), while they are well organized in wild type cross sections (Fig 4.15 E). Strikingly, I often observe manchette MTs that protrude into invagination inside the nucleus of CCP5^{-/-} spermatids (Fig 4.15 G, L, O).

Third, CCP5^{-/-} condensed spermatids do not show well-developed axonemal structures, and thus, flagella. Instead, several MT singlets and/or doublets are visible within the cytoplasm of condensed spermatids (Fig 4.15 N, arrow Fig 4.15Q). Interestingly, mitochondria organize around those MTs (arrowheads, Fig 4.15-Q). Analysis of testis serial sections demonstrates a failure in axoneme maintenance in elongating CCP5^{-/-} condensed spermatids (Fig 4.17). Indeed, while axoneme is still assembled in its proximal tract (Fig 4. 17 A, B), axonemal MTs split apart in more distal regions (Fig 4.17 C-F). This striking observation lead us to the hypothesis that the singlet and doublet MTs observed in the cytoplasm of elongating spermatids are derived from defective single and/or multiple flagella axonemes.

Altogether these data suggest that CCP5 is a key regulator of mouse spermiogenesis. Indeed, suppression of CCP5 lead to defects in all the cellular sub-structures that are developed during spermiogenesis such as the acrosome, the manchette and the flagellum

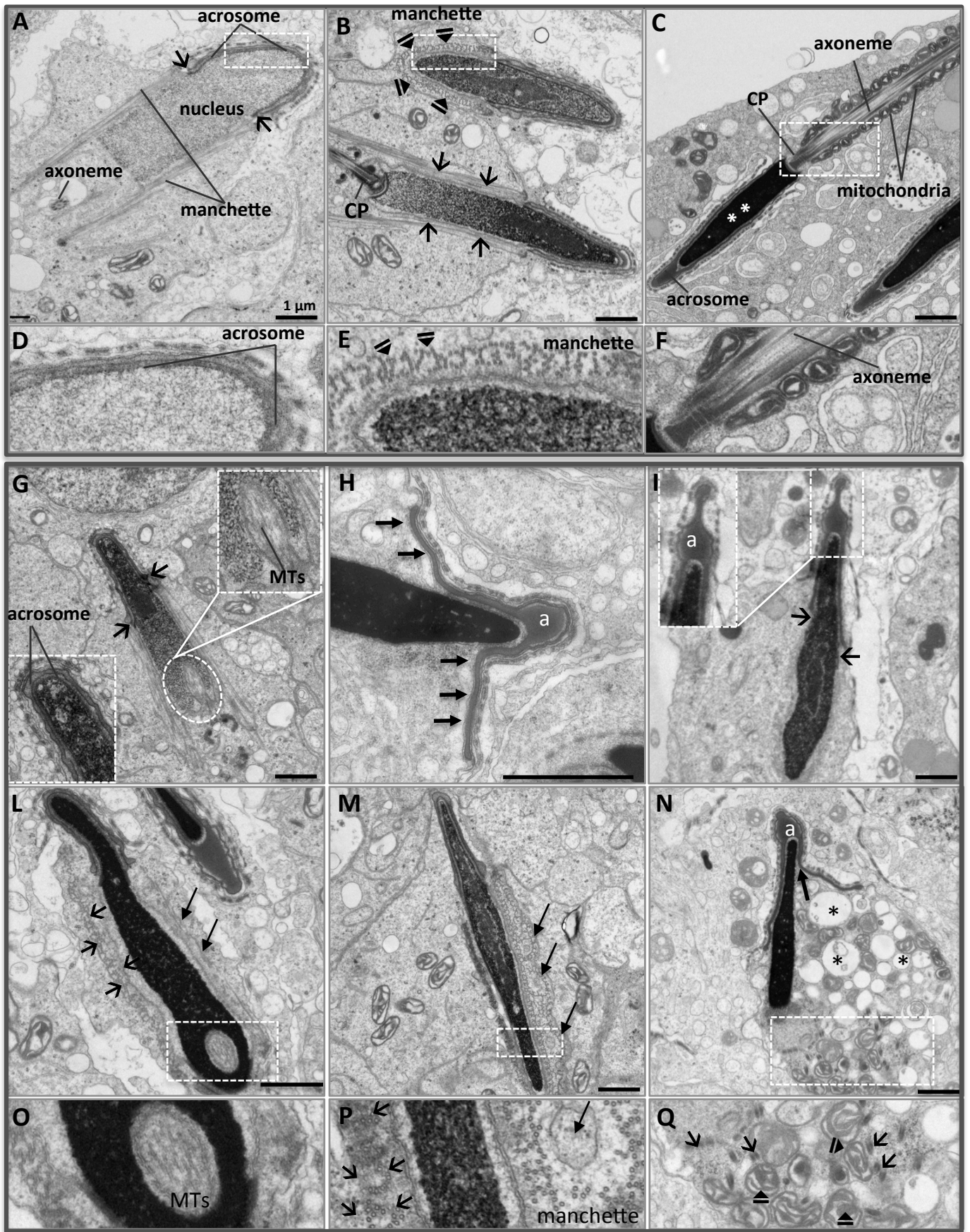


Figure 4.15: Ultrastructural defects in *CCP5*^{-/-} elongating spermatids. (See figure legend at page 127)

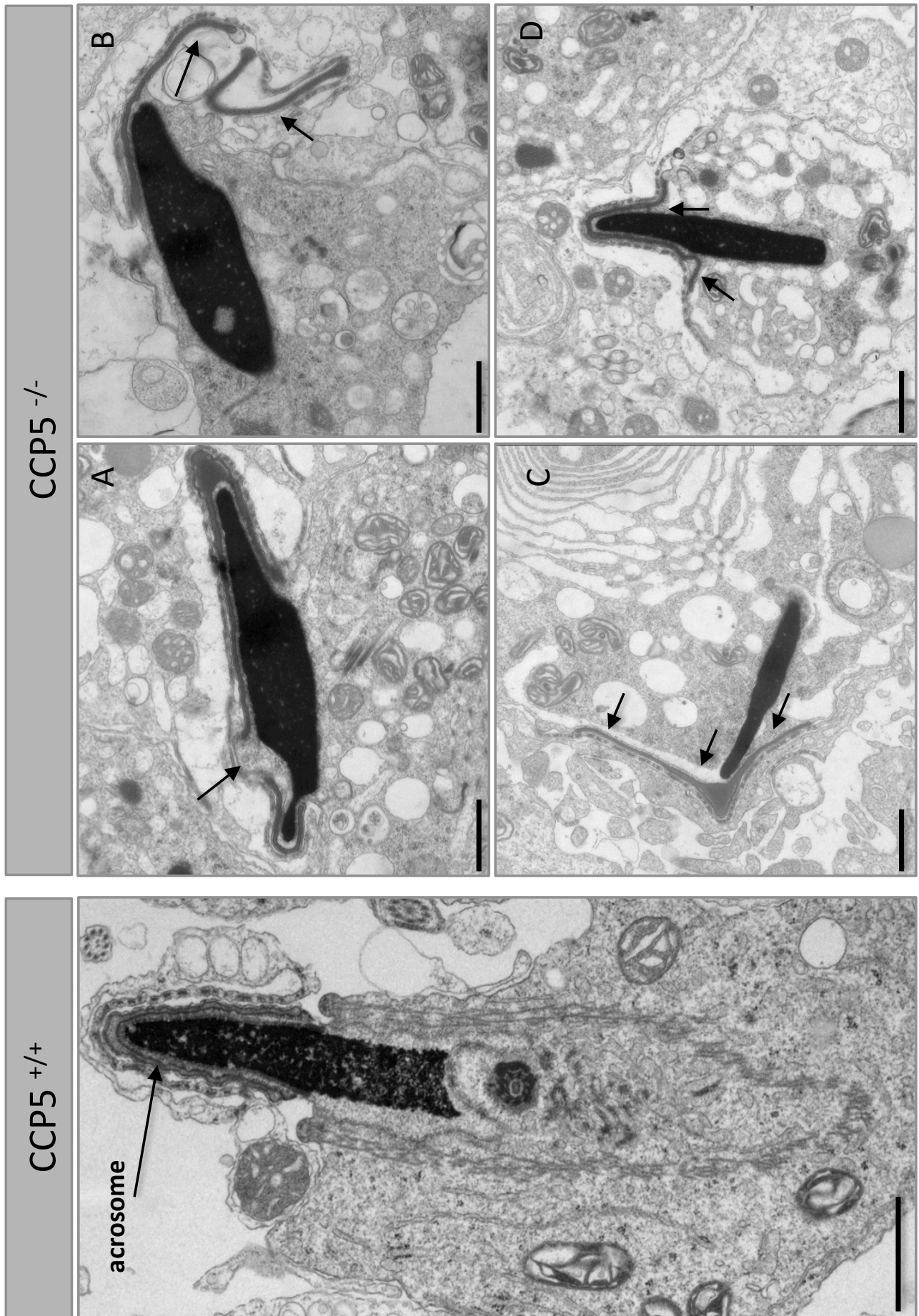


Figure 4.16: The acrosome is detached from the nuclear membrane in degenerating elongated spermatids of $CCP5^{-/-}$. (See figure legend at page 127)

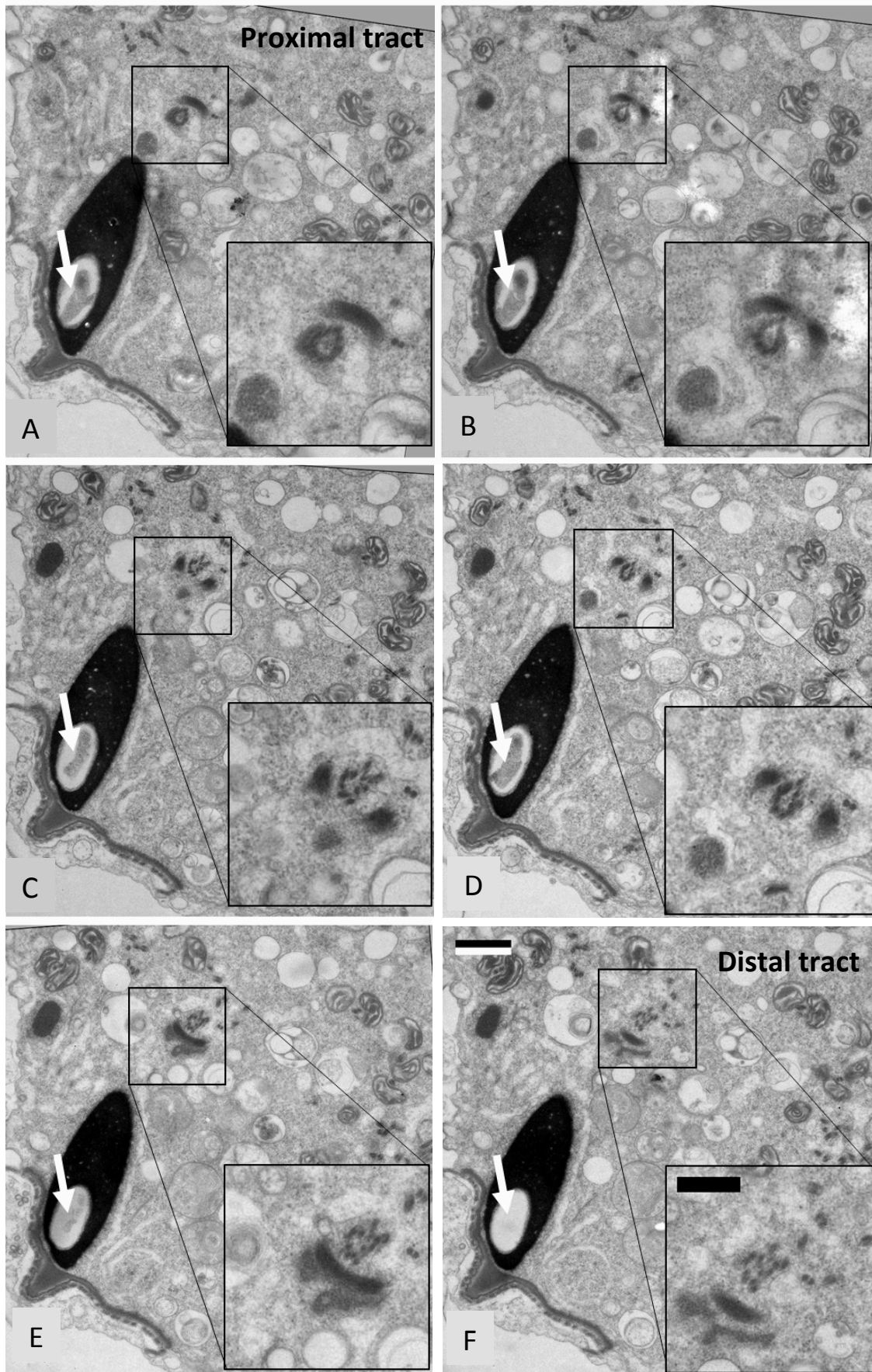


Figure 4.17: Electron microscopy serial sections of a CCP5^{-/-} condensed spermatid showing axonemal integrity defects. (See figure legend at page 127)

Figure 4.15: Ultrastructural defects in CCP5^{-/-} elongating spermatids. Electron microscopy analysis of elongating spermatids from CCP5^{+/+} (upper panel) and CCP5^{-/-} (bottom panel) testis. Scale bar is 1 μ m. (A) Longitudinal section of CCP5^{+/+} elongating spermatids. Arrows indicate belt groove between acrosomal caudal edge and perinuclear ring from which manchette MTs emanate. (B) Coronal (upper cell) and longitudinal section of CCP5^{+/+} elongating spermatids. Arrows indicate longitudinally cut manchette MTs. Arrowheads indicate manchette coronal section. CP is connecting piece. (C) Longitudinal view of a late condensed spermatids and flagellum. CP is connecting piece. (D-F) Higher magnification of dashed boxes in A-C. (G) Longitudinal section of CCP5^{-/-} spermatids. Asymmetric belt groove (arrows), MTs invagination into the nucleus (circle). (H) Mutant spermatids showing acrosome (a) detached from the nucleus (arrows). (I) CCP5^{-/-} elongating spermatid showing a bulb-like shaped acrosome and asymmetric manchette emanation (arrows). (L) Cross section of a CCP5^{-/-} elongated spermatid. The presence of coronally cut manchette MTs (short arrows) and longitudinally cut MTs (long arrows) suggests that manchette MTs are not parallel arranged in CCP5^{-/-} spermatids. MTs inside the nucleus are underlined in a white dashed box. (M) Asymmetric organization of manchette MTs in CCP5^{-/-} elongating spermatid. Note the presence of vesicles inbetween manchette MTs (arrows). (N) Highly defective condensed spermatid showing detached acrosome (arrow), vacuolization (*) and disorganized singlet and/or doublets MTs in the cytoplasm. Note how mitochondria organize around those MTs (white dashed box). (O) Higher magnification of box in L. (P) Higher magnification of box in (M). Long arrows indicate ectopic vesicle, short arrows indicate disorganized manchette MTs. (Q) Higher magnification of box in N. MTs singlets or doublets are marked with arrows whereas arrowheads indicate mitochondria

Figure 4.16: The acrosome is detached from the nuclear membrane in degenerating elongated spermatids of CCP5^{-/-}. (A-D) Electron microscopy CCP5^{-/-} testis show that acrosomes detachment (arrows) correlates with the presence of high degree of vacuolization in the germ cells cytoplasm. Scale bar is 1 μ m. CCP5^{+/+} panel represents a control elongating spermatid.

Figure 4.17: Electron microscopy serial sections of a CCP5^{-/-} condensed spermatid showing axonemal integrity defects. (A-F) Serial sections from the proximal to the distal region of a CCP5^{-/-} spermatid (A-F). Scale bar is 1 μ m. Note how axonemal MTs, initially assembled into the axoneme (A, B), split apart more distally to the sperm head (C-F). Note also the present of a cavity inside the nucleus (arrow).

4.7 Generation of a germ-cell-specific CCP5 conditional knockout

mouse: The CCP5^{ff} STRA8-CRE^{+/-} mouse model

The analyses of the CCP5^{-/-} mouse model demonstrate that the regulation of tubulin glutamylation via CCP5 activity is fundamental for differentiation of elongating spermatids during mouse spermatogenesis. Indeed, absence of the CCP5 enzyme leads to the formation of highly defective elongating spermatids, in which all the organelles/structures that form during spermiogenesis are severely impaired.

Elongating spermatid differentiation depends both on cell-autonomous processes, as well as on interactions between the germ cells and the surrounding Sertoli cells. In order to understand whether some of the phenotypes observed in the CCP5^{-/-} mice are related to defects in Sertoli cells I decided to generate a conditional, germ cells-specific CCP5 knock-out mouse model. The new mouse model was generated by crossing STRA8-CRE^{+/-} mice with CCP5^{ff} mice, and the CCP5^{ff} STRA8-CRE^{+/-} mice were obtained by sequential intercrossing between F1 progeny. The STRA8 promoter is specifically expressed in premeiotic germ cells, but not in the epithelial Sertoli cells (Sadate-Ngatchou et al 2008). Thus, in the CCP5^{ff} STRA8-CRE^{+/-} Sertoli cells are considered to be CCP5^{+/+}, whereas germ cells become CCP5^{-/-}.

As the generation of mouse model was time-consuming, mice were available only in the last year of my PhD. Thus I decided to focus on key experiments in order to observe the main phenotypes in this mouse model, and to compare them with the results obtained in the CCP5^{-/-} mouse line. Although some experiments have still to be repeated, I present here all the data I obtained so far.

From here CCP5^{ff} STRA8-CRE^{+/-} mice will be called conditional CCP5^{-/-} mice whereas CCP5^{-/-} will be called total CCP5^{-/-} mice. During experimental procedures I used age-

matched CCP5^{+/+} STRA8-CRE^{-/-} or CCP5^{+/+} STRA8-CRE^{+/-} or CCP5^{ff} STRA8-CRE^{-/-} or CCP5^{f/+} STRA8-CRE^{-/-} as control animals. Thus, the term "control" will refer to any one of those genotypes.

4.8 Increased sperm production in conditional CCP5^{-/-} mice.

To understand whether CCP5 expression in Sertoli cells allows a total/partial rescue of the CCP5^{-/-}-related impaired differentiation of elongating spermatids into spermatozoa I first analyzed sperm count and morphology in the newly generated conditional CCP5^{-/-} mice. Coomassie blue staining on 3-month-old control and conditional CCP5^{-/-} mice revealed an increased sperm production as compared to the total CCP5^{-/-} mouse. However, spermatozoa present a striking phenotype showing retro-flipped tails at junction between the mid- and principal piece (arrows, Fig 4.18 A). The conditional CCP5^{-/-} mouse presents an increased sperm number (Fig 4.18B) compared to total CCP5^{-/-} mouse (Fig 4.1 B). Indeed I counted respectively 32×10^6 vs 14.5×10^5 sperm cells/ml in 3-month-old control and conditional CCP5^{-/-} mice (N=1) (Fig 4.18B). However, accordingly to the observed sperm count the conditional CCP5^{-/-} mouse is still affected by a milder form of oligospermia. To confirm this observation, two more replicate experiments will be done as soon as more mice are available.

Interestingly, histological analysis of adult conditional CCP5^{-/-} and control cauda epididymis revealed the presence of a mixed population of spermatozoa and immature germ cells in the conditional CCP5^{-/-} mouse (Fig 4.18C).

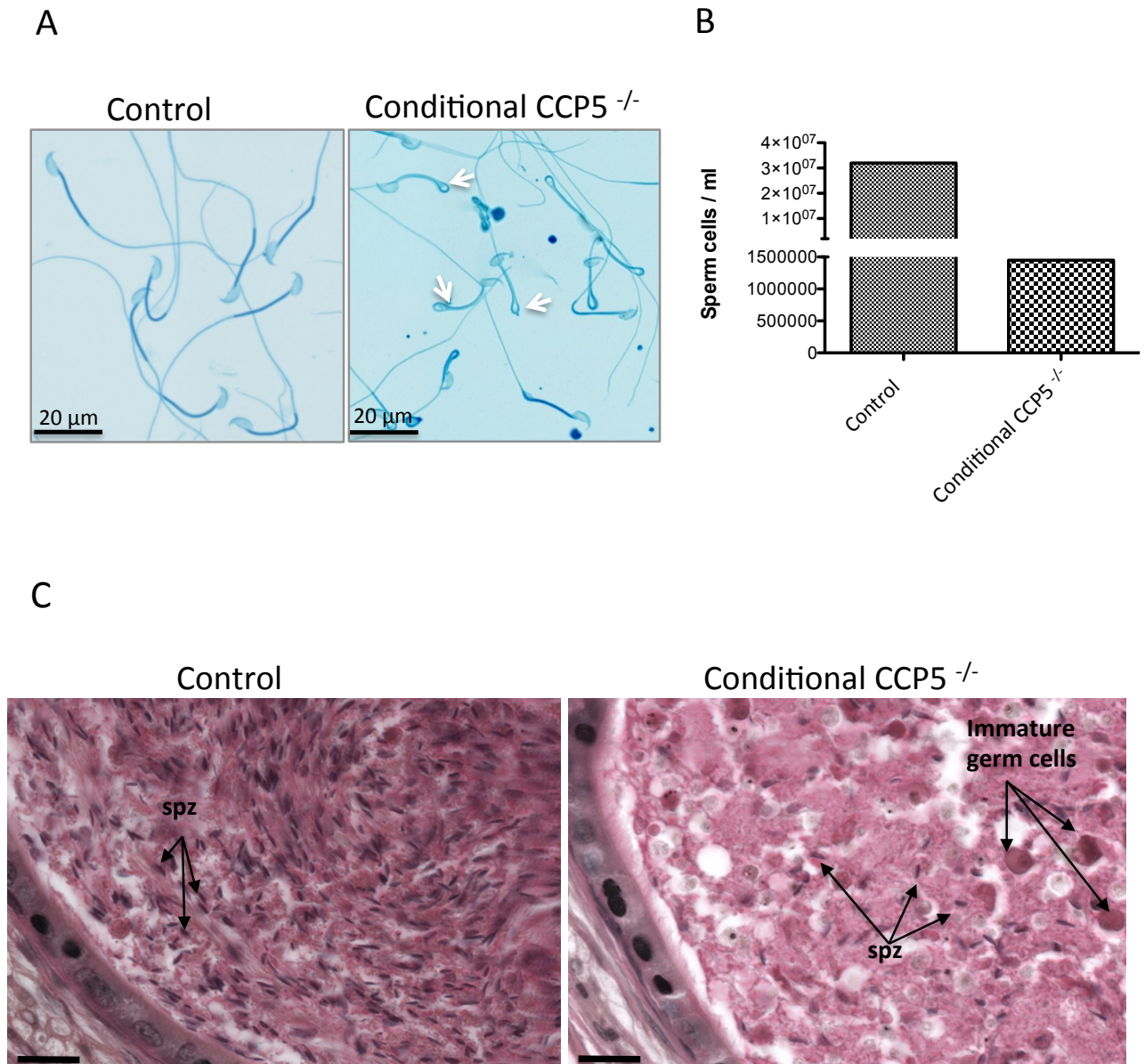


Figure 4.18: Presence of spermatozoa in conditional CCP5^{-/-} semen. CCP5^{fl/fl} STRA8-CRE^{+/-} mice, here called conditional CCP5^{-/-} mice, were obtained in order to assess whether the CCP5^{-/-} observed phenotypes are intrinsic to the spermatogenic germ line. The STRA 8 promoter is specifically expressed in pre-meiotic sperm cells, but not in the epithelial Sertoli cells. Thus in this new mouse model Sertoli cells are to be considered CCP5^{+/+}, whereas germ cells should become CCP5^{-/-}. (A) Coomassie-blue-stained sperm smears from 3 months-old conditional CCP5^{-/-} and control littermates. White arrows indicate spermatozoa heads flipped toward sperm tails, a typical phenotype of conditional CCP5^{-/-} mice. Scale bars, 20 μ m. (B) Sperm cell concentration (n° sperm cells/ml) in 3 months-old conditional CCP5^{-/-} (n=1) and control (n=1) littermates. Conditional CCP5^{-/-} mice are characterized by a mild oligozoospermie (14.5x10⁵ sperm cells/ml vs. 32x10⁶ sperm cells/ml in the control). (C) PAS staining of epididymal cross-sections. Scale bar is 20 μ m. Note the presence of both spermatozoa (spz) and immature germ cells in the conditional mutant semen.

To detect eventual amelioration on testis architecture and/or common histological defects with the total $CCP5^{-/-}$ mouse, I analyzed PAS-stained 2-months old conditional $CCP5^{-/-}$ and control testis cross-sections. Compared to control (*, Fig4.19A), conditional $CCP5^{-/-}$ testis were characterized by less spermatozoa-containing tubules (*, Fig 4.19 D). As in the total $CCP5^{-/-}$ mouse (Fig 4.3 H), no specific loss of any germ cell type was detected when comparing the histology of control (Fig 14.19B) and conditional $CCP5^{-/-}$ (Fig 14.19 E) seminiferous tubules. Although the presence of tubules in spermiation, such as the one shown in Fig 14.19E, were rarely seen in the total $CCP5^{-/-}$ mouse (Fig 4.3 G-N), I detected several $CCP5^{-/-}$ -related histological phenotypes. Indeed, I observed multinucleated cells next to tubules luminal edge (dashed boxes Fig14.19 F,G, and Fig 4.19 I) as well as a great amount of cytoplasm (arrow, Fig 4.19 H) in some seminiferous tubules from the conditional $CCP5^{-/-}$ mouse. Moreover, elongating spermatid heads were in some case unshaped (Insert, Fig 4.19 H) as compared to controls (Insert, Fig 4.19C).

Altogether these data suggest that selective deletion of CCP5 in germ cells, with expression of the protein in Sertoli cells, allows a partial spermatid differentiation into spermatozoa. However, the process of differentiation is most likely not completely rescued considering the observed sperm morphology and counting. Moreover, testicular germ cells still seem to be prematurely released from the seminiferous epithelium, as in the total $CCP5^{-/-}$ mouse and testes from conditional mutant mice seems to be composed by wild-type-like (Fig 4.19 E) and b total $CCP5^{-/-}$ -like (FIG 4.19 F-H) seminiferous tubules.

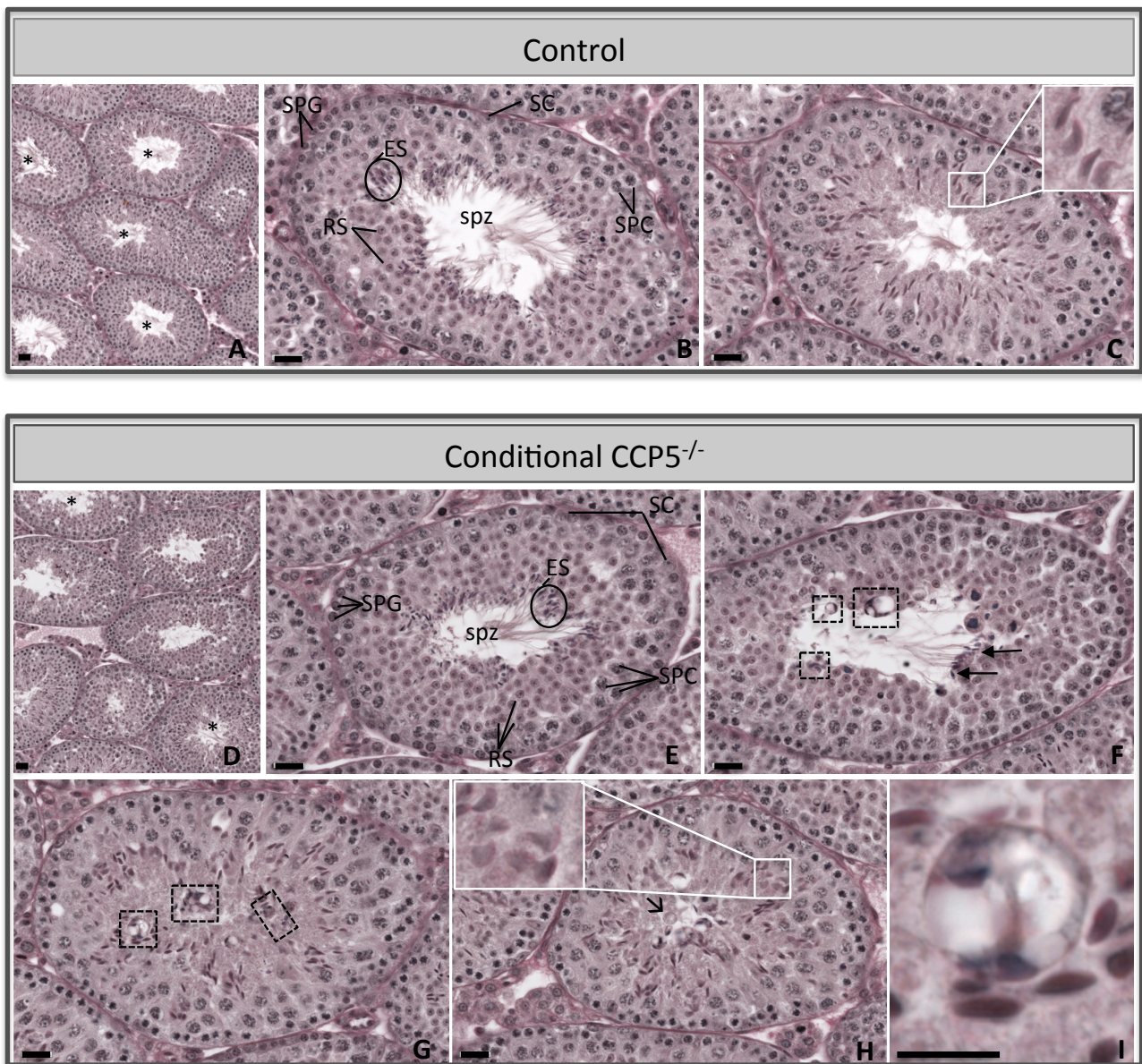


Figure 4.19: Disorganized testis cytoarchitecture in 2-months-old conditional $CCP5^{-/-}$ mice. PAS staining of paraffin-embedded testis cross-sections. SPC= spermatocytes, SPG= spermatogonia, RS= round spermatids, ES= elongating spermatids, SC= Sertoli cells, spz= spermatozoa. Scale bar is 20 μ m. (A) Lower magnification of control seminiferous epithelium showing tubules containing a great amount of sperm cells (*). (B) Control tubule composed of all different germ cell types. From the base to de apex: Sertoli cell and spermatogonia, spermatocytes, round spermatids, elongating spermatids and spermatozoa. (C) Control tubule at later stages showing elongating spermatids (zoomed in the insert) and spermatocytes. (D) Mixture of sperm-filled (*) and empty tubules in the conditional $CCP5^{-/-}$ seminiferous tubules. (E) No differences in cell composition in mutant tubules compared to control (B) could be found. (F) Tubule cross-section showing elongating spermatids in spermiation (arrows) together with multinucleated cells (boxes). (G) Multinucleated cells are detected (dashed boxes). (H) Presence of unshaped elongating spermatids (insert); arrow indicate excess of cytoplasm inside the lumen of the seminiferous tubule. (I) Zoom of a multinucleated cell formed by haploid cell nuclei (maximum projection of dashed squared box in G).

4.9 No changes in PTMs between total CCP5^{-/-} and conditional CCP5^{-/-} testicular germ cells, but lower penetrance of CCP5^{-/-} -like phenotypes

To understand whether specific knockout of CCP5 in sperm cells leads to the same changes in the PTM pattern observed in total CCP5^{-/-} testicular germ cells (Fig 4.9 A), I performed immuno blots of all tubulin PTMs on testicular germ cells fractionated from testes of conditional CCP5^{-/-}. Interestingly, conditional CCP5^{-/-} germ cells show a glutamylation and glycylation pattern similar to the one observed in total CCP5^{-/-} mice (Fig 4.20 A). Conditional CCP5^{-/-} germ cells present an overall increase level of tubulin glutamylation (GT335 and polyE) on both α -tubulin and the unidentified non-tubulin substrate. I also observed changes in glycylation characterized by a stronger positive signal for mono- and polyglycylation on α - and β -tubulin compared to control. Also the non-tubulin substrate, which is detected with monoglycylation antibody in control elongating spermatids (*, Fig 4.20A), is no more detected in conditional CCP5^{-/-} elongating spermatids. Globally no evident changes were detected in the glutamylation and glycylation patterns between germ cells from total- and conditional CCP5^{-/-} mice.

I then analyzed also the levels of detyrosination (detyr) and acetylation (Fig 4.20 A). Although no changes were detected for detyrosinated tubulin levels, I observed a great increase of acetylation on both α -tubulin and on the non-tubulin substrate (**, Fig 4.20 A). It will be interesting in the future to verify whether the non-tubulin substrate is acetylated also in the total CCP5^{-/-} mouse.

As the most-striking phenotypes of the total CCP5^{-/-} mouse were hyperglutamylation of round spermatids, and the formation of a glutamylated MTs-hair like structure, I decided to check whether these phenomena were detectable also in conditional CCP5^{-/-} mice. Glutamylation was visualized using GT335 antibody and nuclei were stained with DAPI. As expected, spermatocytes appear to be unmodified, and no evident morphological defects

were detected in conditional $CCP5^{-/-}$ (Fig 4.20 B-b) compared to control cells (Fig 4.20 B-a). Both, hyperglutamylated (Fig 4.20B-d) and unmodified (data not shown) round spermatids were observed in conditional $CCP5^{-/-}$ testicular dissociated cells, whereas tubulin hyperglutamylation was rarely observed in control round spermatid (Fig 4.20 B-c). Among elongating spermatids I detected both wild type-like cells (Fig 4.20 A-e), showing the typical manchette structure (insert Fig 4.20 B-f), and cells with the MT-hair like structures (Fig. 4.20 B-f). Moreover, I detected both condensed spermatids with defective flagella (insert, Fig 4.20 B-h) and normal spermatids (Fig 4.20 B-h). As in the total $CCP5^{-/-}$ mouse, elongating spermatids showing MT hair-like structures or defective flagella were also characterized by an aberrantly shaped nucleus. Thus, it seems that conditional $CCP5^{-/-}$ testicular dissociated cells are composed by a mixture population of wild-type-like and $CCP5^{-/-}$ -like germ cells. However quantification of those phenotypes (Fig 4.21 B-E) revealed a lower percentage of conditional $CCP5^{-/-}$ cells bearing each analyzed phenotype compared to total $CCP5^{-/-}$ germ cells (Fig 4.21 F).

To confirm these results, it will be necessary to perform at least two replicate experiments in order to perform a statistical analysis on these results

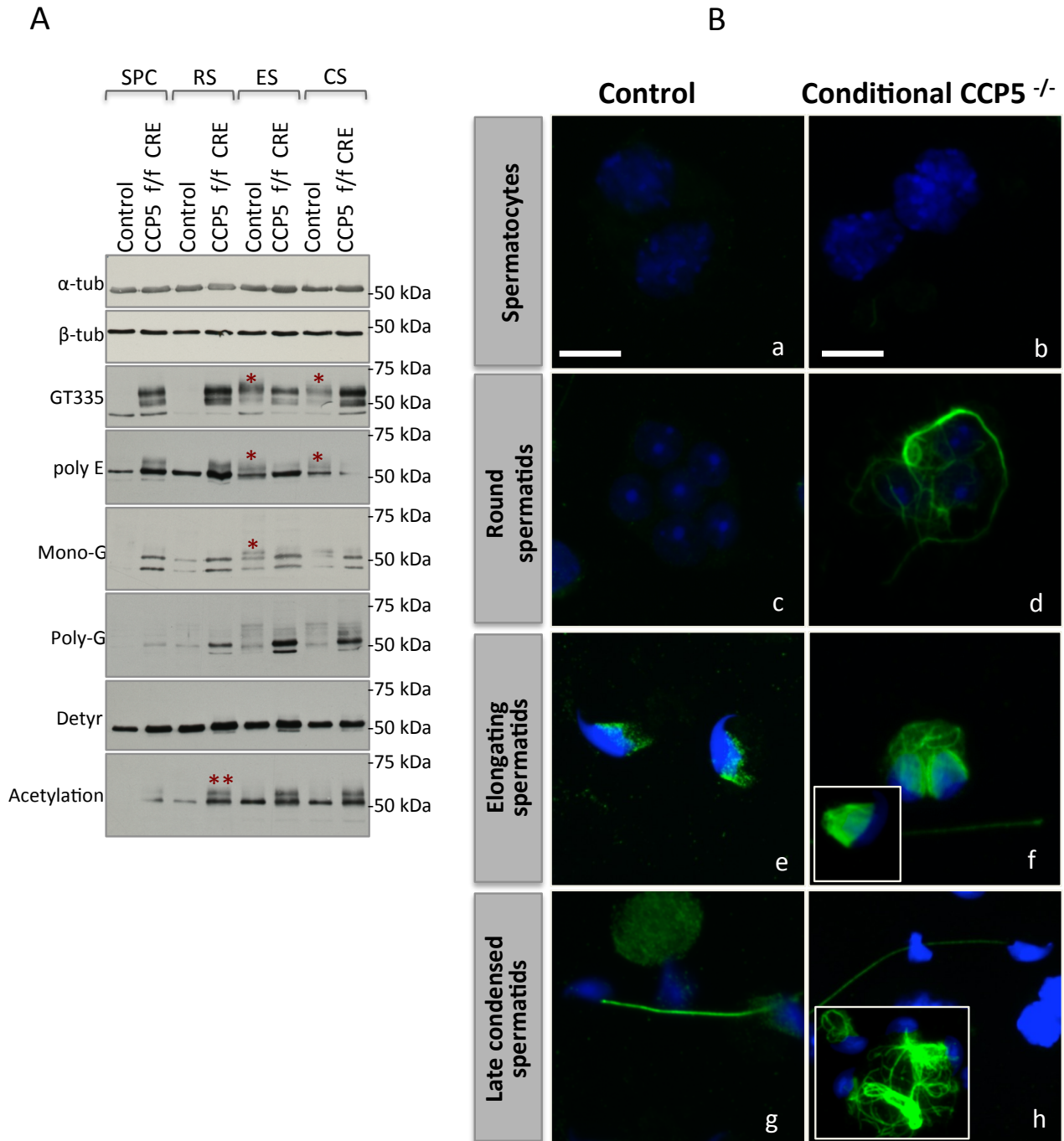


Figure 4.20: Posttranslational modifications in conditional CCP5^{-/-} testicular germ cells. (A) Immunoblot analysis of extract from conditional CCP5^{-/-} and control fractionated spermatocytes (SPC), round spermatids (RS), elongating spermatids (ES) and condensed spermatids (CS). Cell extract were obtained by BSA density gradient- based cell fractionation. From the top to the bottom lane are α -tubulin, β -tubulin, glutamylation, polyglutamylation, monoglycylation, polyglycylation, detyrosination and acetylation. There is an overall increase of most tubulin PTMs in mutant germ cells. (B) Immunodetection of glutamylated tubulin in testicular dissociated cells. GT335 antibody was used to detect glutamylation (green). Nuclei were stained with DAPI (blue). Scale bar is 10 μ m. The mutant germ cell population is characterised by wild type-like cells (insert in f, h) and CCP5^{-/-}-like cells (d, f, insert in h).

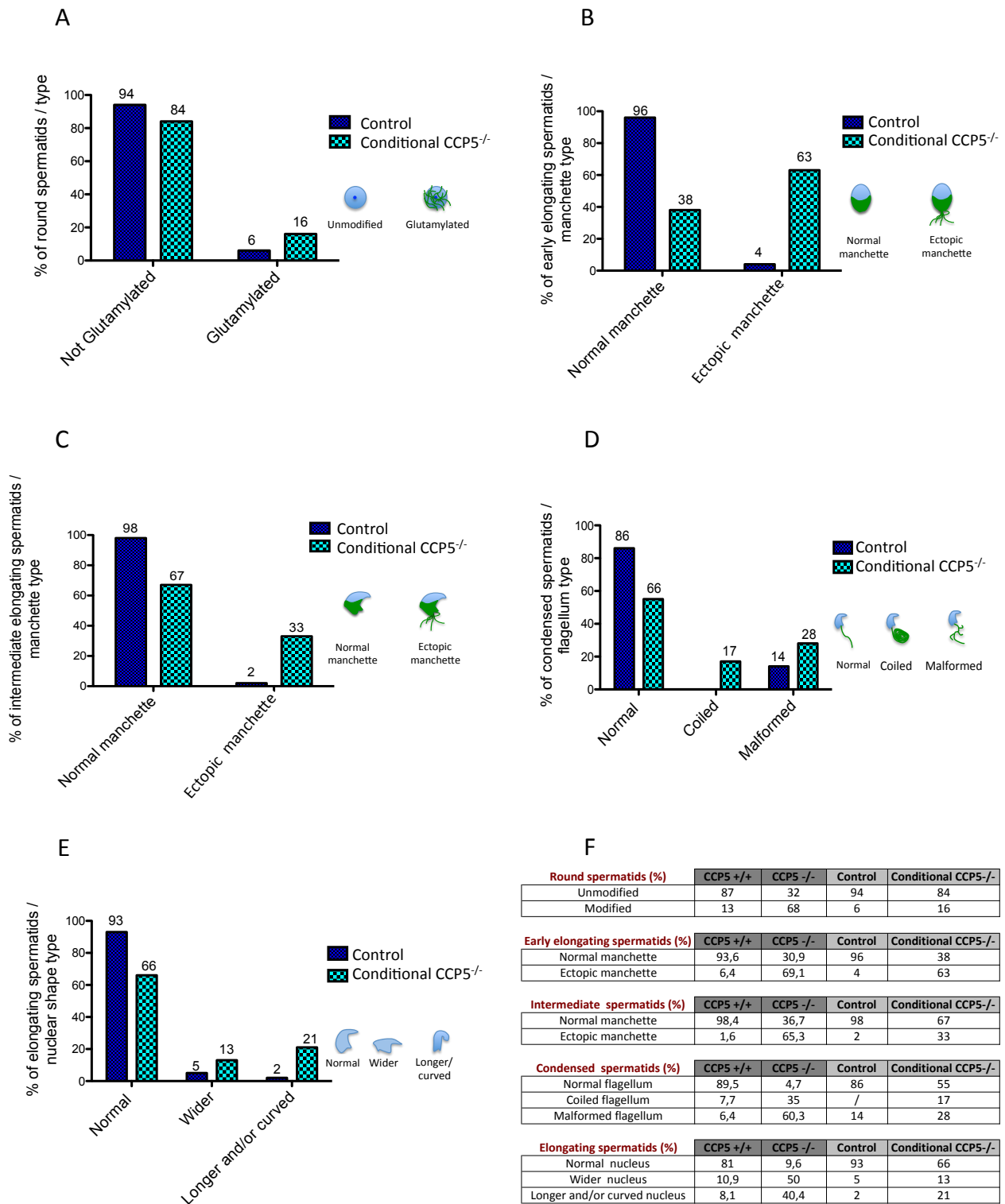


Figure 4.21: Percentage of defective germ cells in conditional CCP5^{-/-} spermatids.

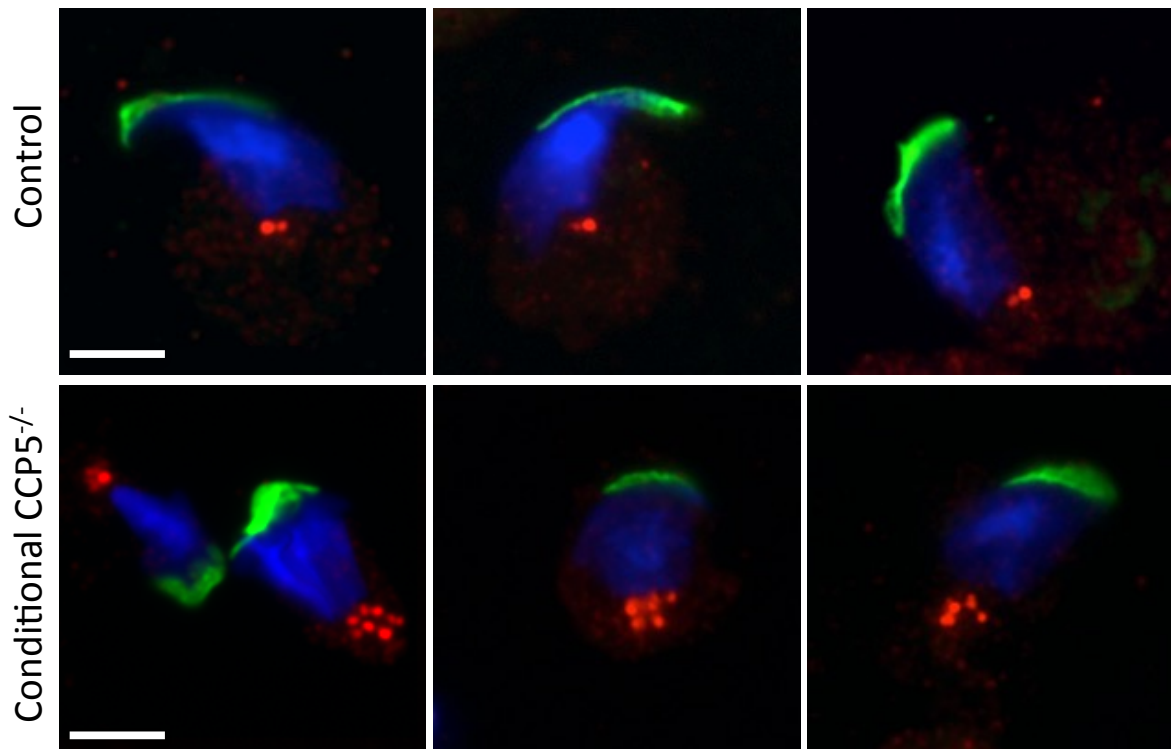
Quantification of conditional CCP5^{-/-} testicular germ cells showing CCP5^{-/-}-like defects. Round spermatids glutamylation (A) ectopic manchette in early (B) and intermediate (C) elongating spermatids, defective flagella (D), misshaped spermatid nuclei (E). Table summarizing percentage of counted defective cells/analyzed phenotype in total CCP5^{-/-} and conditional CCP5^{-/-} line (F).

4.10 Presence of multiple basal bodies in conditional $CCP5^{-/-}$ spermatids.

Another strikingly phenotype observed in $CCP5^{-/-}$ spermatids is the presence of multiple centrioles/basal bodies in elongating spermatids. Thus, I verified by immunofluorescence analysis whether the basal body-related phenotype was also present in conditional $CCP5^{-/-}$ mice. Interestingly, multiple γ -tubulin positive spots are detectable in conditional $CCP5^{-/-}$ elongating spermatids (Fig 4.22 A). This observation was confirmed by electron microscopy analyses that revealed several basal bodies/centriole alterations. I observed both cells showing multiple basal bodies attached to the nucleus, each one connected to a single implantation fossa (Fig 4.22 B-c,e,f), as well as cells with centrioles located in the cytoplasm periphery (Fig 4.22B-d).

It will now be important to quantify the percentage of conditional $CCP5^{-/-}$ spermatids showing this phenotype, and compare it with the $CCP5^{-/-}$ mouse.

A



B

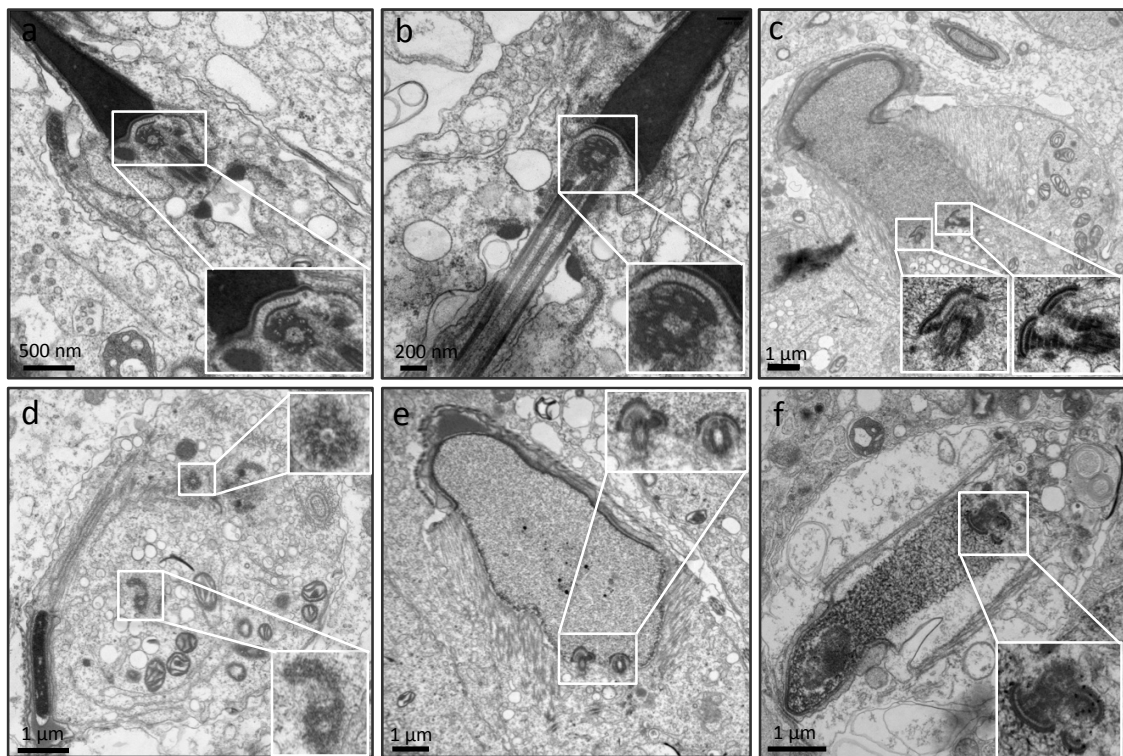


Figure 4.22: Presence of supernumerary basal bodies in conditional CCP5^{-/-} elongating spermatids. (A) Basal body immunolocalisation with anti γ -tubulin antibody (red). Sp56 antibody was used to stain the acrosome (green). DAPI stains nuclei (blue). Scale bar is 5 μ m. (B) Detection of multiple basal bodies by electron microscopy analysis. a, b: longitudinal section of control spermatid. The centriole is zoomed in the insert. C-d: Example of mutant spermatids showing multiple centrioles into the cytoplasm (d), or organizing multiple implantation foci (c, e, f). Scale bars are indicated in the images.

4.11 Common ultrastructural defects in conditional $CCP5^{-/-}$ and total $CCP5^{-/-}$ elongating spermatids.

As mentioned before, electron microscopy analyses of testes from total $CCP5^{-/-}$ mice revealed the presence of exciting ultrastructural defects on acrosomes, manchettes and flagella of elongating spermatids.

Considering that immuofluorescence analysis of testicular dissociate cells from conditional $CCP5^{-/-}$ mice demonstrated the presence of wild-type-like and $CCP5^{-/-}$ -like cells, we decided to further analyze conditional $CCP5^{-/-}$ testes by electron microscopy in order to verify whether the defective cells are characterized by the same ultrastructural defects found in the total $CCP5^{-/-}$ spermatids.

In these analyses, I observed several conditional $CCP5^{-/-}$ spermatids developing a normal acrosomal system and manchette (Fig 4. 23 D), without showing any evident defect compared to control spermatids (Fig 4.23 A, B). However, when defective, conditional $CCP5^{-/-}$ elongating spermatids were characterized by the same ultrastructural defects found in the total $CCP5^{-/-}$ spermatids. The acrosome (a), although still attached to the nucleus at earlier phases of chromatin condensation (Fig 4.23 D, E), where completely detached in fully condensed spermatids (Fig 4.23 H, I), as well as in defective spermatozoa in the epididymis (Fig 4.23 L, N). Manchette MTs appear to be asymmetric and have been eventually seen to emanate from ectopic regions in the spermatids cytoplasm (black arrow, Fig 4.23 E), whereas in wild-type-like cells, manchettes appear to emanate just caudally to the acrosome (black and white arrows FIG 4.23 D). Manchette invagination or presence of MT-filled vesicle in spermatid nuclei was observed as well (Fig 4.23 F, G). Finally, spermatids growing multiple disorganized flagella were observed as in total $CCP5^{-/-}$ mice (Fig 4.23 H, I). In general, those cells were characterized by a

disorganized cytoplasm with many vacuoles (*, Fig 4.24 H, I), as well as by mitochondria mislocalization (Fig 4.24 H).

Ultrastructural analysis of epididymal sperm revealed the presence of wild-type-like spermatozoa showing a normal ultrastructure of the flagellum (black arrows, FIG 4.24 L-N) side-by-side with very defective sperm-like cells. Compared to control spermatozoa (FIG 4.24 C), defective sperm cells present disorganization in the 9+2 axonemal MTs pattern and associated structures (red arrows, Fig 4.24 L-N). The observation of coronally and longitudinally cut midpieces (respectively long red arrow and arrowheads in Fig 4.24L) within the same sperm plasma membranes suggests the presence of multiple, or coiled/flipped flagella. However further studies are needed to analyze eventual ultrastructural defects on the different regions of the flagellum

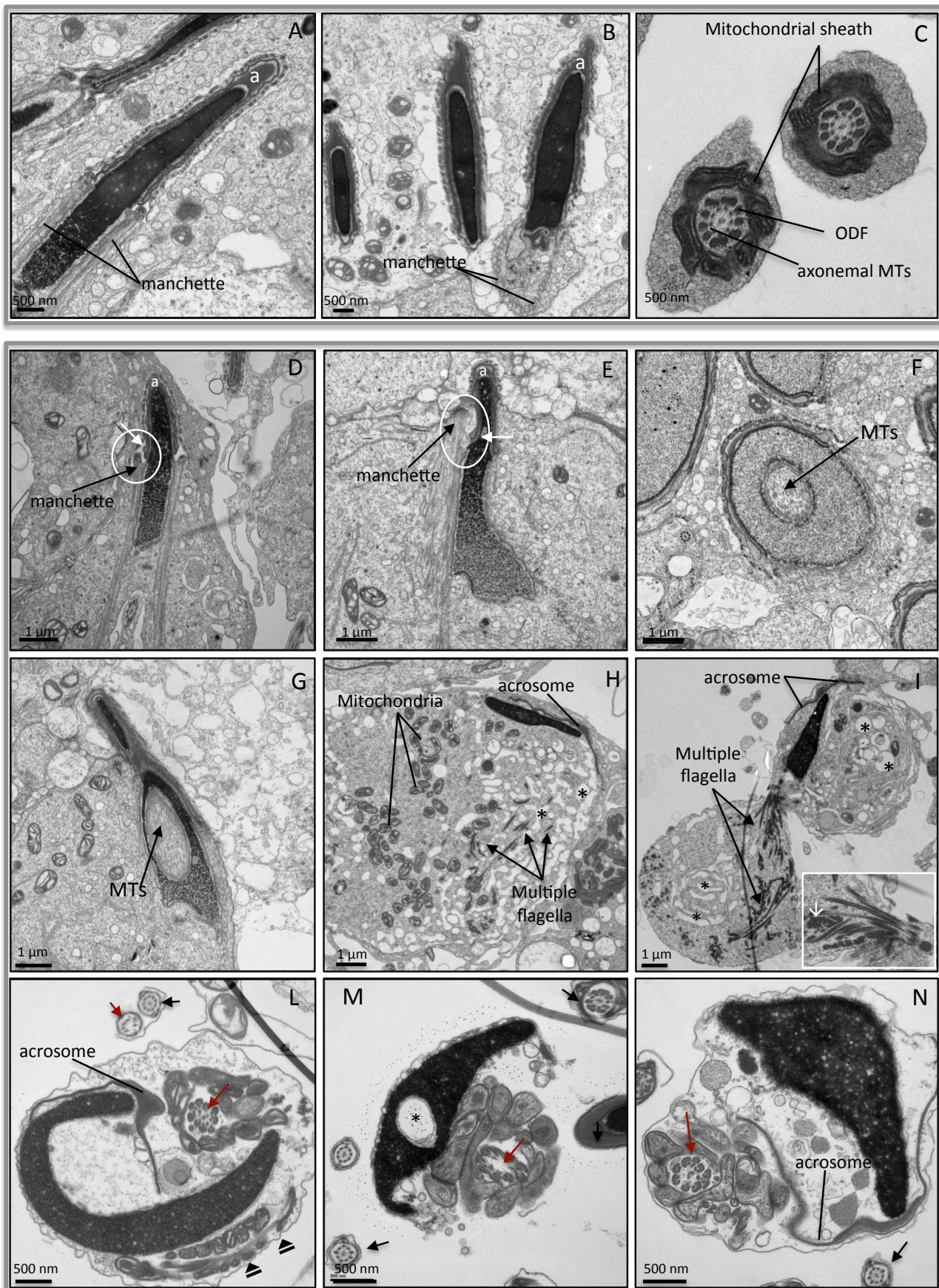


Figure 4.23: Characterization of ultrastructural defects of conditional $CCP5^{-/-}$ spermatids by electron microscopy. (See figure legend at page 142)

Figure 4.23: Characterization of ultrastructural defects of conditional CCP5^{-/-} spermatids by electron microscopy. Upper panel (control), bottom panel (conditional CCP5^{-/-}). Scale bars are indicated in the images. (A-B) Acrosome (a) and manchette appearance in control spermatids. (C) Cross section of a midpiece from control epididymal sperm. (D) Spermatid from mutant testis showing normal acrosome and manchette formation. The white arrow indicates the caudal edge of the acrosome, the black arrow indicates the manchette emanation. (E) Mutant spermatids showing mislocalized manchette (black arrow). White arrows indicate the caudal pole of the acrosome. Presence of ectopic MTs inside the nucleus of mutant round (F) and elongating (G) spermatids. (H-I) Highly defective cell showing detached acrosome and multiple flagella. Note the high degree of vacuolization in those cells (*). The white arrow in the insert indicates the centrioles. (L-N) Epididymal sperm with disorganized axoneme and associated structures (red arrows). Black arrows indicate normal flagellar cross sections. Arrowheads in (L) represent a longitudinal section of the midpiece.

4.12 Incomplete Cre-mediated defloxing in conditional CCP5^{-/-} testicular germ cells

The results so far obtained by the study of the conditional CCP5^{-/-} mouse model could support the hypothesis that CCP5^{+/+} Sertoli cells allow a partial rescue of the phenotypes observed in total CCP5^{-/-}. This is especially obvious in terms of number of defective spermatids that characterize the conditional CCP5^{-/-} seminiferous epithelium. Indeed testes from this germ cell-specific CCP5^{-/-} mice are either normal, either defective as in the total knockout CCP5^{-/-} mice. Based on the assumption that Sertoli cells are responsible for some of the phenotypes observed in the total knockout mouse model, it would be expected that ultrastructural defects are totally or at least partially rescued in germ cell-specific CCP5^{-/-} mice. However, what I really observed was that in the conditional CCP5^{-/-} mice, certain spermatids developed normally, while others are completely defective, similar to the total CCP5^{-/-} mice. Thus, I hypothesized that an incomplete cre-mediate excision of the flox alleles might be the cause of the observed partial phenotypes in the CCP5^{ff} STRA8-cre^{+/-} mice.

To confirm this notion, I performed PCR to genotype both CCP5-flox and -knockout alleles on spermatozoa collected from CCP5^{ff/+} STRA8-CRE^{+/-}, CCP5^{ff/+} STRA8-CRE^{+/-} and CCP5^{ff} STRA8-CRE^{+/-} mice. If CRE-mediated defloxing mechanism is efficient, sperm cells harvested from CCP5^{ff} STRA8-CRE^{+/-} mice should show the genotyping profile of CCP5^{-/-}, which is characterized by a single PCR product of 303 bp, and the two PCR products that characterize flox alleles (294 bp and 265 bp) should not be detected. However the genotyping profile of CCP5^{ff} STRA8-CRE^{+/-} sperm cells shows the two PCR products for the flox-alleles (red box Fig 4.24 A) as well as the CCP5 knockout signal (asterisk Fig, 4.24 A), suggesting that STRA8-CRE mediated knockout was incomplete in these mice.

PCR-based genotyping for CRE alleles was performed as well (Fig 4.24 B). As internal control I also performed PCR-based genotyping for CCP5 wild type, flox and knockout alleles (Fig 4.24 C) as well as for CRE (Fig 4.24 D) on the analyzed mice tails. Strikingly, I detected also the 303 bp knockout band in the tail of CCP5^{ff} STRA8-CRE mouse (Asterisk Fig 4.24 C).

Thus accordingly to the obtained PCR results the sperm cell population of conditional CCP5^{-/-} mice is composed by CCP5^{ff} cells and CCP5^{-/-} cells. The efficiency of flox alleles excision is most-likely variable between mice. These observation suggest that the decrease in the percentage of defective cells in the conditional CCP5^{-/-} mouse might be due to an incomplete Cre-mediated excision of the CCP5 flox alleles. Thus the presence of wild-type-like cells observed in the mouse model is most likely due to germ cells that escape from the defloxing mechanism rather than to CCP5^{+/+} Sertoli cell functions. It thus appears that the phenotypes observed in the total CCP5^{-/-} mouse are germ cell-autonomous, rather than being related to defects in Sertoli cells.

To verify this hypothesis, I characterized the glutamylation profile of Sertoli cells from CCP5^{-/-} and conditional CCP5^{-/-} testis. In order to deplete the testicular germ cells from the testis and obtain a Sertoli cell-only seminiferous epithelium, mice were treated by intra-peritoneal injection of Busulfan (Wang et al 2010). CCP5^{-/-} and conditional CCP5^{-/-} mice and respective control littermates were treated with 30 mg/Kg of Busulfan. Untreated control animals were injected with 200 µl of 50% DMSO. One month post-injection, testes were harvested from treated and untreated animals, and testes extracts were analyzed by immunoblot (Fig 4.25).

The GT335 immunoblot revealed a very weak positive signal on beta-tubulin in treated testes from the conditional CCP5^{-/-} line (Fig 4.25 A). As expected, no differences in signal intensity were observed between treated control and conditional CCP5^{-/-} animals (Fig 4.25 A). Untreated testes do not show any GT335 positive signal on beta-tubulin, most probably

because of the presence of strong alpha-tubulin glutamylation in the germ cell line and the axonemes in the sample extract, which are known to be highly polyglutamylated. Polyglutamylation (Poly E) was detected on both α - and β -tubulin of conditional CCP5^{-/-} and control treated Sertoli cells without observing important changes in signal intensity between the two samples. The absence of tubulin glutamylation up/downregulation in Sertoli cells from the conditional mouse model suggests that in this mouse Sertoli cells are effectively CCP5^{+/+}.

I then compared the glutamylation of Sertoli cells obtained from Busulfan-treated testes of total CCP5^{-/-} and wild type mice (Fig 4.25 B.). Interestingly, I detected an increase in the GT335 signal in both α and β -tubulin in treated testes of the total CCP5^{-/-} mice, as compared to wild type. Furthermore a decrease in the polyE signal is observable in β -tubulin from treated CCP5^{-/-} testis as compared to wild type. Thus, CCP5^{-/-} Sertoli cells present an increase in β -tubulin glutamylation, and this specifically with short glutamate side chains.

Altogether these results show that we cannot exclude that Sertoli cells in total CCP5^{-/-} mice show tubulin hyperglutamylation, and we can thus not exclude that this partially participates in the observed infertility phenotype of these mice. However, the presence of defective CCP5^{-/-}-like germ cells together to the incomplete Cre-mediated flox alleles excision in the conditional CCP5^{-/-} mouse model strongly suggest that CCP5-controlled glutamylation levels in the germ cell line is more important than in Sertoli cells.

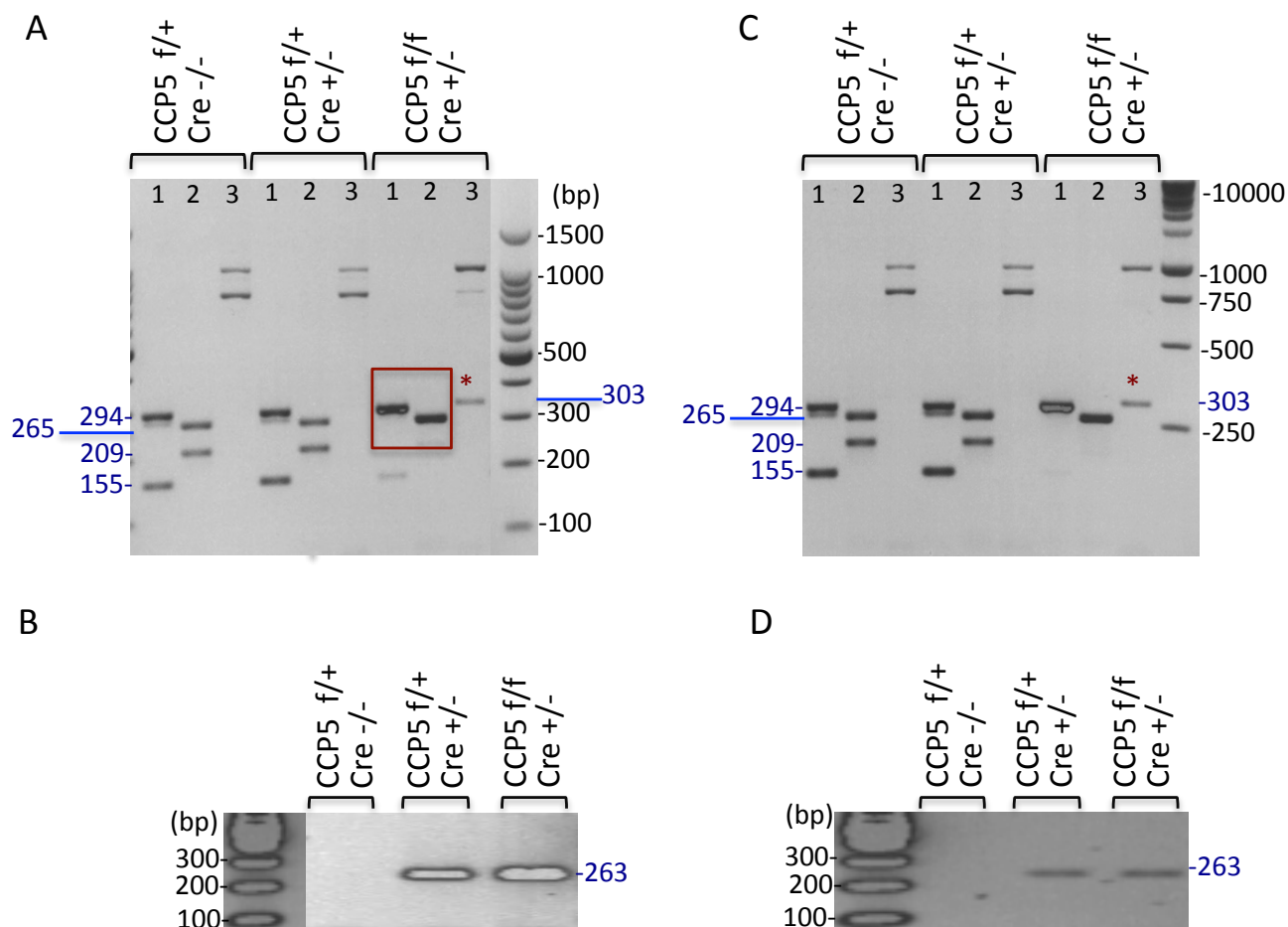
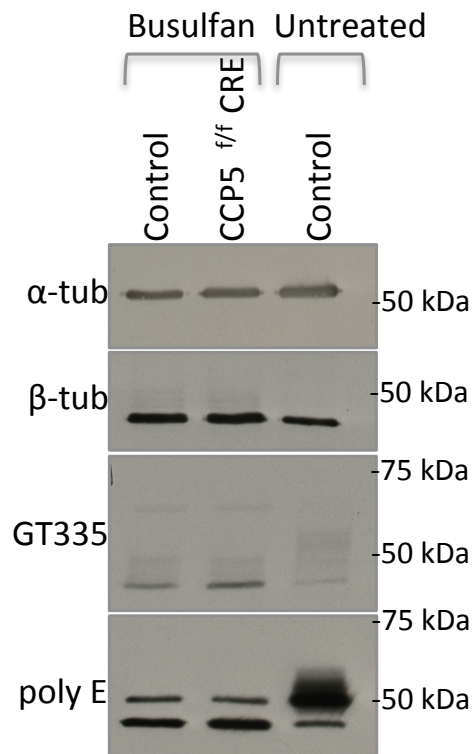


Figure 4.24: Incomplete Cre-mediated defloxing in conditional CCP5^{-/-} testicular germ cells. Wild type alleles (lane1: 155 bp and lane 2: 209 bp), CCP5 flox alleles (lane 1: 294 bp, lane 2: 265 bp); KO allele (lane 3: 303 bp). (A) Representative PCR for CCP5 from wild type (CCP5 f/+ CRE^{+/-}), heterozygous (CCP5 f/+ CRE^{+/-}), knockout (CCP5 f/f CRE^{+/-}) sperm cells. Note the presence of CCP5 Flox alleles in CCP5^{f/f} STRA 8 CRE^{+/-} sperm extract. (B) PCR for STRA 8 CRE (236 bp) from wild type (CCP5 f/+ CRE^{+/-}), heterozygous (CCP5 f/+ CRE^{+/-}), knockout (CCP5 f/f CRE^{+/-}) sperm cells. (C) PCR-based genotyping for CCP5 WT, Flox, and KO alleles from tails of animals used in (A). (D) PCR-based genotyping for STRA 8 CRE from tails of animals used in A.

A



B

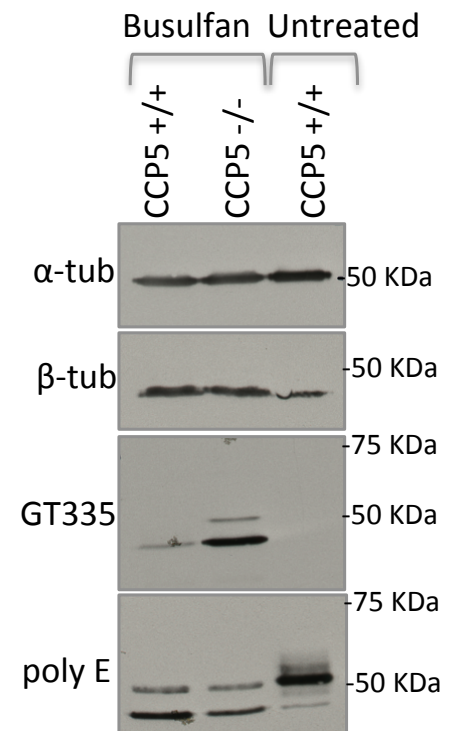


Figure 4.25: Glutamylation levels in wild type and CCP5-mutant Sertoli cells.

Testicular germ cells were deleted from the testis of conditional CCP5^{-/-} (CCP5^{f/f} STRA 8 CRE^{+/-}) (A) CCP5^{-/-} (B) and respective control littermates by intraperitoneal injection of Busulfan at the dose of 30 mg/kg. Control animals were injected with 200 µl of 50% DMSO. One-month post injection mice were sacrificed and testis extracts were used for immunoblot. GT335 detects both long and short glutamate side chains. PolyE recognizes long glutamate side chains.

5. DISCUSSION

Microtubules (MTs) are essential player of the spermatogenesis process. Many of the mechanisms happening during male germ cell development depend on MT organization, their dynamic regulation as well as MT-based traffic (O'Donnell & O'Bryan 2014). Furthermore, germ cells are physically and biochemically supported by the cytoskeleton of the epithelial Sertoli cells (Vogl 1988), in which MTs are able to rapidly respond to changes in shape and position of germ cells (O'Donnell & O'Bryan 2014). Thus, during spermatogenesis MTs have to play many different functions in a perfect coordinated way. This is particularly important during spermiogenesis, the process of maturation of round spermatid into spermatozoa. In this spermatogenetic phase, protein synthesis does not take place anymore, instead a well-coordinated trafficking of proteins and/or organelles has to take place within the germ cell cytoplasm in order to allow each specific cargo to reach its final destination. Consequently, a mechanism allowing spatiotemporal coordination of MT-based traffic must exist. One of the mechanisms that could explain functional regulation of MTs are posttranslational modifications of tubulin, such as polyglutamylation. Polyglutamylation is catalyzed by enzymes of the TTLL family (Janke et al 2005, van Dijk et al 2008b). Polyglutamylation consist in the addition of glutamate side chains of variable length on modification sites that are localized in the carboxy-terminal tails of α - and β -tubulin (Edde et al 1990, Janke et al 2008). Glutamylation is a reversible reaction and enzymes of the CCP family were found to catalyze deglutamylation (Kimura et al 2010, Rogowski et al 2010, Tort et al 2014). CCP5 has a unique enzymatic function among all CCP enzymes: it is the only deglutamylase able to remove the glutamate branching point of the added side chain. Thus, CCP5 specifically regulates the equilibrium

between presence/absence of branching point, and the regulation at this level can influence the presence of short, but indirectly also of longer glutamate side chains.

Glutamylation has been demonstrate to a be enriched on axonemes of different cilia and flagella, and a regulator of axonemal beating (Bre et al 1996, Fouquet et al 1997, Fouquet et al 1996, Fouquet JP. et al 1994, Plessman U & Weber K 1997 , Pringent Y. et al 1996, Redeker et al 1994). However, only the recent generation of knockout mice for TTLL and CCP enzymes allowed to study the role of glutamylation in spermatogenesis *in vivo*. Among glutamylase enzymes, TTLL1 (Campbell et al 2002, Vogel et al 2010) and TTLL5 (Lee et al 2013) has been demonstrate to regulate axoneme assembly and/or maintenance during spermiogenesis, whereas TTLL9 has been shown to regulate both axoneme maintenance and switching of flagellar bending direction in epididymal sperm (Konno et al 2016). Among all CCP enzymes, only CCP1 has been so far linked to spermatogenesis. CCP1 depletion leads to a decreased number of epididymal sperm showing a defective bulbous shaped head and motility defects (Handel & Dawson M. 1981, Kim et al 2011). In this mouse the decreased epididymal sperm output has been linked to an increased number of apoptotic spermatocytes and spermatids (Kim et al 2011) in the mutant testis.

Here I show that CCP5 is another deglutamylase fundamental for mouse male fertility. CCP5^{-/-} mice are affected by oligoasthenoteratospermia, the most common pathology of human infertility. Oligoasthenoteratospermia consists in a combination of several infertility-related defects: decreased sperm output, defective sperm morphology and motility. Thus, the goal of my PhD was to understand which spermatogenesis-related mechanisms are impaired in the CCP5^{-/-} mouse, thus allowing a deeper understanding about which phases of spermatogenesis are regulated by CCP5-mediated tubulin glutamylation.

5.1 Reduced sperm output in CCP5^{-/-} is due to defects in the post-meiotic phase of spermatogenesis

Spermatogenesis is divided in three main phases: mitotic, meiotic and post-meiotic phases. Defects in each of those phases can lead to infertility.

Generally, defects that happen during mitotic or meiotic phases lead to spermatogenesis arrest with apoptosis of the defective germ cells and consequent lacking of post-meiotic germ cells within the seminiferous epithelium. However, several lines of evidence suggest that the infertility phenotype observed in the CCP5^{-/-} mouse is most likely due to defects in spermiogenesis rather than in earlier phases of spermatogenesis. Indeed, although a disorganized cytoarchitecture, the CCP5^{-/-} seminiferous epithelium is composed of all different germ-cell types, from spermatogonia to condensed spermatids. However, the release of spermatozoa from the seminiferous tubules was rarely observed. Histological analysis of epididymis reveal that, instead of spermatozoa, epididymis are filled with premature post-meiotic germ cells, suggesting that one cause of the decreased sperm output in CCP5^{-/-} mice is the premature exfoliation of the seminiferous epithelium. The premature release of germ cells might be the consequence of defects in MT organization of Sertoli cells. However, it has been shown that the MT-disrupting agent colchicine leads to non-selective germ cell sloughing in the seminiferous epithelium (Correa et al 2002). This is not the case in CCP5^{-/-}, where I observed a selective releasing of post-meiotic germ cells. On the other hand, a mutation in the testis-specific MT-severing enzyme Katanin-like protein 1 (KATNAL1) led to the disruption of MT dynamics in Sertoli cells, and consequently sloughing of spermatids (Smith et al 2012) in the seminiferous epithelium. However in this mouse model, defective MT severing in Sertoli cells correlated with decreased testes size because of the massive loss of post-meiotic germ cells from the epithelium (Smith et al 2012). In contrast, in CCP5^{-/-}, I did not observe testicular atrophy

suggesting that the release of elongating spermatids might take place during late phases of spermiogenesis, and is most likely not mediated by MT defects in Sertoli cells. However, the presence of dislocated elongating spermatids in the seminiferous epithelium suggests a defective mechanism of spermatid transportation through the seminiferous epithelium. Indeed, although the biological function of this process is not well understood, cytoplasmic dynein of Sertoli cells is known to mediate this movement in concert with the ectoplasmic specialization of elongating spermatids (Guttman et al 2000). As I observed an increase in both α - and β -tubulin glutamylation in CCP5^{-/-} Sertoli cells, it might be that those changes in tubulin PTM levels interfere with the MT-based transport of elongating spermatids within the seminiferous epithelium.

Altogether my results demonstrate that the reduced sperm count in CCP5^{-/-} is most likely due to impairment of one or more steps of differentiation of spermatid into spermatozoa. Moreover, as I did not observe testicular atrophy over time I can exclude major defects in Sertoli cell MT dynamics and organization, or an age-related phenotype.

5.2 The entire process of spermiogenesis is defective in the CCP5^{-/-} mouse

Spermiogenesis is the process by which round spermatids undergo a series of complex morphological changes to generate spermatozoa that are composed of a condensed hydrodynamic, hook-shaped head, and a long flagellum composed by the axoneme and its associated structures.

During their differentiation spermatids develop 5 specific structures that are necessary for the formation of healthy and functional spermatozoa:

- The acrosome is formed at the apical pole of round spermatids nucleus
- The centrioles migrate to the caudal pole of the round spermatid and undergo a functional shift to basal body

- The axoneme is fully ensembled in round spermatids at early stages of spermiogenesis, whereas its accessory elements such as ODF, mitochondria- and fibrous sheath will be added throughout spermiogenesis.
- The transient MT-based manchette assembles as soon as the spermatid nucleus starts its elongation contributing with mechanical forces at the nuclear shaping of the cell.
- Elongating spermatid chromatin undergoes compaction process by the replacement of histones with transition proteins and protamines.

As we supposed that the infertility phenotype in $CCP5^{-/-}$ was due to impairments in spermiogenesis, I analyzed which of the above-mentioned processes are impaired in $CCP5^{-/-}$ mice in order to understand which mechanisms could be regulated by CCP5-mediated glutamylation.

Interestingly, my results demonstrate that in $CCP5^{-/-}$ spermatids, all the important steps characterizing spermiogenesis are impaired, suggesting that CCP5 is a major regulator of MT functions during spermiogenesis.

5.2.1 CCP5 is important for acrosome elongation as well as for nucleus-acrosome anchoring.

Electron microscopy analysis of $CCP5^{-/-}$ testis revealed several defects on acrosome formation and integrity. Acrosome biogenesis takes place in round spermatids during the Golgi and Cap phases of spermiogenesis, whereas its elongation happens during the acrosomal phase, which coincides with the beginning of the nuclear elongation process (Abou-Haila & Tulsiani 2000, Kierszenbaum et al 2003). So far, MTs have been shown to regulate the Golgi and Cap phase, during which a disruption of the MT network by MT

depolymerizing agents lead to formation of a fragmented acrosome (Huang & Ho 2006, Moreno et al 2006). However, once the acrosome is formed, MT depolymerization has not been shown to disrupt acrosome integrity or attachment to the nuclear envelope in elongating spermatids (Moreno et al 2006).

My results show that in $CCP5^{-/-}$ elongating spermatids, characterized by an overall increased level of glutamylated tubulin, the acrosomes show abnormal shapes. In some spermatids, the acrosome presents a constriction in its apical pole, giving rise to a bulb-like shape. Furthermore, acrosome elongation does not seem to happen in a symmetrical way, as I observed spermatids with an asymmetrically extended acrosome. Finally, in late condensed spermatids the acrosome is completely or partially detached from the nuclear membrane. Altogether my results suggest that unbalancing of MT glutamylation level due to lacking CCP5 gives rise to several acrosomal defects, most likely happening during late phases of acrosome development. However, as I observed MT hyperglutamylation in $CCP5^{-/-}$ round spermatids, we cannot exclude that unbalancing of the glutamylation level interferes with MT-based transport of some acrosomal proteins during early steps of acrosome biogenesis, thus causing defects later during acrosome development. Acrosome elongation, as well as its anchoring to the nucleus, depend both on acroplaxome (Kierszenbaum et al 2003) and perinuclear theca development (Oko & Sutovsky 2009). Indeed the acrosome extension is caudally guided by the descending of the acroplaxome marginal ring toward the caudal pole of the cell (Kierszenbaum et al 2003). Although MTs have so far not been linked to acroplaxome function or structure, many acroplaxome-related proteins are still to be characterized. Interestingly, acrosome detachment has been observed in epididymal spermatozoa after Lamin A/C silencing by siRNA injection in the rete testis (Shen et al 2014). The Lamin A/C protein, also known as LMNA, is a component of the acroplaxome, but has been shown to participate also in manchette formation (Shen et al 2014). Moreover immuno pull-down analyses have shown

that Lamin A/C interact with the MT plus-end tracking protein CLIP-170, which in turn is localized at the manchette and perinuclear ring (Akhmanova et al 2005). Thus, although a direct interaction between these two proteins has not been described yet, it strongly suggests that interactions between MT-associated proteins and acroplaxome protein components are possible, and consequently we cannot exclude that MTs participate in acrosome-acroplaxome-manchette interactions. The perinuclear theca has also been implicated in the acrosome-nucleus attachment. It has been shown that proteins of the post-acrosomal sheath of the perinuclear theca reach their final destination by intra-manchette transport (Okou & Sutovsky 2009, Tovich et al 2004). Thus it might be possible that the observed high levels of tubulin PTMs in CCP5^{-/-} elongating spermatid manchettes lead to defects in intra-manchette transport, thus affecting perinuclear theca protein composition, which then leads to acrosome detachment. It would be interesting for future studies to further analyze acrosome biogenesis in CCP5^{-/-} round spermatids, as well as to study the ultrastructure of acroplaxome and perinuclear theca in CCP5^{-/-} elongating spermatids.

5.2.2 CCP5^{-/-} elongating spermatids are characterized by a hypermodified and ultrastructural defective manchettes

The appearance of the manchette coincides with the first steps of nuclear elongation in spermatids. It is later disassembled by an unknown mechanism when nuclear elongation is completed. This suggests that the manchette plays a major role in the shaping of sperm nuclei (O'Donnell & O'Bryan 2014). Although manchette is a transient structure, it is known so far to be composed of acetylated, glutamylated and detyrosinated MTs (Fouquet JP. et al 1994, Hermo et al 1991, Mochida et al 1999) suggesting that, when assembled, MTs are stable. However, those stable MTs have to be disassembled at later stages of

spermiogenesis. This implicates that a spatio-temporal fine control of MT PTMs could allow for enhancing MT severing and disassembly at the right developmental step.

Here I show for the first time that CCP5^{+/+} manchette MTs are subjected to two so-far not described PTMs: glycylation (mono- and poly-) and the Δ 2-tubulin modification. Recently several works have underlined the importance of intra-manchette transport in spermatid development (Kierszenbaum 2002a, Kierszenbaum et al 2011b, Lehti et al 2013, Liu et al 2015). It is thus intuitive that manchette MTs are subjected to a broad range of tubulin PTMs to generate a MT-identity code that most likely participates in the regulation of the intra-manchette transport.

Interestingly, CCP5^{-/-} manchettes are characterized by an overall increased level of tubulin PTMs, including a higher level of short glutamate side chains as compared to wild type. Moreover, electron microscopy analysis revealed several ultrastructural defects such as non-parallel organization of manchette MTs, as well as asymmetric and/or ectopic emanation of MTs from the perinuclear ring. Also, manchette abnormalities correlate with aberrantly shaped elongating spermatid nuclei in CCP5^{-/-} mice. Interestingly, asymmetric or mislocalized manchettes have been already observed in the CLIP-170-KO mice, where dysfunctions of the manchette have been linked to mislocalization of the dynactin-dynein complex along the nuclear envelope (Akhmanova et al 2005), thus interfering with manchette movement along the nucleus (Yoshida et al 1994). Another MT-related protein that has been shown to regulate manchette structure is katanin p80, the regulatory subunit of the MTs-severing enzyme katanin (O'Donnell et al 2012). Mutation in p80 cause abnormal, bulbous-shaped sperm heads due to a delayed manchette clearing and descending of the perinuclear ring (O'Donnell et al 2012), suggesting that MT-severing activity is important for manchette disassembly and movement.

Another interesting phenotype that has been observed in CCP5^{-/-} spermatids is the ectopic localization of manchette MTs within the nucleus. Interestingly, this phenomenon has been

reported in Taxol- (Russell et al 1991) and Carbendazim- (Nakai et al 1997) treated testes, linking MT hyperstability to the nuclear indentation of the manchette. The overall increased level of tubulin PTMs together with the presence of ectopic MTs inside spermatid nuclei thus strongly suggests that the lacking of CCP5 leads to MT hyperstabilization in CCP5^{-/-} spermatids. To test this hypothesis I tried to measure the resistance of MTs to depolymerization by incubation of CCP5^{+/+} and CCP5^{-/-} testicular dissociated cells at 4°C during different incubation times (Data not shown). However, I did not manage to find the right experimental conditions to allow MTs depolymerization in CCP5^{+/+} cells. Thus the experiment needs to be optimized in order to verify this hypothesis.

Altogether my results demonstrate that CCP5-mediated glutamylation is important for normal manchette formation and functions. Based on the hypothesis that tubulin glutamylation might participate in the regulation of MT-based traffic, thus in the localization of MAPs within the manchette, my results suggests that CCP5 is an upstream regulator of manchette function and structure.

5.2.3 Formation of multiple defective flagella in CCP5^{-/-} elongating spermatids

The most striking phenotype observed I observed in CCP5^{-/-} elongating spermatids by immunofluorescence was the presences of MTs situated caudally to the manchette, and that are organized into hair-like structures. Those MTs appear to be highly modified, and are only found in CCP5^{-/-} spermatids, suggesting that either they are newly nucleated in the mutant cells, or that they are not disassembled. Our electron microscopy analysis revealed that these MT hair-like structures are most likely composed of singlet and/or doublet MTs, which are scattered in the cytoplasm. Interestingly disorganized mitochondria and ODFs are seen around those MTs indicating that they might carry a flagellar identity code. In serial sections of elongating spermatids is possible to observe the presence of an

axoneme that is assembled in its proximal tract, but splits apart in more distal regions. Moreover, in the same cells, others MT doublets are seen in the cytoplasm. These data strongly suggest the presence of multiple instable defective flagella in CCP5^{-/-} elongating spermatids, which is supported by, the presence of multiple basal bodies in CCP5^{-/-} elongating spermatids.

Two mechanisms could explain the observed supernumerary centrioles: failure of meiotic division, or centriole overduplication. Defects in cytokinesis are often correlated with the presence of multinucleated spermatids within the seminiferous epithelium (O'Donnell 2014). These cells are most likely composed of 2-4 nuclei (O'Donnell 2014), however the multinucleated cells that I observed in CCP5^{-/-} testis are composed of several, dark-stained defective nuclei, which are more likely degenerating spermatids. Vacuolated, multinucleated and highly defective cells were often observed in the testes of the conditional CCP5^{-/-} mouse (data not shown), supporting this hypothesis. In the future, others studies are needed to understand the mechanism leading to supernumerary centrioles in CCP5^{-/-} spermatids.

Interestingly, CCP5 ablation in Zebrafish Fleer mutant larvae, characterized by impaired multiciliogenesis and decreased levels of glutamylation because of a miss-targeting of TTLL6 into cilia (Pathak et al 2007), leads to the rescue of the ciliary phenotype (Pathak et al 2014). Interesting, CCP1 and/or CCP6 ablation does not rescue the phenotype (Pathak et al 2014). This observation together with the formation of multiple defective flagella in CCP5^{-/-} mouse spermatids opens new questions about a potential role of CCP5 as regulator of multi-cilia/flagella-genesis.

5.2.4 CCP5-mediated glutamylation participates in the regulation of the acrosome-acroplaxome-manchette-tail system.

The study of several knockout mice has allowed for a deep understanding of the acrosome-acroplaxome-manchette-tail system. Indeed it has been demonstrated that during spermatid development, several proteins are localized first in the acroplaxome, later in the manchette and, once the manchette disassembles, in the sperm flagellum (Kierszenbaum 2002a, Kierszenbaum et al 2011b, Lehti et al 2013, Liu et al 2015, Zhou et al 2012). IFT88, a member of the IFTB complex, together with the Golgi-MTs associated protein 210 (GMAP 210), have been shown to mediate the pro-acrosomal vesicle trafficking in round spermatids (Kierszenbaum et al 2011b). In elongating spermatids both, IFT88 and GMAP 210 are detected in the acrosome-acroplaxome region as well as in the manchette. After manchette clearing, IFT88 localizes both to acroplaxome and tail region whereas GMAP210 is detected only in the flagellum (Kierszenbaum et al 2011b), suggesting that a mechanism allowing a fine-tuned spatial-temporal subcellular localization of those proteins might exist. The study of the hypomorphic IFT88 mouse model revealed the presence of ultrastructural defects quite similar to the one observed in CCP5^{-/-} elongating spermatids (Kierszenbaum et al 2011b). Indeed IFT88 mutant spermatids are characterized by misshaped nuclei, ectopic manchette emanations, presence of multiple basal bodies, as well as a tail “stump” formation. Interestingly, the tail stump has been shown to be formed by randomly arranged MTs, mitochondria and ODFs, which are dispersed in the germ cell cytoplasm, an organization quite similar to the one characterizing the MT hair-like structure that I am presenting here.

MT organization, as well as the capacity of MTs to act as tracks for movement of proteins within the manchette and the cytoplasm are extremely important during spermiogenesis, when protein synthesis ceases. Throughout spermatid development, a great numbers of

proteins and organelles have to be transported to specific places at given time points in order to develop healthy spermatozoa. The observation that mice carrying mutation on these proteins develop several ultrastructural defects on acrosome, manchette and flagellum underscore the importance of a fine-tuned regulation of the MT-based transport. Tubulin glutamylation, together with other PTMs of tubulin, might provide a guide that selectively regulates the affinity of MTs for motor proteins and MT-associated proteins, thus regulating the traffic of several sperm components.

My results demonstrate that in $CCP5^{-/-}$ spermatids the whole spermatid differentiation process is impaired. Considering that I observed an increase in tubulin modified with short glutamate side chains, as well as in other tubulin PTMs, we hypothesized that the ultrastructural defects observed in $CCP5^{-/-}$ spermatids are due to a misregulation of the MT-based traffic. In order to assess the molecular mechanism underlining some of the ultrastructural defects observed in $CCP5^{-/-}$ spermatids, it will be interesting to analyze whether the localization pattern of IFT88 or of other described proteins is defective in $CCP5^{-/-}$ spermatids. However, as I also observed a premature and stronger glutamylation signal on a yet not identified non-tubulin substrate, we cannot exclude the possibility that CCP5 regulates one or more mechanism in spermiogenesis via glutamylation of other proteins. The identification of this new substrate by mass spectrometry analysis could clarify some aspects of mechanisms impaired in $CCP5^{-/-}$ spermiogenesis.

5.3 Implication of Sertoli cells in the $CCP5^{-/-}$ infertility phenotype

One of the open questions that arose from the study of $CCP5^{-/-}$ mouse model was which of the observed phenotypes were due to the lacking of CCP5 in the germ cells, and which to the epithelial Sertoli cells. To answer this question I generated the conditional $CCP5^{-/-}$ ($CCP5^{ff}$ STRA8-iCRE^{+/-}) mouse. In this mouse model only testicular germ cells are $CCP5^{-/-}$

, whereas Sertoli cells remain CCP5^{+/+}. Strikingly, testes from this mouse model are composed of a mixed population of wild-type-like and CCP5^{-/-}-like germ cells. This observation was quite astonishing as in the conditional CCP5^{-/-} mouse all the Sertoli cells are supposed to be CCP5^{+/+}, a hypothesis that is strongly supported by the detection of equal glutamylation levels on Sertoli-cell-only testes from conditional CCP5^{-/-} and control mice. Thus, if the observed CCP5^{-/-} phenotype would be only due to defective Sertoli cell functions, I should have observed a complete absence of the ultrastructural defects in the conditional CCP5^{-/-} testes. On the other hand, if CCP5^{-/-} infertility would be due to germ-cell autonomous mechanisms, both total and conditional CCP5^{-/-} mice should have shown the same phenotype. However the mixed phenotype in conditional CCP5^{-/-} is more difficult to explain. One explanation could be that some of the defects observed in total CCP5^{-/-} mice are related to Sertoli-cell malfunction, while others are germ-cell-intrinsic defects. In this case I should have detected a partial or total rescue of some ultrastructural CCP5^{-/-} defects. However I observed that of most cell populations, both, defective and normal cells were present. The most likely explanation for this phenotype could be an incomplete cre-mediated excision of the flox alleles in some of the germ cells, leading to a less penetrant, mosaic phenotype of germ cells.

This problem has already been observed in others cases (Bao et al 2013) and it has been shown that STRA8-icre-mediated excision of flox alleles is more efficient in mice carrying one copy of the flox alleles and one copy of knockout alleles (Bao et al 2013). To confirm this notion, I am actually generating the CCP5^{f/f} STRA8-iCRE mouse model for future analysis. However, it is possible to conclude from the study of the CCP5^{f/f} STRA8-iCRE^{+/-} mice that most of not all of the observed phenotypes of the CCP5^{-/-} mice are germ-cell intrinsic, as among defective cells in the conditional CCP5^{-/-} mouse show the same ultrastructural defects. Moreover, both, complete and conditional CCP5^{-/-} mice show the same PTM patterns in germ cells of different developmental stages, suggesting that CCP5

plays a major role in germ cells rather than in Sertoli cells. Moreover, as I did not detect changes in the expression of others tubulin-modifying enzymes (TTLLs and CCPs) in CCP5^{-/-} testicular germ cells, we can exclude that others glutamylases or deglutamylases significantly participate in the generation of the CCP5^{-/-} phenotypes. This strongly suggests that the observed spermiogenetic failures are mainly due to the lacking of CCP5 in germ cells. However, we cannot entirely exclude that Sertoli cells partially participate in the generation of the CCP5^{-/-} phenotypes, as we also detected increased α - and β -tubulin glutamylation signals in CCP5^{-/-} Sertoli cells-only testes.

6. CONCLUSION

The goal of my PhD was to understand by which mechanism CCP5 regulates spermatogenesis, and how its deglutamylases activity affects the MTs cytoskeleton as well as its posttranslational modifications during mouse spermatogenesis. To answer these questions I characterized and compared the spermatogenic processes wild type and CCP5^{-/-} mice.

My results demonstrate that CCP5 is a central regulator of several MT-based functions during mouse spermiogenesis:

- CCP5 is generally highly expressed in wild type testicular germ cells and its deletion does not provoke any evident change in the expression level of others CCP and TTLL enzyme suggesting a non-redundant function of CCP5 during spermatogenesis.
- The lack of CCP5 is associated with a premature glutamylation of cortical MTs in round spermatids, and with an overall increase in the levels of glutamylation of α -tubulin in elongating spermatids.
- The lack of CCP5 leads to changes in the glutamylation of a yet unidentified protein (here called non-tubulin substrate), suggesting that CCP5 might regulate spermatogenesis also via MT-independent mechanisms.
- Absence of CCP5 correlates with overall increased levels of other PTMs, suggesting that MTs are hyper-stabilized in round and elongating spermatids.
- CCP5^{-/-} mice are oligoasthenoteratospermic because a severe impairment of spermatid maturation during spermiogenesis

- The lack of CCP5 causes acrosome elongation defects, as well as failures in nucleus-acrosome attachment in condensed spermatids, suggesting that CCP5 might regulate the development of acrosome, acroplaxome and perinuclear theca.
- Manchette MTs present several ultrastructural defects such as an ectopic emanation, a non-parallel organization of manchette MTs and nuclear invagination in CCP5^{-/-} elongating spermatids, suggesting that the deregulation of the PTM profile in elongating spermatids might be responsible for the generation of structural and functional defective manchette in CCP5^{-/-} mice.
- The lack of CCP5 leads to the presence of supernumerary centrioles, and thus basal bodies in elongating spermatids
- CCP5^{-/-} elongating spermatids fail to build a single well-developed flagellum. Instead, disorganized doublet or singlet MTs are found in the germ cell cytoplasm together with disorganized ODFs and mitochondria. Electron microscopy analyses revealed the presence of multiple unstable defective flagella in CCP5^{-/-} spermatids.
- The analysis of the conditional CCP5^{-/-} mouse model suggest that the observed phenotypes are most likely due to the lacking of CCP5 in germ cells rather than in the epithelial Sertoli cells.

BIBLIOGRAPHY

- Abou-Haila A, Tulsiani DR. 2000. Mammalian sperm acrosome: formation, contents, and function. *Arch Biochem Biophys* 379: 173-82
- Aillaud C, Bosc C, Saoudi Y, Denarier E, Peris L, et al. 2016. Evidence for new C-terminally truncated variants of alpha- and beta-tubulins. *Mol Biol Cell* 27: 640-53
- Akhmanova A, Mausset-Bonnefont A-L, van Cappellen W, Keijzer N, Hoogenraad CC, et al. 2005. The microtubule plus-end-tracking protein CLIP-170 associates with the spermatid manchette and is essential for spermatogenesis. *Genes Dev* 19: 2501-15
- Akhmanova A, Steinmetz MO. 2008. Tracking the ends: a dynamic protein network controls the fate of microtubule tips. *Nat Rev Mol Cell Biol* 9: 309-22
- Alexander JE, Hunt DF, Lee MK, Shabanowitz J, Michel H, et al. 1991. Characterization of posttranslational modifications in neuron-specific class III beta-tubulin by mass spectrometry. *Proc Natl Acad Sci U S A* 88: 4685-9
- Bao J, Ma HY, Schuster A, Lin YM, Yan W. 2013. Incomplete cre-mediated excision leads to phenotypic differences between Stra8-iCre; Mov10l1(lox/lox) and Stra8-iCre; Mov10l1(lox/Delta) mice. *Genesis* 51: 481-90
- Berezniuk I, Lyons PJ, Sironi JJ, Xiao H, Setou M, et al. 2013. Cytosolic carboxypeptidase 5 removes alpha- and gamma-linked glutamates from tubulin. *J Biol Chem* 288: 30445-53
- Bettencourt-Dias M, Glover DM. 2007. Centrosome biogenesis and function: centrosomics brings new understanding. *Nat Rev Mol Cell Biol* 8: 451-63
- Bonnet C, Boucher D, Lazereg S, Pedrotti B, Islam K, et al. 2001. Differential binding regulation of microtubule-associated proteins MAP1A, MAP1B, and MAP2 by tubulin polyglutamylation. *J Biol Chem* 276: 12839-48

- Bornens M. 2012. The Centrosome in Cells and Organisms. *Science* 335: 422-26
- Bosch Grau M, Gonzalez Curto G, Rocha C, Magiera MM, Marques Sousa P, et al. 2013. Tubulin glycylation and glutamylases have distinct functions in stabilization and motility of ependymal cilia. *J Cell Biol* 202: 441-51
- Boucher D, Larcher J-C, Gros F, Denoulet P. 1994. Polyglutamylation of Tubulin as a Progressive Regulator of in Vitro Interactions between the Microtubule-Associated Protein Tau and Tubulin+. *Biochemistry* 33: 12471-77
- Bre MH, Redeker V, Quibell M, Darmanaden-Delorme J, Bressac C, et al. 1996. Axonemal tubulin polyglycylation probed with two monoclonal antibodies: widespread evolutionary distribution, appearance during spermatozoan maturation and possible function in motility. *J Cell Sci* 109 (Pt 4): 727-38
- Campbell PK, Waymire KG, Heier RL, Sharer C, Day DE, et al. 2002. Mutation of a novel gene results in abnormal development of spermatid flagella, loss of intermale aggression and reduced body fat in mice. *Genetics* 162: 307-20
- Chemes HE. 2012. Sperm Centrioles and Their Dual Role in Flagellogenesis and Cell Cycle of the Zygote. 33-48
- Cooke HJ, Saunders PT. 2002. Mouse models of male infertility. *Nat Rev Genet* 3: 790-801
- Correa LM, Nakai M, Strandgaard CS, Hess RA, Miller MG. 2002. Microtubules of the mouse testis exhibit differential sensitivity to the microtubule disruptors Carbendazim and colchicine. *Toxicol Sci* 69: 175-82
- de Boer P, de Vries M, Ramos L. 2015. A mutation study of sperm head shape and motility in the mouse: lessons for the clinic. *Andrology* 3: 174-202
- de Rooij DG. 2001. Proliferation and differentiation of spermatogonial stem cells. *Reproduction* 121: 347-54

- Drewes G, Ebner A, Preuss U, Mandelkow EM, Mandelkow E. 1997. MARK, a novel family of protein kinases that phosphorylate microtubule-associated proteins and trigger microtubule disruption. *Cell* 89: 297-308
- Edde B, Rossier J, Le Caer JP, Desbruyeres E, Gros F, Denoulet P. 1990. Posttranslational glutamylation of alpha-tubulin. *Science* 247: 83-5
- Eddy EM, Toshimori K, O'Brien DA. 2003. Fibrous sheath of mammalian spermatozoa. *Microsc Res Tech* 61: 103-15
- Ersfeld K, Wehland J, Plessmann U, Dodemont H, Gerke V, Weber K. 1993. Characterization of the tubulin-tyrosine ligase. *J Cell Biol* 120: 725-32
- Fawcett DW. 1975. The mammalian spermatozoon. *Dev Biol* 44: 394-436
- Fawcett DW, Anderson WA, Phillips DM. 1971. Morphogenetic factors influencing the shape of the sperm head. *Dev Biol* 26: 220-51
- Fawcett DW, Phillips DM. 1969. The fine structure and development of the neck region of the mammalian spermatozoon. *Anat Rec* 165: 153-64
- Fernandez-Gonzalez A, La Spada AR, Treadaway J, Higdon JC, Harris BS, et al. 2002. Purkinje cell degeneration (pcd) phenotypes caused by mutations in the axotomy-induced gene, Nna1. *Science* 295: 1904-6
- Fouquet JP, Kann ML, Pechart I, Prigent Y. 1997. Expression of tubulin isoforms during the differentiation of mammalian spermatozoa. *Tissue Cell* 29: 573-83
- Fouquet JP, Prigent Y, Kann ML. 1996. Comparative immunogold analysis of tubulin isoforms in the mouse sperm flagellum: unique distribution of glutamylated tubulin. *Mol Reprod Dev* 43: 358-65
- Fouquet JP., Edde B., Kann ML., Wolff A., Desbruyeres E., Denoulet P. 1994. Differential distribution of glutamylated tubulin during spermatogenesis in mammalian testis. *Cell Motil Cytoskeleton* 27: 49-58

- Fukushima N, Furuta D, Hidaka Y, Moriyama R, Tsujiuchi T. 2009. Post-translational modifications of tubulin in the nervous system. *J Neurochem* 109: 683-93
- Gagnon C, White D, Cosson J, Huitorel P, Eddé B, et al. 1996. The polyglutamylated lateral chain of alpha-tubulin plays a key role in flagellar motility. *Journal of Cell Science* 109: 1545-53
- Goode BL, Drubin DG, Barnes G. 2000. Functional cooperation between the microtubule and actin cytoskeletons. *Current Opinion in Cell Biology* 12: 63-71
- Gundersen GG, Khawaja S, Bulinski JC. 1987. Postpolymerization detyrosination of alpha-tubulin: a mechanism for subcellular differentiation of microtubules. *J Cell Biol* 105: 251-64
- Guttman JA, Kimel GH, Vogl AW. 2000. Dynein and plus-end microtubule-dependent motors are associated with specialized Sertoli cell junction plaques (ectoplasmic specializations). *J Cell Sci* 113 (Pt 12): 2167-76
- Handel MA, Dawson M. 1981. Effects on Spermiogenesis in the Mouse of a Male Sterile Neurological Mutation, Purkinje Cell Degeneration. *Gamete Research* 4: 185-92
- Hawkins T, Mirigian M, Selcuk Yasar M, Ross JL. 2010. Mechanics of microtubules. *J Biomech* 43: 23-30
- Hermo L, Oko R, Hecht NB. 1991. Differential post-translational modifications of microtubules in cells of the seminiferous epithelium of the rat: a light and electron microscope immunocytochemical study. *Anat Rec* 229: 31-50
- Hermo L, Pelletier RM, Cyr DG, Smith CE. 2010a. Surfing the wave, cycle, life history, and genes/proteins expressed by testicular germ cells. Part 2: changes in spermatid organelles associated with development of spermatozoa. *Microsc Res Tech* 73: 279-319
- Hermo L, Pelletier RM, Cyr DG, Smith CE. 2010b. Surfing the wave, cycle, life history, and genes/proteins expressed by testicular germ cells. Part 3: developmental changes

in spermatid flagellum and cytoplasmic droplet and interaction of sperm with the zona pellucida and egg plasma membrane. *Microsc Res Tech* 73: 320-63

Hess RA, Renato de Franca L. 2008. Spermatogenesis and cycle of the seminiferous epithelium. *Adv Exp Med Biol* 636: 1-15

Holstein AF, Schulze W, Davidoff M. 2003. Understanding spermatogenesis is a prerequisite for treatment. *Reprod Biol Endocrinol* 1: 107

Hoyer-Fender S. 2010. Centriole maturation and transformation to basal body. *Semin Cell Dev Biol* 21: 142-7

Hoyer-Fender S. 2012. Centrosomes in fertilization, early embryonic development, stem cell division, and cancer *Atlas of Genetics and Cytogenetics in Oncology and Haematology* 16

Huang WP, Ho HC. 2006. Role of microtubule-dependent membrane trafficking in acrosomal biogenesis. *Cell Tissue Res* 323: 495-503

Ikegami K, Heier RL, Taruishi M, Takagi H, Mukai M, et al. 2007. Loss of alpha-tubulin polyglutamylation in ROSA22 mice is associated with abnormal targeting of KIF1A and modulated synaptic function. *Proc Natl Acad Sci U S A* 104: 3213-8

Ikegami K, Sato S, Nakamura K, Ostrowski LE, Setou M. 2010. Tubulin polyglutamylation is essential for airway ciliary function through the regulation of beating asymmetry. *Proc Natl Acad Sci U S A* 107: 10490-5

Inaba K. 2011. Sperm flagella: comparative and phylogenetic perspectives of protein components. *Mol Hum Reprod* 17: 524-38

Infante C, Ramos-Morales F, Fedriani C, Bornens M, Rios RM. 1999. GMAP-210, A Cis-Golgi Network-associated Protein, Is a Minus End Microtubule-binding Protein. *THE JOURNAL OF CELL BIOLOGY* 145: 83-98

- Ishijima S, Baba SA, Mohri H, Suarez SS. 2002. Quantitative analysis of flagellar movement in hyperactivated and acrosome-reacted golden hamster spermatozoa. *Mol Reprod Dev* 61: 376-84
- Ishikawa H, Marshall WF. 2011. Ciliogenesis: building the cell's antenna. *Nat Rev Mol Cell Biol* 12: 222-34
- Jan SZ, Hamer G, Repping S, de Rooij DG, van Pelt AM, Vormer TL. 2012. Molecular control of rodent spermatogenesis. *Biochim Biophys Acta* 1822: 1838-50
- Janke C. 2014. The tubulin code: Molecular components, readout mechanisms, and functions. *The Journal Of Cell Biology:Review* 206: 461-72
- Janke C, Bulinski JC. 2011. Post-translational regulation of the microtubule cytoskeleton: mechanisms and functions. *Nat Rev Mol Cell Biol* 12: 773-86
- Janke C, Kneussel M. 2010. Tubulin post-translational modifications: encoding functions on the neuronal microtubule cytoskeleton. *Trends Neurosci* 33: 362-72
- Janke C, Rogowski K, van Dijk J. 2008. Polyglutamylation: a fine-regulator of protein function? 'Protein Modifications: beyond the usual suspects' review series. *EMBO Rep* 9: 636-41
- Janke C, Rogowski K, Wloga D, Regnard C, Kajava AV, et al. 2005. Tubulin Polyglutamylase Enzymes Are Members of the TTL Domain Protein Family. *SCIENCE* 308: 1758-62
- Jaworski J, Hoogenraad CC, Akhmanova A. 2008. Microtubule plus-end tracking proteins in differentiated mammalian cells. *Int J Biochem Cell Biol* 40: 619-37
- Kalebic N, Sorrentino S, Perlas E, Bolasco G, Martinez C. 2013. α TAT1 is the major α -tubulin acetyltransferase in mice. *Nature communications*
- Kalinina E, Biswas R, Berezniuk I, Hermoso A, Aviles FX, Fricker LD. 2007. A novel subfamily of mouse cytosolic carboxypeptidases. *FASEB J* 21: 836-50

- Kann M-L, Soues S, Levilliers N, Fouquet J-P. 2003. Glutamylated Tubulin: Diversity of Expression and Distribution of Isoforms. *Cell Motility and the Cytoskeleton* © 2003 55: 14-25
- Kierszenbaum AL. 2001. Spermatid manchette: plugging proteins to zero into the sperm tail. *Mol Reprod Dev* 59: 347-9
- Kierszenbaum AL. 2002a. Intramanchette transport (IMT): managing the making of the spermatid head, centrosome, and tail. *Mol Reprod Dev* 63: 1-4
- Kierszenbaum AL. 2002b. Keratins: unraveling the coordinated construction of scaffolds in spermatogenic cells. *Mol Reprod Dev* 61: 1-2
- Kierszenbaum AL, Gil M, Rivkin E, Tres LL. 2002. Ran, a GTP-binding protein involved in nucleocytoplasmic transport and microtubule nucleation, relocates from the manchette to the centrosome region during rat spermiogenesis. *Mol Reprod Dev* 63: 131-40
- Kierszenbaum AL, Rivkin E, Tres LL. 2003. Acroplaxome, an F-actin-keratin-containing plate, anchors the acrosome to the nucleus during shaping of the spermatid head. *Mol Biol Cell* 14: 4628-40
- Kierszenbaum AL, Rivkin E, Tres LL. 2011a. Cytoskeletal track selection during cargo transport in spermatids is relevant to male fertility. *Spermatogenesis* 1: 221-30
- Kierszenbaum AL, Rivkin E, Tres LL, Yoder BK, Haycraft CJ, et al. 2011b. GMAP210 and IFT88 are present in the spermatid golgi apparatus and participate in the development of the acrosome-acroplaxome complex, head-tail coupling apparatus and tail. *Dev Dyn* 240: 723-36
- Kierszenbaum AL, Tres L. 2004. The acrosome-acroplaxome-manchette complex and the shaping of the spermatid head. *Arch Histol Cytol* 67: 271-84
- Kim N, Xiao R, Choi H, Jo H, Kim JH, et al. 2011. Abnormal sperm development in *pcd(3J)*^{-/-} mice: the importance of *Agtbbp1* in spermatogenesis. *Mol Cells* 31: 39-48

- Kimura Y, Kurabe N, Ikegami K, Tsutsumi K, Konishi Y, et al. 2010. Identification of tubulin deglutamylase among *Caenorhabditis elegans* and mammalian cytosolic carboxypeptidases (CCPs). *J Biol Chem* 285: 22936-41
- Knoblaugh D, L. T. 2012. Male Reproductive System. *Comparative Anatomy and histology: A Mouse and human Atlas*: 285-308
- Kollman JM, Merdes A, Mourey L, Agard DA. 2011. Microtubule nucleation by gamma-tubulin complexes. *Nat Rev Mol Cell Biol* 12: 709-21
- Komada M, McLean DJ, Griswold MD, Russell LD, Soriano P. 2000. E-MAP-115, encoding a microtubule-associated protein, is a retinoic acid-inducible gene required for spermatogenesis. *Genes Dev* 14: 1332-42
- Konno A, Ikegami K, Konishi Y, Yang HJ, Abe M, et al. 2016. Ttl9^{-/-} mice sperm flagella show shortening of doublet 7, reduction of doublet 5 polyglutamylation and a stall in beating. *J Cell Sci* 129: 2757-66
- Konno A, Setou M, Ikegami K. 2012. Chapter three – Ciliary and Flagellar Structure and Function—Their Regulations by Posttranslational Modifications of Axonemal Tubulin. *International Review of Cell and Molecular Biology* 294: 133-70
- Kubo T, Yanagisawa HA, Yagi T, Hirono M, Kamiya R. 2010. Tubulin polyglutamylation regulates axonemal motility by modulating activities of inner-arm dyneins. *Curr Biol* 20: 441-5
- L'Hernault SW, Rosenbaum JL. 1985. Chlamydomonas alpha-tubulin is posttranslationally modified by acetylation on the epsilon-amino group of a lysine. *Biochemistry* 24: 473-8
- Lacroix B, van Dijk J, Gold ND, Guizetti J, Aldrian-Herrada G, et al. 2010. Tubulin polyglutamylation stimulates spastin-mediated microtubule severing. *J Cell Biol* 189: 945-54

- Lee GS, He Y, Dougherty EJ, Jimenez-Movilla M, Avella M, et al. 2013. Disruption of Ttl5/stamp gene (tubulin tyrosine ligase-like protein 5/SRC-1 and TIF2-associated modulatory protein gene) in male mice causes sperm malformation and infertility. *J Biol Chem* 288: 15167-80
- Lehti MS, Kotaja N, Sironen A. 2013. KIF3A is essential for sperm tail formation and manchette function. *Mol Cell Endocrinol* 377: 44-55
- Lehti MS, Sironen A. 2016. Formation and function of the manchette and flagellum during spermatogenesis. *Reproduction* 151: R43-54
- Lie PP, Mruk DD, Lee WM, Cheng CY. 2010. Cytoskeletal dynamics and spermatogenesis. *Philos Trans R Soc Lond B Biol Sci* 365: 1581-92
- Liu Y, DeBoer K, de Kretser DM, O'Donnell L, O'Connor AE, et al. 2015. LRGUK-1 is required for basal body and manchette function during spermatogenesis and male fertility. *PLoS Genet* 11: e1005090
- Ludueña RF, Banerjee A. 2008. The isotypes of tubulin: distribution and functional significance. *Cancer Drug Discovery and Development: The Role of Microtubules in Cell Biology, Neurobiology, and Oncology*: 123-75
- Lyons PJ, Sapio MR, Fricker LD. 2013. Zebrafish cytosolic carboxypeptidases 1 and 5 are essential for embryonic development. *J Biol Chem* 288: 30454-62
- Manandhar G, Simerly C, Schatten G. 2000. Highly degenerated distal centrioles in rhesus and human spermatozoa. *Hum Reprod* 15: 256-63
- Manandhar G, Sutovsky P, Joshi HC, Stearns T, Schatten G. 1998. Centrosome reduction during mouse spermiogenesis. *Dev Biol* 203: 424-34
- Martin M, Iyadurai SJ, Gassman A, Gindhart JG, Jr., Hays TS, Saxton WM. 1999. Cytoplasmic dynein, the dynactin complex, and kinesin are interdependent and essential for fast axonal transport. *Mol Biol Cell* 10: 3717-28

- Mary J, Redeker V, Caer J-PL, Rossier J, Schmitter J-M. 1997. Posttranslational Modifications of Axonemal Tubulin. *Journal of Protein Chemistry* 16
- Mendoza-Lujambio I, Burfeind P, Dixkens C, Meinhardt A, Hoyer-Fender S, et al. 2002. The Hook1 gene is non-functional in the abnormal spermatozoon head shape (azh) mutant mouse. *Hum Mol Genet* 11: 1647-58
- Mochida A, Tres LL, Kierszenbaum AL. 1999. Structural and Biochemical Features of Fractionated Spermatid Manchettes and Sperm Axonemes of the Azh/Azh Mutant Mouse. *MOLECULAR REPRODUCTION AND DEVELOPMENT* 52: 434-44
- Moreno RD, Palomino J, Schatten G. 2006. Assembly of spermatid acrosome depends on microtubule organization during mammalian spermiogenesis. *Dev Biol* 293: 218-27
- Moreno RD, Schatten G. 2000. Microtubule configurations and post-translational alpha-tubulin modifications during mammalian spermatogenesis. *Cell Motil Cytoskeleton* 46: 235-46
- Mujica A, Navarro-Garcia F, Hernandez-Gonzalez EO, De Lourdes Juarez-Mosqueda M. 2003. Perinuclear theca during spermatozoa maturation leading to fertilization. *Microsc Res Tech* 61: 76-87
- Mullen RJ, Eicher EM, Sidman RL. 1976. Purkinje cell degeneration, a new neurological mutation in the mouse. *Proc Natl Acad Sci U S A* 73: 208-12
- Nakai M, Hess RA, Matsuo F, Gotoh Y, Nasu T. 1997. Further observations on carbendazim- induced abnormalities of spermatid morphology in rats. *Tissue & Cell* 29: 477-85
- O'Donnell L. 2014. Mechanisms of spermiogenesis and spermiation and how they are disturbed. *Spermatogenesis* 4: e979623
- O'Donnell L, Nicholls PK, O'Bryan MK, McLachlan RI, Stanton PG. 2011. Spermiation: The process of sperm release. *Spermatogenesis* 1: 14-35

- O'Donnell L, O'Bryan MK. 2014. Microtubules and spermatogenesis. *Semin Cell Dev Biol* 30: 45-54
- O'Donnell L, Rhodes D, Smith SJ, Merriner DJ, Clark BJ, et al. 2012. An essential role for katanin p80 and microtubule severing in male gamete production. *PLoS Genet* 8: e1002698
- O'Hagan R, Piasecki BP, Silva M, Phirke P, Nguyen KC, et al. 2011. The tubulin deglutamylase CCPP-1 regulates the function and stability of sensory cilia in *C. elegans*. *Curr Biol* 21: 1685-94
- Oko R, Maravei D. 1995. Distribution and possible role of perinuclear theca proteins during bovine spermiogenesis. *Microsc Res Tech* 32: 520-32
- Oko R, Sutovsky P. 2009. Biogenesis of sperm perinuclear theca and its role in sperm functional competence and fertilization. *J Reprod Immunol* 83: 2-7
- Oliva R. 2006. Protamines and male infertility. *Hum Reprod Update* 12: 417-35
- Otazo MRdIV, Lorenzo J, Tort O, Avilés FX, Bautista JM. 2013. Functional segregation and emerging role of cilia-related cytosolic carboxypeptidases. *The FASEB Journal* 27: 424-31
- Parvinen M. 1982. Regulation of the seminiferous epithelium. *Endocr Rev* 3: 404-17
- Pathak N, Austin-Tse CA, Liu Y, Vasilyev A, Drummond IA. 2014. Cytoplasmic carboxypeptidase 5 regulates tubulin glutamylation and zebrafish cilia formation and function. *Mol Biol Cell* 25: 1836-44
- Pathak N, Obara T, Mangos S, Liu Y, Drummond IA. 2007. The zebrafish fleer gene encodes an essential regulator of cilia tubulin polyglutamylation. *Mol Biol Cell* 18: 4353-64
- Peris L, Wagenbach M, Lafanechere L, Brocard J, Moore AT, et al. 2009. Motor-dependent microtubule disassembly driven by tubulin tyrosination. *J Cell Biol* 185: 1159-66

- Petersen C, Aumuller G, Bahrami M, Hoyer-Fender S. 2002. Molecular cloning of Odf3 encoding a novel coiled-coil protein of sperm tail outer dense fibers. *Mol Reprod Dev* 61: 102-12
- Petersen C, Fuzesi L, Hoyer-Fender S. 1999. Outer dense fibre proteins from human sperm tail: molecular cloning and expression analyses of two cDNA transcripts encoding proteins of approximately 70 kDa. *Mol Hum Reprod* 5: 627-35
- Petry S, Groen AC, Ishihara K, Mitchison TJ, Vale RD. 2013. Branching microtubule nucleation in *Xenopus* egg extracts mediated by augmin and TPX2. *Cell* 152: 768-77
- Piperno G, LeDizet M, Chang XJ. 1987. Microtubules containing acetylated alpha-tubulin in mammalian cells in culture. *J Cell Biol* 104: 289-302
- Plessman U, Weber K. 1997 Mammalian sperm tubulin: an exceptionally large number of variants based on several posttranslational modifications. *J Protein Chem.* 16: 385-90
- Pringent Y., Kann M. L., Larsh-Gar H., Péchart I., Fouquet J.P. 1996. Glutamylated tubulin as a marker of microtubule heterogeneity in the human sperm flagellum. *Molecular Human Reproduction* 2: 573-81
- Prota AE, Magiera MM, Kuijpers M, Bargsten K, Frey D, et al. 2013. Structural basis of tubulin tyrosination by tubulin tyrosine ligase. *J Cell Biol* 200: 259-70
- Rathke C, Baarends WM, Awe S, Renkawitz-Pohl R. 2014. Chromatin dynamics during spermiogenesis. *Biochim Biophys Acta* 1839: 155-68
- Raybin D, Flavin M. 1995. An enzyme tyrosylating α -tubulin and its role in microtubule assembly. *Biochemical and Biophysical Research Communications* 65: 1088-95
- Redeker V, Levilliers N, Schmitter JM, Le Caer JP, Rossier J, et al. 1994. Polyglycylation of tubulin: a posttranslational modification in axonemal microtubules. *Science* 266: 1688-91

- Refik-Rogers J, Manova K, Koff A. 2006. Misexpression of cyclin B3 leads to aberrant spermatogenesis. *Cell Cycle* 5: 1966-73
- Regnard C, Desbruyeres E, Huet J-C, Beauvallet C, Pernollet J-C, Edde B. 2000. Polyglutamylation of Nucleosome Assembly Proteins. *THE JOURNAL OF BIOLOGICAL CHEMISTRY* 275: 15969-76
- Regnard C, Fesquet D, Janke C, Boucher D, Desbruyeres E, et al. 2003. Characterisation of PGs1, a subunit of a protein complex co-purifying with tubulin polyglutamylase. *J Cell Sci* 116: 4181-90
- Rogowski K, Juge F, van Dijk J, Wloga D, Strub JM, et al. 2009. Evolutionary divergence of enzymatic mechanisms for posttranslational polyglycylation. *Cell* 137: 1076-87
- Rogowski K, van Dijk J, Magiera MM, Bosc C, Deloulme JC, et al. 2010. A family of protein-deglutamylating enzymes associated with neurodegeneration. *Cell* 143: 564-78
- Rosenbaum JL, Witman GB. 2002. Intraflagellar transport. *Nat Rev Mol Cell Biol* 3: 813-25
- Rüdiger M, Plessman U, Kloppel KD, Wehland J, Weber KCIt, the major brain beta tubulin isotype is polyglutamylated on glutamic acid residue 435. *FEBS Lett* 308, 101-105. 1992. Class II tubulin, the major brain beta tubulin isotype is polyglutamylated on glutamic acid residue 435. *FEBS Lett* 308: 101-05
- Russell LD, Russell JA, Macgregor GR, Meistrich MI. 1991. Linkage of Manchette Microtubules to the Nuclear Envelope and Observations of the Role of the Manchette in Nuclear Shaping- During Spermiogenesis in Rodents. *The American Journal of Anatomy* 192: 97-120
- Sadate-Ngatchou PI, Payne CJ, Dearth AT, Braun RE. 2008. Cre recombinase activity specific to postnatal, premeiotic male germ cells in transgenic mice. *Genesis* 46: 738-42

- San Agustin JT, Pazour GJ, Witman GB. 2015. Intraflagellar transport is essential for mammalian spermiogenesis but is absent in mature sperm. *Mol Biol Cell* 26: 4358-72
- Sassone-Corsi P. 2002. Unique chromatin remodeling and transcriptional regulation in spermatogenesis. *Science* 296: 2176-8
- Satir P. 1985. Switching mechanisms in the control of ciliary motility. *Mod. Cell Biol* 4: 1-46
- Satir P. 1979. Basis of flagellar motility in spermatozoa: current status. *The spermatozoon*: 81-90
- Schroder HC, Wehland J, Weber K. 1985. Purification of brain tubulin-tyrosine ligase by biochemical and immunological methods. *J Cell Biol* 100: 276-81
- Schulze E, Asai DJ, Bulinski JC, Kirschner M. 1987. Posttranslational modification and microtubule stability. *J Cell Biol* 105: 2167-77
- Sharp DJ, Ross JL. 2012. Microtubule-severing enzymes at the cutting edge. *J Cell Sci* 125: 2561-9
- Shen J, Chen W, Shao B, Qi Y, Xia Z, et al. 2014. Lamin A/C proteins in the spermatid acroplaxome are essential in mouse spermiogenesis. *Reproduction* 148: 479-87
- Sirajuddin M, Rice LM, Vale RD. 2014. Regulation of microtubule motors by tubulin isoforms and posttranslational modifications. *Nat Cell Biol* 16: 335-44
- Smith LB, Milne L, Nelson N, Eddie S, Brown P, et al. 2012. KATNAL1 regulation of sertoli cell microtubule dynamics is essential for spermiogenesis and male fertility. *PLoS Genet* 8: e1002697
- Tanos BE, Yang HJ, Soni R, Wang WJ, Macaluso FP, et al. 2013. Centriole distal appendages promote membrane docking, leading to cilia initiation. *Genes Dev* 27: 163-8

- Tort O, Tanco S, Rocha C, Bieche I, Seixas C, et al. 2014. The cytosolic carboxypeptidases CCP2 and CCP3 catalyze posttranslational removal of acidic amino acids. *Mol Biol Cell* 25: 3017-27
- Toshimori K, Ito C. 2003. Formation and organization of the mammalian sperm head. *Arch Histol Cytol* 66: 383-96
- Tovich PR, Sutovsky P, Oko RJ. 2004. Novel aspect of perinuclear theca assembly revealed by immunolocalization of non-nuclear somatic histones during bovine spermiogenesis. *Biol Reprod* 71: 1182-94
- Tres LL, Rivkin E, Kierszenbaum AL. 1996. Sak 57, an intermediate filament keratin present in intercellular bridges of rat primary spermatocytes. *MOLECULAR REPRODUCTION AND DEVELOPMENT* 45: 93-105
- Valenstein ML, Roll-Mecak A. 2016. Graded Control of Microtubule Severing by Tubulin Glutamylation. *Cell* 164: 911-21
- van Dijk J, Miro J, Strub JM, Lacroix B, van Dorsselaer A, et al. 2008a. Polyglutamylation is a post-translational modification with a broad range of substrates. *J Biol Chem* 283: 3915-22
- van Dijk J, Rogowski K, Miro J, Lacroix B, Edde B, Janke C. 2008b. A targeted multienzyme mechanism for selective microtubule polyglutamylation. *Mol Cell* 26: 437-48
- Vogel P, Hansen G, Fontenot G, Read R. 2010. Tubulin tyrosine ligase-like 1 deficiency results in chronic rhinosinusitis and abnormal development of spermatid flagella in mice. *Vet Pathol* 47: 703-12
- Vogl AW. 1988. Changes in the distribution of microtubules in rat Sertoli cells during spermatogenesis. *Anat Rec* 222: 34-41

- Vogl AW, Pfeiffer DC, Mulholland D, Kimel G, Guttman J. 2000. Unique and multifunctional adhesion junctions in the testis: ectoplasmic specializations. *Arch Histol Cytol* 63: 1-15
- Walker WH. 2011. Testosterone signaling and the regulation of spermatogenesis. *Spermatogenesis* 1: 116-20
- Wang DZ, Zhou XH, Yuan YL, Zheng XM. 2010. Optimal dose of busulfan for depleting testicular germ cells of recipient mice before spermatogonial transplantation. *Asian J Androl* 12: 263-70
- Winder BS, Strandgaard CS, Miller MG. 2001. The role of GTP Binding and microtubule-associated proteins in the inhibition of microtubule assembly by carbendazim. *Toxicol Sci* 59: 138-46
- Wloga D, Webster DM, Rogowski K, Bre MH, Levilliers N, et al. 2009. TTLL3 Is a tubulin glycine ligase that regulates the assembly of cilia. *Dev Cell* 16: 867-76
- Wolff A, de Nechaud B, Chillet D, Mazarguil H, Desbruyeres E, et al. 1992. Distribution of glutamylated alpha and beta-tubulin in mouse tissues using a specific monoclonal antibody, GT335. *Eur J Cell Biol* 59: 425-32
- Yan HH, Mruk DD, Lee WM, Cheng CY. 2008. Cross-talk between tight and anchoring junctions-lesson from the testis. *Adv Exp Med Biol* 636: 234-54
- Yoshida T, Ioshii SO, Imanaka-Yoshida K, Izutsu K. 1994. Association of cytoplasmic dynein with manchette microtubules and spermatid nuclear envelope during spermiogenesis in rats. *J Cell Sci* 107 (Pt 3): 625-33
- Zamboni L, Stefanini M. 1971. The fine structure of the neck of mammalian spermatozoa. *Anat Rec* 169: 155-72
- Zhang Y, Ou Y, Cheng M, Saadi HS, Thundathil JC, van der Hoorn FA. 2012. KLC3 is involved in sperm tail midpiece formation and sperm function. *Dev Biol* 366: 101-10

Zhou J, Yang F, Leu NA, Wang PJ. 2012. MNS1 Is Essential for Spermiogenesis and Motile Ciliary Functions in Mice. *PLOS Genetics* 8

RESUME SUBSTANTIEL EN FRANÇAIS

La spermatogenèse est le processus par lequel les cellules germinales sont transformées en spermatozoïdes par le déroulement de 3 phases: la phase méiotiques et meiotique et la spermiogénèse. Pendant la spermiogénèses d'importantes structures sont formées afin de générer un spermatozoïde fonctionnel : l'acrosome, la manchette et le flagelle. La manchette est une structure transitoire situé caudalement à l'acrosome, composée par un manteau de microtubules longeant le noyau du spermatide. La manchette est connue pour participer au remodelage du noyau afin de lui conférer une forme falciforme ainsi que pour son rôle dans le développement de l'acrosome et du flagelle. En effet, pendant la toutes les molécules nécessaires pour la formation du flagelle et de l'acrosome doivent être transportées sur leur site d'assemblage. Les microtubules forment la manchette permettent le mouvement de protéines entre la région pre-acrosomique et la zone d'assemblage du flagelle. Cependant ce transport doit être finement régulé dans l'espace et dans le temps car la localisation aberrante et/ou manquante de certaines protéines peut causer des malformations de l' acrosome, de la manchette et du flagelle. Un mécanisme qui peut expliquer la façon dont ce processus de transport peut être régulé est la génération de modification post-traductionnelles de la tubuline forment les microtubules car ces modifications peuvent réguler les interactions avec les moteurs moléculaires et les protéines associées aux microtubules. La polyglutamylation correspond à un attachement covalent de chaines de glutamates latérales sur la queue terminale de la tubuline. Cette modification est contrôlée par la coordination des enzymes glutamylase (TTLLs) et déglutamylase (CCPs). De récentes études ont souligné l'importance potentielle de certaines de ces enzymes dans la formation et la maintenance du flagelle. Mon projet est centré sur l'étude des fonctions exercées par CCP5 pendant la spermatogenèse chez la souris.. L'analyse de la souris CCP5-knockout a permis de souligner le rôle essentiel

mené par CCP5 pendant la spermiogénèse. J'ai constaté que les souris CCP5-KO produisent 100 fois moins de sperme, défectueux et immobile, comparé aux contrôles. De plus, des nombreuses cellules haploïdes immatures sont prématurément libérées de l'épithélium germinatif. Une analyse approfondie a révélée que la réduite production de sperme est due à plusieurs défaut ultrastructurelles qui surgissent pendant la spermiogénèse. J'ai observé que l'acrosome n'était pas bien développée et que cela se détachait du noyau chez les spermatides matures condensés. De plus l'organisation des microtubules formant la manchette était aussi affectée par une émanation ectopique, ainsi que par une localisation défectueuse dans le noyau. Ces défauts corrént avec la formation des spermatides allongée que n'ont pas la typique forme falciforme. De plus, j'ai constaté la présence de centrioles surnuméraires chez les spermatides allongées CCP5-KO. Ce défaut corréle avec l'observation de microtubules « doublets » et « singlets » dispersés dans le cytoplasme de la cellule. De plus, les structures accessoires du flagelle se positionnaient, de façon désorganisé, à côté de ces microtubules. On a pu constater que ces microtubules sont très probablement issus de plusieurs axonemes qui s'ouvrent dans leur région. Le processus entier de spermiogénèse semble être défectueux dans la souris CCP5-KO et cela est accompagné par d'importants changements de niveaux de glutamylation chez les spermatides rondes et allongés. Par conséquent la régulation des niveaux de glutamylation faites par CCP5 lors de la spermiogénèse semble être fondamentale pour garantir un développement normal des spermatides en spermatozoïdes.

RESUME EN FRANÇAIS

Titre: Etude du rôle de l'enzyme deglutamylase CCP5 dans la régulation de la fonction des microtubules au cours de la spermiogénèse chez la souris

Mots clés: Microtubules, Glutamylaton, Spermiogénèse, Stérilité

La spermatogénèse est le processus par lequel les cellules germinales sont transformées en spermatozoïdes. Pendant la spermiogénèse d'importantes structures sont formées afin de générer un spermatozoïde fonctionnel: l'acrosome, la manchette et le flagelle. La manchette est une structure transitoire, composée par un manteau de microtubules longeant le noyau du spermatide. La manchette est connue pour participer au remodelage du noyau afin de lui conférer une forme falciforme ainsi que pour son rôle dans le développement de l'acrosome et du flagelle. Les microtubules forment la manchette permettent le mouvement de protéines entre la région pre-acrosomique et la zone d'assemblage du flagelle. Cependant ce transport doit être finement régulé dans l'espace et dans le temps car la localisation aberrante et/ou manquante de certaines protéines peut causer des malformations de l'acrosome, de la manchette et du flagelle. Un mécanisme qui peut expliquer la façon dont ce processus de transport peut être régulé est la génération de modification post-traductionnelles de la tubuline. Ces modifications peuvent réguler les interactions avec les moteurs moléculaires et les protéines associées aux microtubules. La polyglutamylaton correspond à un attachement covalent de chaînes de glutamates latérales sur la queue terminale de la tubuline. Cette modification est contrôlée par la coordination des enzymes glutamylase (TTLLs) et déglutamylase (CCPs). Mon projet est centré sur l'étude des fonctions exercées par la deglutamylase CCP5 pendant la spermatogénèse chez la souris. L'analyse de la souris CCP5-knockout a permis de souligner le rôle essentiel mené par CCP5 pendant la spermiogénèse. J'ai constaté que les souris CCP5-KO produisent 100 fois moins de sperme, défectueux et immobile, comparé aux contrôles. Une analyse approfondie a révélée que la réduite production de sperme est due à plusieurs défaut ultrastructurales qui surgissent pendant la spermiogénèse. Ces défauts corrélaient avec la formation des spermatides allongée que n'ont pas la typique forme falciforme. Le processus entier de spermiogénèse semble être défectueux dans la souris CCP5-KO et cela est accompagné par d'importants changements de niveaux de glutamylaton chez les spermatides rondes et allongés. Par conséquent la régulation des niveaux de glutamylaton faites par CCP5 lors de la spermiogénèse semble être fondamental pour garantir un développement normal des spermatides en spermatozoïdes.

ENGLISH SUMMARY

Title: Study of the role of the deglutamylating enzyme CCP5 in microtubules function regulation during mouse spermatogenesis.

Key words: Microtubules, Glutamylaton, Spermiogenesis, Sterility

Spermatogenesis is the process by which germ cells are transformed into spermatozoa. To allow the final maturation of haploid germ cells into spermatozoa specific structures have to be developed during the spermiogenesis: the acrosome, the manchette and the flagellum. The manchette is a microtubules-based structure. It is known to participate in the shaping of the nucleus conferring it the typical hook-like shape and several studies have underlined its importance in acrosome and flagellum formation. During spermiogenesis manchettal microtubules allow the movement of molecules and organelles necessary for both acrosome and flagellum formation to their destination sites. However this MTs-based traffic has to be regulated both in space and time as it has been shown that ectopic or mislocalization of certain proteins can lead to failures in acrosome, manchette and flagellum development. The generation of posttranslationally modified MTs might explain a possible mechanism of traffic regulation since it has been demonstrated that posttranslational modifications (PTMs) can regulate the interaction between MTs and molecular motors and microtubules binding proteins. Polyglutamylaton, consist in the addition of glutamate side chains of variable length on α - and β - tubulin carboxy-terminal tails. Glutamylaton levels are determined by the combined action of glutamylase (TTLLs) and deglutamylase (CCPs) enzymes. During my PhD I investigated about the functional role of CCP5 during mouse spermatogenesis. CCP5 is the only enzyme able to remove the glutamate branching point of the added side chain. The study of the CCP5-KO mouse reveals that CCP5 has an essential role during mouse spermiogenesis. CCP5-KO male produces 100-fold less sperm cells than controls and released sperm cells are highly defective and immotile. A deep-analysis reveals that the reduced sperm output is due to several ultrastructural defects emerging during the spermatids differentiation process that correlate with increased level of glutamylaton on round spermatids' cortical MTs and elongating spermatids' manchettal MTs. Taken together, this study strongly suggests that CCP5-mediated glutamylaton regulation is fundamental for spermatids' differentiation into healthy functional spermatozoa.